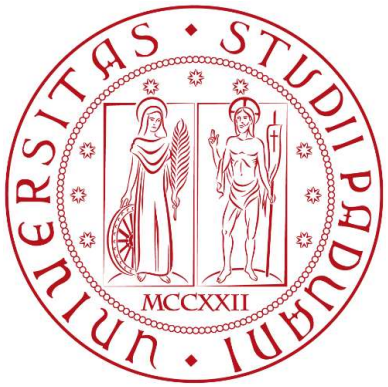

UNIVERSITÀ DEGLI STUDI DI PADOVA

DIPARTIMENTO DI INGEGNERIA INDUSTRIALE

CORSO DI LAUREA MAGISTRALE IN INGEGNERIA DEI MATERIALI

Tesi di Laurea Magistrale in
Ingegneria dei Materiali

GRAPHENE FILLED POLYAMIDE-6

Relatore: Prof.ssa Alessandra Lorenzetti

Correlatore: Prof. Tony McNally

Laureando: Francesco Cugola

ANNO DI ACCADEMICO 2017-2018

Abstract

In this thesis the electrical, mechanical, thermal, rheological, chemical and morphological properties of a semi-crystalline polymeric material (polyamide 6, PA6) filled with 2-dimensional (2-D) graphene nanoplatelets (GNPs) were investigated. In order to promote chemical compatibility between the polar polyamide matrix and the apolar filler, graphene with some oxygen functionality has been employed. The melt-mixing process of polyamide 6/graphene nanocomposite via twin screw extrusion has been conducted in order to examine how the various properties of the material change with different nanofiller concentration, and by altering the characteristics of the polymer matrix. GNPs have been added to the polymer matrix with increasing loading from 0.1wt% to 5wt% in order to produce several specimens of different geometries via injection-moulding and compression moulding processes. Two different grades of polyamide 6 were utilised, each characterised by a distinct molecular weight, to investigate the effects of matrix characteristics on the properties of the composites.

The results of this research indicated that mechanical properties of the nanocomposites varied only slightly and a change from ductile to brittle behaviour was observed. Thermal conductivity measurements did not show any significant improvement of the heat transfer through the composite structure. However, a rheological as well as electrical percolation threshold was achieved between 1-3 wt% GNPs; in particular the electrical resistivity decreased of approximately 7 orders of magnitude compared to neat PA6.

In conclusion it can be assessed that, even if a percolated network has been formed, no perfect contact between nanofillers and matrix was achieved throughout the network. Therefore, the increase in the chemical compatibility between graphene and polar polyamide matrix, by using graphene containing oxygen functionality, is not enough to obtain a good matrix-filler adhesion. One of the key feature in achieving significant improvement of the polymer nanocomposites properties still remain the processing conditions.

This thesis work was developed at International Institute for Nanocomposites Manufacturing (IINM) at the University of Warwick.

Riassunto

In questa tesi sono state studiate le proprietà elettriche, meccaniche, termiche, reologiche, chimiche e morfologiche di un materiale polimerico semicristallino (poliammide 6, PA6) caricato con nanoparticelle di grafene bidimensionale (2-D) (GNP). Al fine di promuovere la compatibilità chimica tra la matrice poliammidica polare e l'additivo apolare, è stata impiegata polvere di grafene funzionalizzata con una varietà di gruppi chimici contenenti ossigeno. I nanocompositi polimerici poliammide 6 – grafene sono stati prodotti mediante il metodo *melt blending* in estrusore, con l'obbiettivo di esaminare come le proprietà del materiale cambino al variare della concentrazione di additivo e alterando le caratteristiche della matrice polimerica. Le nanoparticelle di grafene sono state aggiunte alla matrice polimerica con una concentrazione crescente dallo 0,1 al 5% in peso, per produrre diversi campioni a geometria variabile tramite processi di stampaggio a iniezione e compressione. Sono stati utilizzati due diversi gradi di poliammide 6, ciascuno caratterizzato da un distinto peso molecolare, al fine di studiare gli effetti delle caratteristiche della matrice sulle proprietà dei materiali compositi.

I risultati di questa ricerca hanno indicato una debole variazione delle proprietà meccaniche dei nanocompositi ed è stata osservata una transizione duttile-fragile all'aumentare del contenuto di carica. Le misure di conducibilità termica non hanno mostrato alcun miglioramento significativo per quanto riguarda il trasferimento di calore attraverso la struttura del materiale composito. Tuttavia, è stata raggiunta una soglia di percolazione, sia reologica che elettrica, tra l'1 e il 3% in peso di grafene; in particolare la resistività elettrica è diminuita di circa 7 ordini di grandezza rispetto alla poliammide pura. In conclusione si può notare che, nonostante si sia assistito ad un fenomeno percolativo, non è stato ottenuto un perfetto contatto tra l'additivo e la matrice in tutto il reticolo. Pertanto, l'aumento della compatibilità chimica tra l'additivo e la matrice poliammidica polare, utilizzando grafene funzionalizzato, non è stata sufficiente a garantire una buona adesione matrice-carica. Una possibile soluzione, ai fini di un miglioramento delle proprietà dei nanocompositi polimerici rimane l'ottimizzazione delle condizioni di processo. Questo lavoro di tesi è stato sviluppato presso l'*International Institute for Nanocomposites Manufacturing* (IINM) dell'Università di Warwick.

Contents

Introduction

In recent years, there has been a growing interest in the development of extrinsically conductive polymers, with the goal of producing a new concept of plastic materials characterised by a metal-like behaviour. With the continuous development of higher powered electronic device and smaller packages of integrated circuits, the use of materials with excellent electrical and thermal properties has started growing in importance. Polymers are industrially attractive materials because of their remarkable characteristics such as corrosion resistance, miniaturization capabilities, durability, light weight, and low production cost [1]. These features enable the substitution of metal parts in several applications including electromagnetic interference (EMI) shielded computer cables and housing, anti-static packaging, high strength and lightweight automotive/aerospace components, printable and flexible electronics, and thermal interface materials (TIMs) [2, 3]. However, the majority of polymers are electrically and thermally insulating, with values of thermal conductivity typically between 0.1 and 0.5 W m^{-1} K^{-1} [4] and electrical resistivity values between 10^{14} and 10^{16} ohm-cm [5]. These characteristics constitute a barrier to heat dissipation and good electronic performance, thus making the use of polymers challenging for modern electronic devices and heat transfer components. One way to improve the thermal and electrical conductivity (TC and EC, respectively) of a polymer is through the incorporation of one or more conductive filler materials, thus creating a composite. The final properties of this kind of material derived from the combination of two or more constituents and depend on both the loading, type, shape, size of the filler, and processing conditions of the composite [6]. Particularly, if the fillers are incorporated into sufficient quantities and dispersed properly, the creation of a percolated network structure could be possible, thus enabling the transfer of heat and electric current. The critical amount of conductive fillers at which the polymer nanocomposites change from insulator to conductor behaviour, is named as the percolation threshold [7]. Several studies demonstrated that a good enhancement of mechanical and electrical properties can be obtained when a physical percolation threshold is present in the composite structure [8, 9]. However, other researchers stated that is not obvious to observe the same improvement in term of heat transfer [10]. This

fact is largely due to the different fundamental mechanisms between thermal and electric transport in plastic based composite materials. Polymers are typically filled with carbon-based and/or metals materials, for enhancing thermal and electrical properties. The best intrinsic thermal conductivity of these materials does not always provide a good thermal conductivity in the composite, because in this system, heat transfer in mainly controlled by phonons (crystal vibrations) rather than electrons. Generally, phonons are greatly affected by the structure of the material in which they move. Therefore, even if a filler percolated network is formed into the polymer matrix, the presence of any defect/discontinuity in the filler crystalline structure, and weak filler/matrix interfaces will hinder the mechanisms of phonon transfer (by scattering phenomena), hence reducing the thermal conductivity [11].

This research intends to formulate, produce and characterise an extrinsically conductive polymeric material, consisting of polyamide 6 (PA6) filled with graphene nanoplatelets (GNPs). The conductive fillers were melt blended with two different grades of polyamide 6, differing for molecular weight, by using a co-rotating twin screw extruder. Subsequently, several composite specimens were manufactured through mini-injection moulding followed by testing (mechanical properties, volume electrical resistivity, and through-plane thermal conductivity) and analysis (fillers' size and morphology, defects density, thermal stability, filler surface chemistry, composite rheological properties). This study attempts to study the mechanical, thermal and electrical properties of the PA6/GNPs composites. More specifically, it will be explored how the filler concentration and the polymer characteristics can alter the possibility to form a mechanical and electrical percolated network in the composite structure. In order to promote chemical compatibility between the polar polyamide matrix and the apolar filler, graphene with some oxygen functionality has been employed.
The thesis is divided in the following sections:

- Chapter 1 begins by laying out the difference between intrinsically and extrinsically conductive polymers, the phenomenon of percolation, the electrical and thermal insulating nature of polymers, and the potential applications of conductive polymer composites.

- Chapter 2 describes the characteristics of polymeric nanocomposites with the main factors affecting their final properties.
- Chapter 3 contains the information related to the raw materials used for this research, and their remarkable features.
- Chapter 4 deals with the description of the processing and characterisation techniques used for the production and analysis of the PA6/GNPs nanocomposites, respectively.
- Chapter 5 presents the practical procedure and the processing parameters utilised for the nanocomposites preparation.
- Chapter 6 shows all the experimental results and their discussion.

Chapter 1

Conductive Polymers

The aim of this chapter is to introduce limits and solutions in relation to the electrically and thermally insulating nature of polymeric materials. Initially, a distinction between intrinsically and extrinsically electrically conducting polymers is provided, with further explanation of the current flow mechanisms in composite materials. Subsequently, a description of the causes related to the poor thermal conductivity of the materials is given, by focusing on the heat transfer mechanisms in pure polymers and in composites. Lastly, an overview of the main industrial applications of conductive polymer composites is illustrated.

1.1 Intrinsically Conductive Polymers

One of the most significant characteristics of polymers is their capacity to manifest negligible conduction when exposed to high electric fields, due to the high energy differences between the valence electronic states and the conduction band [12]. Even though each electron and nucleus of the material is subjected to an external electric force, the presence of tight molecular bondings prevents the free movements of these charges, thus making polymers more suitable for insulating applications. However, since 1977, with the discovery of polyacetylene and its high intrinsic electrical conductivity, the belief that polymers have obvious limits in carrying electric current has started being contradicted. Generally, there are two main categories of electrically active polymer system. The first group of conducting system is named as intrinsically conductive polymers (ICPs) or conjugated polymers. These polymers have a specific atomic configuration which consists of alternate single and double bonds, forming an extended π-network. Electrical conductivity arises from the transit of electrons along this π-framework, but the presence of specific dopants is required in order to trigger the

electrons mobility. The second family consists of extrinsically conductive polymers which derived from the addition of particulate and/or fibrous conductive fillers (such as carbon or metal) to the insulating polymer, in order to transmit high conductivity at the composite. The conductivity of these materials is related to the filler loading and dispersion as well as on the polymer type and viscosity. The first ICP to be synthesised was polyacetylene, followed with the synthesis of other electrically conducting organic compounds such as polypyrrole (PPY), polythiopene, polyaniline (PANI), poly(p-phenylene) etc. These organic materials exhibit alternating carbon single and double bonds which have delocalised π electrons that can flow along the polymer chain and have the potential to carry the charge. Metal-like conductivity can be achieved by adding/removing electrons from the polymer chain. Shirakawa, MacDiarmid and Heeger observed that partial oxidation of polyacetylene with iodine or other reagents led the conductivity to increase by 10^9 times more than the one of the undoped polymer [13]. When an electron is expelled from the highest point of the valence band of an ICP, a vacancy (hole o radical cation) is formed and does not delocalised completely. Only partial delocalisation took place, extending over different monomeric units and forcing them to deform structurally. In solid-state physics, a radical cation that is partly delocalised over some polymer chains is defined as a polaron. Upon increasing the doping more and more polarons are formed and, at higher doping concentration, it is possible to form a bipolaron which results from the removal of the unpaired electron from the level of the first polaron. Oxidative doping leads to the creation of two new electronic states between the valence and the conduction bands, as shown in Figure 1.1.

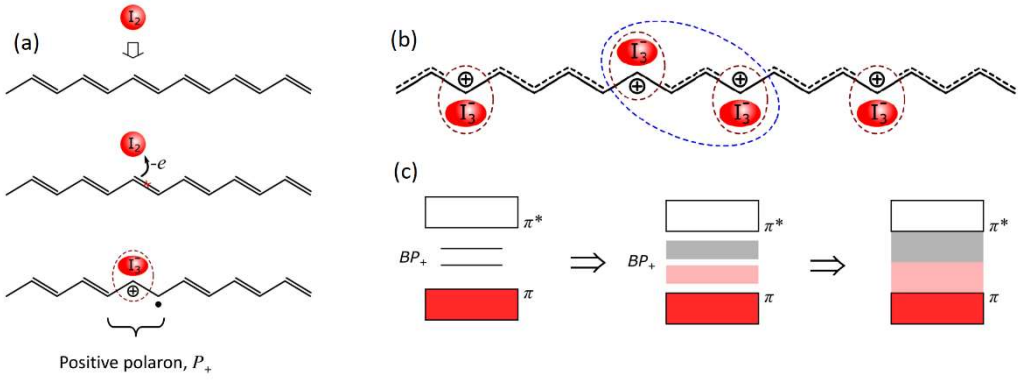

Fig. 1.1. *Schematic of: (a) Doping mechanism and polaron formation, (b) formation of a bipolaron and, (c) intercalated nanocomposites and (b) overlapping between conduction and valence bands [14].*

The polarons and bipolarons are mobile along the polymer chain and therefore charge transport is mediated by them as well as by hopping electrons. The conductivity of MacDiarmid's doped polyacetylene reached 10^3 S·cm and opened the way to the development of a new concept of polymer material with a metal-like behaviour. In a previous work in the area of polyacetylene, the research was focused on the use of ICPs as "easily processable and lightweight plastic metals" [15]. However, even though the conductivity of polyacetylene is similar to that of copper, its durability on air/moisture and processability are very low compared to those of common used thermoplastic polymers. Conversely, other conjugated polymers such as polypyrrole, polythiophene and PANI are characterised by higher stability and processability than polyacetylene, but are less conductive. These characteristics make the conjugated polymers not perfectly suitable for producing macroscopic components with the most widely used manufacturing techniques. Polymers composites containing ICPs as conducting fillers are becoming much more attractive because of the combination of enhanced processability and good mechanical properties together with a high conductivity. However, there are still difficulties in exploiting the high degree of conductivity of ICPs and, at the same time, make them applicable in industrial processing along with a thermoplastic matrix.

1.2 Extrinsically Conductive Polymers

A completely different approach to make a polymer electrically conductive consists in creating a mixture between the polymeric matrix and the conductive material in order to alter the electrical properties of the resulting composite. Through the use of this method, almost every polymer can be made electrically conductive, due to the fact that this property is not related to the intrinsic molecular structure of the polymer, as for ICP. In order to use a material as a conductive filler it is necessary to understand the mechanisms and interactions that occur at the micro and nanometric level between the additive and the matrix of the composite. The main factors regulating these interactions depend on the characteristics of the chosen filler, such as its conductivity, size, shape, surface morphology, orientation and dispersion within the matrix. The latter depends mainly on the production process of composites [16]. The most commonly used fillers for producing conductive polymeric composites are: carbon black, graphene, carbon nanotubes, ICPs,

metal nanoparticles and graphite fibers. In this study, polymer composites obtained by dispersing graphene nanoplatelets will be studied and analysed in depth.

The above listed fillers, characterised by a high intrinsic electrical conductivity, help to enhance the electrical properties of the polymer. This enhancement derives from the formation of a continuous three-dimensional lattice within the matrix, which occurs when the dispersed conductive particles are in such an amount as to be adjacent to one another. The lattice formation depends on the percentage and on the geometry of the additives. Moreover, a good dispersion of the fillers is fundamental, and this characteristic discriminates the various methods of production of the composites. One of the common issues which arise with the use of conductive fillers, in fact, is the formation of aggregates caused by Van der Walls forces which established between the particle surfaces. These aggregates do not allow a good homogenisation of the additives in the composite, making it necessary to increase the percentage of additive in order to obtain a good conductivity. The percentage at which the material manifests a transition from an insulating behavior to a semi-conductive/conductive behavior is defined as the percolation threshold.

1.2.1 Percolation Threshold

The percolation threshold corresponds to the percentage of additive at which the formation of a continuous network of the dispersed particles occurs. Below this threshold, the conductivity is low, but tend to abruptly increase above the filler concentration at which the particles come into contact with each other (see Fig. 1.2). The percolation threshold is characterised by a sudden leap in the conductivity of several orders of magnitude, attributed to the formation of the three-dimensional filler network within the matrix.

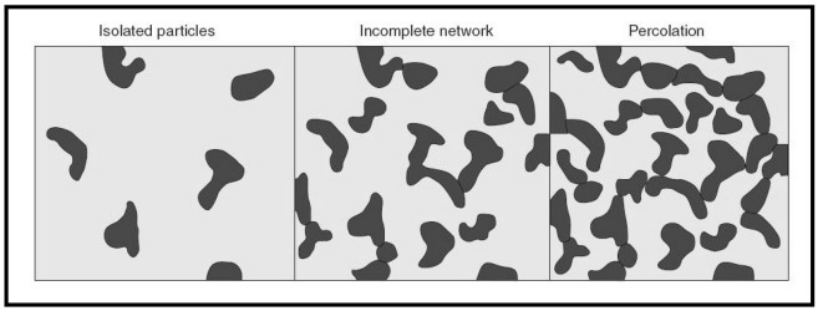

Fig. 1.2. *Schematic of percolation threshold formation.*

An important parameter which regulates the percentage of percolation is the aspect ratio. On one hand, additives with a low aspect ratio, i.e. with the shape of more or less spherical particles, are characterised by a high percolation threshold value. On the other hand, fillers with a high aspect ratio have a larger surface area with the same volume and consequently, the percolation threshold is reached at lower filler concentration. In addition to the aspect ratio, the filler dimensions are also fundamental in lowering the percolation threshold; for example, the nanometric dimensions of graphene and nanotubes favor the formation of an interconnected lattice between the particles with respect to a micrometric charge such as carbon black. Near percolation, electrical conductivity is affected by a non-linear change (as shown in Fig 1.3) which can be described according to the following power law:

$$\sigma = \sigma_c (V - V_p)^t \tag{1.1}$$

where σ_c is the intrinsic electrical conductivity of the filler, V is the filler volumetric fraction, V_p is the percolation volume fraction and t is a critical exponent related to the system dimensions. With composite materials consisting of two phases, a conductor and an insulator, three different modes of current transport can be taken in account, depending on whether the filler concentration is approaching the percolation threshold:

1. When the additive concentration is well below the conductivity threshold, the average distance between two filler particles is wide (or in any case greater than 10 nm), which means that electric transport mechanisms are not possible between one particle and another. Therefore, the material will manifest a conductivity value close to that of the neat polymer matrix.

2. In the second case the particles are still well separated but have a distance average less than 10 nm. Even though the particles are not geometrically connected, electric transport is possible in the presence of an external electric field by mean of quantum tunneling phenomena between adjacent conductive fillers.

3. When the filler loading is quite high, an intimate connection between adjacent particles occurs. In this case, the electrons' transport takes place through the continuous structure formed by the conductive fillers, thus the value of

conductivity will depend mainly on the properties of filler particles (presence of defect, intrinsic conductivity, geometry) and on the quality of filler-filler interfaces.

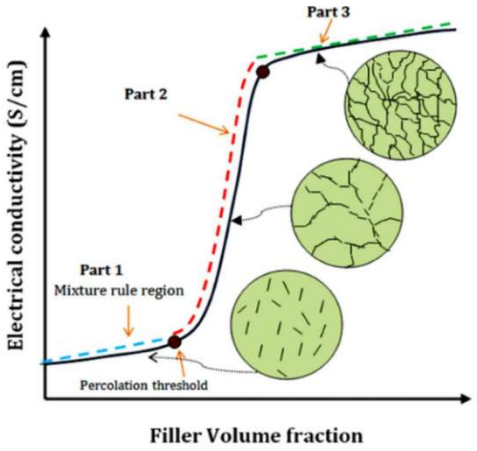

Fig. 1.3. *Schematic of non-linear variation of electrical conductivity as a function of filler volume fraction [17].*

1.3 Thermal Conductivity in Polymers

Thermal transport in polymers represents a complex process due to their amorphous state. Generally, in solid matter, heat transfer is mediated by charge carriers (holes or electrons) or by phonons which consist in "quantised modes of vibration in a rigid crystal lattice" [18]. In polymers, thermal conduction is mainly controlled by phonons, while in metals the electrons dominate with respect the other heat carriers. It is possible to estimate the thermal conductivity of polymer through the use of the Debye equation:

$$k = \frac{C_p v l}{3} \tag{1.2}$$

Where C_p represents the specific heat capacity per unit volume, l is the phonon mean free path and v is the phonon speed. All these variables are influenced by several intrinsic and extrinsic polymer parameters such as temperature, crystallinity, orientation of macromolecules, number of defects etc. Although it has been found that individual extended polymer chains can reach rather high values of thermal conductivity [19], bulk polymers are thermal insulators, with values of TC in the range 0.1-0.5 W/m K. The great

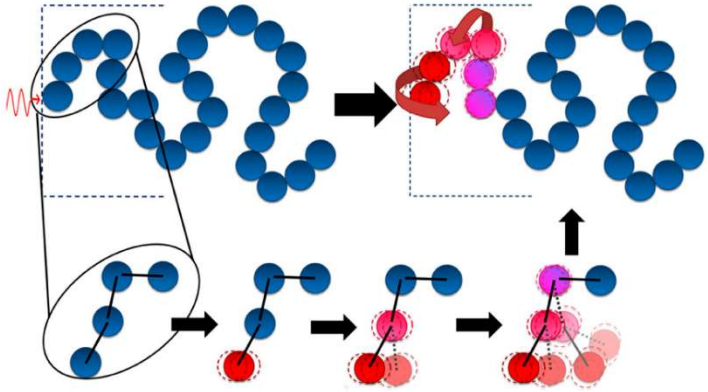

Fig. 1.4. *Thermal conductivity mechanism in an amorphous polymer [4].*

majority of bulk polymers are characterised by the same heat capacity (C_p) and phonon group velocity (v) of those of single chains. Hence, the difference in thermal conductivity between individual chains and the bulk polymer is strictly related to the phonon mean free path (l). This parameter has been found to be large in single chains because of the reduced anharmonicity of lattice vibrations related to covalent bonds, whereas in bulk polymers the abundance of intermolecular weak bondings (Van der Waals forces) which connect random oriented polymeric chains, lead to a much smaller mean free phonon path. Moreover, the presence of defects such as impurities, voids, entanglements and polymer chain ends, contribute to the reduction of the mean free path of phonons, thus further lowering the thermal conductivity. Burger at al. [20] showed a schematic representation of the mechanism of heat transfer in amorphous polymers. The thermal transport is achieved much more slowly in polymers because the heat tends not to propagate like a wave as in crystalline solids (where the phonons diffuse quickly from one atom to the other), but it diffuses irregularly, due to the disordered rotations and vibrations and of atoms around their equilibrium positions. Therefore, a large amount of heat kinetic energy is spread into several directions because of the disordered polymeric structure and the thermal conductivity is significantly reduced. Furthermore, the presence of any defect or discontinuity in the crystalline phase of semycrystalline polymers, will decrease the thermal transfer. The defects are responsible for generation of the so-called phonon scattering which consists in a combination of refraction, diffraction and reflection effects at which the phonons are subjected, yielding to the shortening of the mean free path. Also, the temperature can influence the thermal conductivity of amorphous and

semycrystalline polymers. Recent studies proved that the conductivity of amorphous polymers increased by approaching the glass transition temperature (T_g) while it decreased once above T_g [21, 22].

1.3.1 Nanocomposites for Thermal Conductivity

In order to enhance the thermal conductivity of insulating material such as polymers, the incorporation of high-TC fillers into the polymer matrix can be taken in account. The degree of improvement in thermal transfer depends on the type and structure of the fillers, which determine how the heat is propagated between the conductive particles. Generally, high values of thermal conductivity are achieved by using metallic and carbon-based fillers in which the heat transfer is mainly controlled by free electrons movements. In contrast, fillers characterised by purely phonon heat transfer are less efficient because more affected by scattering phenomena. Outstanding results have been obtained in improving the thermal conductivity of polymer composites by introducing 2D thermally conductive fillers such as graphene [23-25]. In general, most of the manufactured thermally conductive composites based on graphene, utilise this kind of filler in form of multi-layer graphene such as graphene nanoplatelets or nanosheets. When the graphene atoms come in contact with the source of heat and start to vibrate, the phonons are quickly transferred to the surrounding atoms thanks to the strong covalent bondings of the graphene structure. However, vibrations are more limited to diffuse to the adjacent graphene layers due to the weak Van der Walls forces and consequently, anisotropic heat transfer usually occur in the multilayer graphene.

The thermal conductivity of polymer-composites is dependent on several factors such as filler size, filler shape, filler surface treatment, filler orientation, processing method, filler dispersion, filler/matrix interface etc. Among all these variables, the filler/matrix interface is considered as one of the major parameter to be controlled for improving thermal conductivity [26]. When the conductive particles are dispersed in the polymer matrix, large amount of filler/matrix interfaces are produced. Figure 1.5 illustrates the mechanism of heat transfer at the interface between the polymer matrix and the conductive crystalline filler. As explained above, when the crystalline filler is exposed

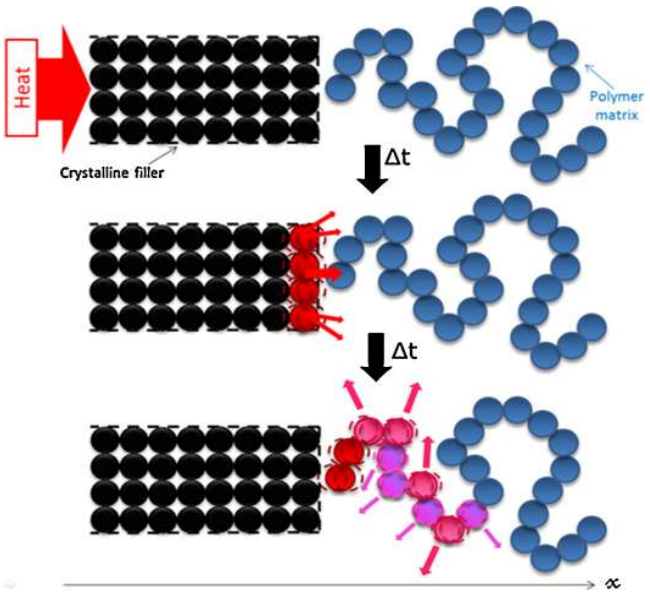

Fig. 1.5. *Schematic of heat transfer mechanism at filler-matrix interface [4].*

to a heat source, the thermal transfer occurs quickly in a specific direction through the material's atoms, within a certain amount of time (Δt). In the same time range, the distance covered by the heat along the polymer chain is much shorter than the corresponding path through the crystalline filler. The high discrepancy between the heat transfer mechanisms along the two constituents leads to a dramatic decreasing of the thermal conductivity at the interface. More specifically, a mismatch in harmonicity of the phonon normal modes (vibration of different frequencies) between the filler and the polymer matrix occur, which is responsible of a strong scattering effect. This phenomenon is also called as "Kapitza resistance" or "thermal resistance" [27]. Several authors have focused their research on matrix/filler interfaces in order to limiting thermal resistance. One of the most commonly used approaches is the filler functionalisation, by which it can be obtained high compatibility between the composites constituents and promote a better thermal transfer through the material. Even though this treatment would reduce the filler/ matrix interface and decrease phonon scattering between at the boundaries, the functionalisation can cause a decreasing of the filler's intrinsic thermal conductivity, due to the intensified phonon scattering at the grafted parts. For instance, Gulotty *et al*. [28] adopted acid treatment in order to introduce carboxylic groups on the surface of carbon nanotubes. The functionalisation improved the interface coupling but

led to defects formation, thus reducing the phonon transport along the filler. Alternatively, it is possible to exploit other treatments such as sol-gel methods, plasma treatments, hybrid materials, coatings, etc.

1.4 Applications

In the last 20 years, there has been an increasing demand in emerging industries for the development of thermally and/or electrically conductive applications. Compared to other traditional conductive materials such as metals and ceramics, polymer composites have started to gain considerable importance, due to the following characteristics:

- Light weight and corrosion resistance;
- Easy processability in parts of different and complex geometries;
- Vibration-damping capacity;
- Electrical and thermal conductivity can be regulated by selecting appropriate fillers;

Applications of electrically and thermally conductive polymer composites involve different areas such as electronics, automotive, solar, aerospace, biomedical etc. In automotive, conductive polymers are commonly used as metal electrodeposition supports. Moreover, by presenting antistatic properties, they are used for bodyworks of motor vehicles. The mechanical reinforcement provided by inorganic filler such as graphene (or other carbon base materials) presents potential applications in weight-sensitive automotive and aerospace applications such as tires, which can also exploit the high conductivity of the filler. One of the main fields of application of conductive composites is that of electronic devices. Thanks to the high electrical conductivity, high mobility of the carriers, and good optical transmittance in the visible range, these composites are used as electrodes for solar cells, liquid crystal devices, light-emitting diodes (LEDs) and field effect transistors (FETs). In the area of energy conservation, composites have been developed with carbon additives to be applied to lithium batteries with the aim of increasing the recharging capacity. Another area of innovation in which these materials are involved, such as the composites filled with graphene, is that of sensors for the detection of pressure, pH and temperature, and of gas or biomolecules, thanks to the high specific surface of the additives. An important application is the

shielding of electromagnetic radiation produced by electronic devices, telecommunication systems such as mobile phones, and internet networks. These radiations interfere with household appliances and electronic instrumentation. Materials, such as conductive polymers, which shield this radiation are therefore indispensable for increasing the life of electronic equipment as they reduce or suppress electromagnetic noise. Increasing interest is also the development of these nanocomposites in the biomedical field. These materials possessing excellent bacterial toxicity and at the same time low cytotoxicity for human cells, are excellent candidates for applications in this sector.

Chapter 2

Polymer Nanocomposites

This chapter is concerned with a description of the theoretical background of polymeric nanocomposites material. Specifically, principal methods of production and factors affecting the mechanical, thermal and electrical properties of the nanocomposites will be dealt.

2.1 Characteristics of Composite Materials

The term composite material refers to a specific class of material which is constituted by at least two distinct phases from a physical or chemical point of view. This definition, however, is very broad and is related to the vast majority of existing materials: for instance, almost all the materials obtained through a solidification process have numerous crystals with different orientations, which have several characteristics between the border and the center of the grain. For this reason, a most appropriate definition of composite material from a functional point of view is given as follows:

A composite material is the result of thy union of several materials, carried out in order to obtain a product with properties superior to those of the single components used.

Particle composites are usually composed of two main phases: a dispersion of reinforcing particles (filler) within a continuous phase (matrix). Furthermore, the presence of the matrix-filler interface and of any porosity must be considered. The physical and geometrical characteristics of the dispersed charges are of fundamental importance and decisive in improving the mechanical, thermal, electrical and rheological characteristics of the final product. There are different composite typologies according to the dimensions of the filler, as listed below:

- In a traditional composite material, the size and shape of the fillers can range from a few millimeters (short fibers), to long fibers, particles, or textures. The variability in this sector is very high and there is great versatility of the product obtainable by the process. There are also composite materials in nature: wood, for example, can be seen as a material in which the long cellulose fibers are contained in a matrix that binds them. Concrete is another example of material belonging to this category: the filler is represented by sand and crushed stone or by long steel bars in the case of reinforced concrete, and is inserted and dispersed in a cement matrix.
- A microcomposite material is a material in which particles of varying size, between the micron (10^{-6} meters) and tens of microns, are dispersed as uniformly as possible in the matrix. Normally, the processing does not modify the dimensions and the characteristics of the filler, but simply distributes and eventually orients the particles inside the matrix.
- In nanocomposite materials the filler in their final configuration are represented by particles characterised by one, two or three dimensions of less than 100 nanometers (nm). From a mechanical point of view, nanocomposites differ from traditional composite materials due to the high surface to volume ratio of the fillers and aspect ratio.

2.2 Polymer Nanocomposites

Polymer nanocomposites constitutes a category of nano-sized materials which comprises several solid phases, in which at least one of the dimensions of the dispersed filler is in the order of magnitude of the nanometer (10^{-9} m). Generally, various types of filler can be utilised as reinforcement such as, semiconductors, ceramics, carbon-based materials and metals. Research and development activities in this sector are increasing due to the possibility of improving mechanical, thermal and electrical characteristics of traditional polymer-based composites, along with a possible cost containment. For instance, it is possible to achieve the same mechanical properties of a traditional 20% micro-reinforced composite with quantities of nanofillers included in the range of 3-6%.

Three types of nanocomposites sub-categories can be distinguished, depending on how many dimensions of the dispersed particles are within the order of the nanometer [29]:

- Nanocomposites with *isodimensional nanofiller*, where all three dimensions of the reinforcement is within the order of nanometer such as, silica spherical nanoparticles or semiconductor nanoinclusions.
- Nanocomposites filled with *nanotubes or whiskers*, in which two dimensions are within the nanometer order of magnitude (elongated structure).
- Nanocomposites with *lamellar/layered nanofillers,* where only one dimension is within the order of the nanometer. One example is represented by lamellar silicates.

Graphene-based polymer nanocomposites have a structure similar to that widely studied of lamellar silicates, so it is possible to extend the terminology also to this type of materials [30]. Depending on the preparation method and on the nature of the constituents used, two principal types of composites can be produced by associating layered nanofillers with polymers, as shown in Fig. 2.1.

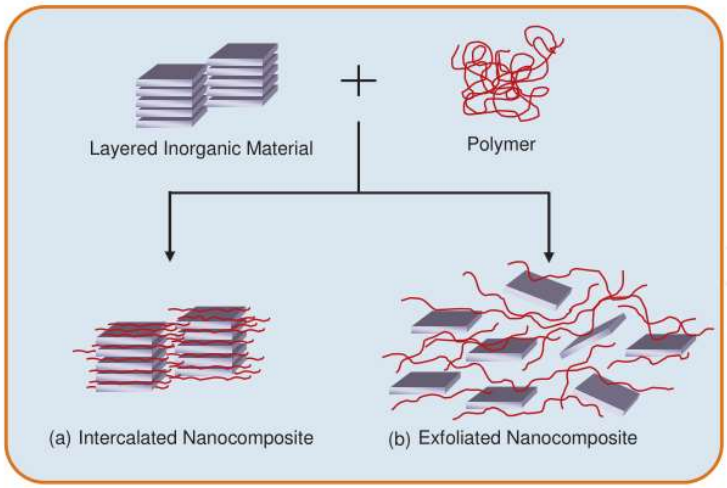

Fig. 2.1. *Schematic of the two different kinds of interations between layered nanofillers and the polymer matrix which lead to: (a) intercalated nanocomposites and (b) exfoliated nanocomposites [31].*

In the first case (see Fig. 2.1a), one or more polymer chains interleave between the individual layers of the reinforcement, thus an ordered structure is obtained through the

alternation of polymer and filler. In the second case, the inorganic layers are uniformly dispersed in the matrix (see Fig. 2.1b), thus creating an exfoliated or delaminated structure [32]. The properties of nanocomposites strongly depend on several parameters such as, the filler concentration, the filler distribution in the matrix, the ability to transfer the load from the matrix to the filler through the interface, and the filler aspect ratio. Generally, if these conditions are respected, the material shows an increase in the mechanical properties as well as in the thermal stability and the gas barrier property. Moreover, the electrical conductivity of the polymer can be enhanced, in the case of incorporation of conductive fillers.

2.2.1 Preparation Techniques

The dispersion of the filler in a polymer represents a critical step during the synthesis of nanocomposites. With a well dispersed filler, a maximum contact area between the filler and the polymer chains is achieved, thus affecting the entire matrix behaviour [33]. Moreover, the type of interaction that arise between the matrix and the filler during the mixing process is an important parameter which affects the dispersion of the reinforcement agent. There are three main ways to incorporate the fillers into the polymer matrix:

- Solution mixing
- Melt blending
- In situ polymerisation

A brief description of these methods will be given in this section, even if only melt-blending was used for this research.

2.2.1.1 Solution Mixing

This technique involves the solubilisation of the polymer in a suitable solvent (water, acetone, chloroform, toluene etc.) followed by the incorporation of the filler in order to create a suspension. A good homogenisation of the filler suspension in the solvent can be reached by the use of sonication technique, in which the exposure time and power are crucial parameters to be controlled in order to avoid the formation of defects and

damaging of the fillers. During the solvent mixing, the fillers are covered by the polymer, yielding to their interconnection once the solvent is evaporated. Surface functionalisation can be used in order to enhance the compatibility between the matrix and the fillers [34, 35]. By grafting functional groups on the filler surface, it is possible to improve the interaction with the polymer chains, yielding to the optimisation of the filler dispersion. Solution mixing involves a simply preparation process if compared to other method of synthesis of nanocomposites, but the use of organic solvent makes this technique unhealthy and environmental unfriendly. Gong *et al.* [36] obtained a good result in term of mechanical properties improvement via solution mixing of graphene oxide (GO) and PA6. They have been able to graft the polymer chain efficiently through an environmental friendly method, yielding to a high interfacial adhesion and dispersion of the filler.

2.2.1.2 Melt Blending

Melt blending is an economical and practical method used for the production of polymer nanocomposites. This technique employs high temperatures to melt the polymer and disperse the filler through the use of high shear stresses. It does not involve toxic solvents, and allows the material to be processed according to the common techniques used for thermoplastic polymers (typically extrusion).

Due to the high versatility of the method, it is believed that melt-blending is suitable for mass-fabrication. However, compared to the other methods, it is the one that provides less dispersion of the filler due to the high viscosity of the composite as the content of the additive increases [37]. Therefore, the chemical modification of the filler prior mixing is necessary to provide strong interactions within the matrix and improve the dispersion. Alternatively, an optimisation of the processing parameters such as mixing speed and temperature can be performed. Mayoral *et al*. [2] studied the result in the variation of extrusion screw speed and filler content on the thermal, electrical and mechanical properties of PA6/GNPs nanocomposites. An enhancement in Young's modulus and electrical conductivity was achieved due to the better dispersion of the nanofiller in the matrix with increasing screw speed. Kim *et al.* [38] noticed an improvement in the thermal conductivity of PC/GNPs nanocomposites produced by melt mixing.

2.2.1.3 In Situ Polymerisation

In situ polymerisation technique consists in the dispersion of the nanofiller in the pure monomer, followed by the polymerisation reaction after the introduction of a suitable initiator. This technique allows the formation of covalent and non-covalent bonds, between the filler particles and the polymer matrix, through various condensation reactions. With layered filler, an interlayer expansion occurs when the additive is poured in the monomer solution. When the polymerisation takes place, the polymer forms between the layers, creating an intercalated nanocomposite structure.

2.2.2 Factors Affecting the Properties of Nanocomposites

Until now, several nanocomposites systems have been formulated in order to improve one or more properties of the starting polymer, leading to a variety of good results. Although it has been shown that the addition of nanosizes fillers leads to significant improvements of the properties of the bulk polymer phase, there are still many factors influencing the morphology and the final properties of the composites that need to be identified and strictly controlled. Thus, a description of the principal parameters affecting the nanocomposites characteristics will be dealt in the next sections, with particular attention to those influencing the morphological, thermal, electrical, rheological and mechanical properties, objects of this research. Numerous factors such as the interfacial interactions between the polymer and the filler, the features of the filler (size, geometry, aspect ratio, etc.), the polymer nature (molecular weight, polarity, melt flow index), the processing techniques, the filler loading etc., play a fundamental role in the production of high quality composite materials.

2.2.2.1 Processing Conditions

Among the abovementioned producing methods, attention will be paid to the melt-blending influencing parameters which condition the filler dispersion during the process. In order to achieve a good mixing between the constituents, twin-screw extrusion represents one of the most popular option. Crucial factors to be controlled during the process are temperature, screws speed and residence time. An increase in temperature

could help to enhance the polymer mobility but, it also leads to reduce the viscosity thus making more difficult to break the filler agglomerates by the action of the shear stresses. In contrast, a high residence time provides a better mixing but, at the same time, it will enhance polymer degradation and process cost. Generally, an increase in screw speed is related to a higher filler dispersion thanks to the de-agglomeration of the nanoparticles promoted by higher shear stresses [39, 40], which leads to the acceleration of exfoliation and intercalation processes. The feed rate has also been reported to be associated with the final dispersion state. Different authors [41, 42] stated that by decreasing the feed rate a significant improvement of the exfoliation occurs, whereas the intercalation is not particularly affected. Paul *et al.* [39] investigated the morphological properties of PA6/clay nanocomposites through the optimisation of melt-blending processing parameters (temperature, shear and residence time). They found that tensile strength and modulus of the composites could be enhanced, either by increasing the residence time or the screw speed.

The optimisation of the processing conditions is very important in order to promote an efficient dispersion of the filler in the polymer matrix. The state of dispersion of the filler represents a key point of affecting the percolation threshold and electrical conductivity of composites. Indeed, several researchers demonstrated that an improvement of the electrical properties of the nanocomposite took place as the dispersion state of the nanoparticles increased [43-45]. Specifically, in the case of melt-mixing processes, it has been reported that an increase of the screw speed provides a better dispersion and disentanglement of the filler, thus facilitating the formation of more conductive filler pathways [46, 47]. A comparison between the percolation thresholds obtained with different type of polymers and production methods has been proposed by Verdejo *et al*. [33]. From this, it is apparent that a quite higher percolation threshold was achieved with PA6/GNPs composites obtained by melt-processing, with respect the one obtained through solution-mixing and in situ polymerisation. Despite these last two methods of preparation are the most appropriate to promote a good dispersion of the filler, melt-compounding process remains the most economical and environmentally friendly among the all production techniques. Moreover, it is compatible with many industrial practices

and suitable for mass production, which provide sufficient reasons for the research to develop new strategies for improving the dispersion by this method.

2.2.2.2 Filler Size, Shape and Aspect Ratio

An aspect that play an important role in influencing the final properties of the nanocomposites consists in the nanoparticle size and shape. The first type of fillers to be used in the context of polymer nanocomposites is represented by spherical nanoparticles such as carbon black and fumed silica, whose great advantage derived primarily from filler size reduction and high surface area. A perturbation effect of the polymer chains in close contact with the filler surface led to a global increase of the composite stiffness, which is related to the volume fraction of the reinforcement and that of the interfacial region that surrounds the particles, characterised by different properties than the bulk polymer. In recent years, more attention was paid on platelets (such as graphene and clays) and carbon-based nanotubes, because of their anisotropic nature which is believed can lead to mechanical and electrical percolation at low loading level. Moreover, the anisotropic aspect of the filler was seen to improve the thermal conductivity of the polymer in the filler direction [48, 49].

The size and the shape of the filler are considered the key-point of the "nano" effect on the properties in nanocomposites, due to their ability to regulate the surface-to-volume ratio of the reinforcements. This parameter indicates the amount of interfacial region compared to bulk polymer in the composite. The interfacial zone controls new structural molecular arrangements and is responsible for the efficient transmission of stress across the composite constituents. Therefore, by increasing the fraction of interfacial region it is possible to maximize the probability of enhancing the material properties. The properties of a nanocomposites are also strictly related with the aspect ratio of the filler. For instance, it has been found that longer fillers with high aspect ratios provide a better enhancement of thermal and electrical conductivity. Mortazavi *et al.* [50] demonstrated that a higher improvement of the thermal conductivity occurred with platelet filler than using spherical fillers. Graphene sheets are characterised by extremely high aspect ratios

and typically present very low value of percolation threshold, as proposed by the study of Stankovic [51].

2.2.2.3 Filler Orientation and Networking

In order to produce multi-functional and high performance composite materials a good orientation and network formation of the fillers within the polymer matrix should occur. In particular, this represents a crucial aspect when dealing with conductive fillers such as graphene. Usually, the rheological response evaluation of the composite system at the molten state is performed in order to verify the formation of filler networks. At this stage, the material shows a visible change of the variables during the analysis, which indicates the transition from a non-percolated system to a percolated one. Gang *et al*. [52] found the existence of a correlation between the rheological and electrical percolation in graphite filled HDPE, with electrical and viscoelastic percolation threshold close to each other. This result is associated to the degree of filler dispersion, filler alignment and filler surface area. A different behavior was observed by Du *et al.* [53], with single wall nanotube filled PMMA system, where the rheological percolation resulted significantly smaller than the electrical one, suggesting that there is a difference in term of minimum inter-filler distances required for electrical conduction, than respect the distance for varying the viscoelastic properties of the matrix. They concluded that a higher dispersion and lower alignment of the fillers, conjugated to a higher molecular weight of the matrix, led to a decrease in the mobility of the polymer chains.

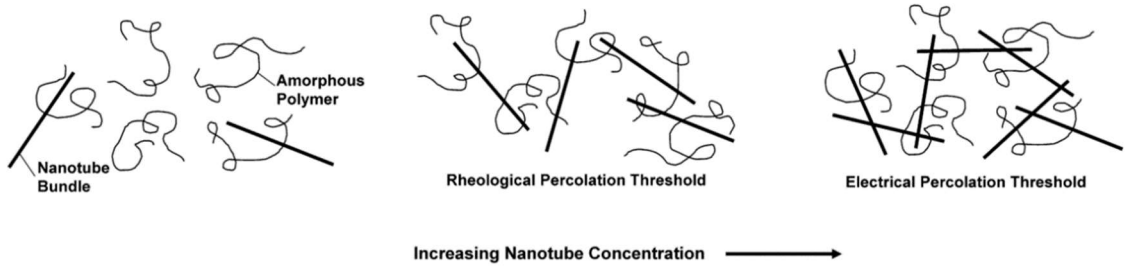

Fig. 2.2. *Schematic of the rheological and electrical percolation differences in PMMA/SWNT nanocomposites [53].*

The orientation of the fillers can affect the percolation threshold and electrical properties of polymer nanocomposites. Generally, randomly distributed fillers have a low contribution to electrical conductivity, whereas the orientation and formation of a continuous conductive network can lead to a great enhancement of the electrical behaviour of the composite. Zhao *et al*. [54] observed that CNTs and graphene sheets are difficult to disperse in the HDPE matrix by using a melt-mixing method. However, the not uniformly distributed fillers had the tendency to form segregated networks by dispersing along specific pathways, thus yielding to an increase in their contact probability and enhancement of the electrical conductivity. Orientation of the filler is also important for improving the heat transfer through the composite. It is believed that the formation of an interconnected structure of fillers act as adequate thermal pathway through the polymer. Shtein *et al.* [55] achieved a high value of thermal conductivity by subjecting the fillers (GNPs) to high compression forces in order to close the gaps between them. The presence of polymer gaps between the GNPs results in higher interfacial thermal resistance and phonon scattering, thus decreasing the global thermal conductivity.

2.2.2.3 Matrix

In addition to the abovementioned factors, the achievement of good mechanical, thermal and electrical properties in nanocomposites can be also influenced by the matrix characteristics such as the molecular weight, polarity or anti-polarity nature, viscosity etc. More specifically, the polymer matrix nature could affect the formation of mechanical, thermal and/or electrical percolated network constituted by the dispersed fillers. When the additives are incorporated in the polymer matrix, their dispersion is strictly dependent on the interactions between the composites constituents. The percolation threshold tends to increase if the filler is introduced in a matrix of higher polarity, lower degree of crystallisation, higher viscosity and larger surface tension, because these parameters contribute to obstruct the homogeneous dispersion of the fillers in the polymer [56]. Particularly, the viscosity of the matrix represents one of the most crucial parameters. The reason of this consists in the fact that a restricted mobility of the fillers occurs when a high viscous matrix is used for producing nanocomposites. Min and Kim [57] observed

an increase in surface resistivity of ethylene-propylene-diene (EPDM) polymer filled with MWCNTs, when EPDM matrix with higher viscosity was used. Similarly, Ha and Kim [58] detected a decrement of MWCNT dispersion by using SEM, due to the use of high molecular weight polycarbonate (PC) and polypropylene (PP) as composite's matrix.

Chapter 3

Materials

This chapter will focus on the characteristics and properties of the materials utilised in the production of the nanocomposites: the matrix in Nylon 6 (PA6), and the filler constituted by Graphene nanoplatelets (GNPs).

3.1 Polyamides

3.1.1 General

Polyamide, otherwise known as Nylon 6, was the first synthetic fiber to be produced in the world, invented by Wallace Charoters in 1935 [59]. This class of thermoplastic polymers is characterised by the presence of the amide group (-CONH-) in the molecular structure, and is divided in two main groups: the aliphatic and the aromatic polyamides. The aromatic polyamides, also referred as aramids, possess higher strength and better flame and heat resistance with respect the aliphatic amides (Nylons) but are more difficult to synthesised and more expensive. Aliphatic polyamides represent one of the most important class of engineering thermoplastics, due to the easy processability and unique set of properties. Examples are the large deformation capacity of the molten polymer, which allows continuous production of filaments or other geometries by mean of extrusion process, and the semycristalline crystalline nature of the material, which enable to fabricate fibers or films by increasing the degree of crystallinity via mechanical stretching.

Polyamides can be produced in two different forms: nylon Z and nylon XY, via two distinct reactions. The first type is produced by ring-opening polymerisation of cyclic amides (lactams), with Z index related to the number of carbon atoms in the monomer.

Type XY derived from the polycondensation reaction of a diacid with a diamine [60]. X and Y indicates the number of carbon atom in the diamine and diacid monomer, respectively. Nylon 6 (or PA6) and Nylon 6-6 (or PA66) are two examples of Z and XY types, respectively, and represent two of the most manufactured polyamides. This work will focus only on Nylon 6 properties and its carbon-filled composites.

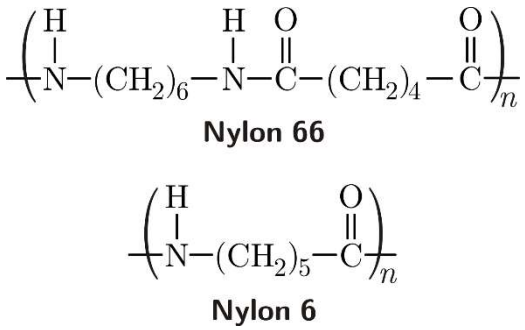

Fig. 3.1. *Nylon 66 and Nylon 6 repeating unites.*

Nylon 6 is synthesised through the ring-opening polymerisation of the monomer ε-caprolactam. This kind of step-growth polymerisation is followed by condensation reaction with the elimination of water at each step. Generally, the reaction is initiated by water which reacts with few percent of the monomer leading to the production of ε-aminocaproic acid. NH_2 groups of this acid starts the ring-opening polymerisation of the monomer.

3.1.1 Properties of Nylon 6

Polyamide 6 is semicrystalline material, which means that the polymer is characterised by crystalline and amorphous domains in its structure. Nylon 6 crystalline structure is constituted by folded chains, cross-linked one each other by hydrogen bonding, which connects carbonyl (-CO-) and NH groups of adjacent chains. Two crystal forms exist in Nylon 6 structure: α-crystals, which contains anti-parallel chains, connected by hydrogen bonds, and γ crystal form, where adjacent chains are aligned parallel to one another. These two crystal forms are distinguished by different strength and density, which are both higher in α-form. Moreover, at high temperatures (≥ 170 °C) γ crystal tend to be converted into α-crystals, which are more thermally stable. The amorphous regions of the polymer

are characterised by a much lower degree of hydrogen bonding [61], responsible for crystallinity. The semicrystalline nature of polyamides allows them to manifest a good balance of properties. The physical linking due to the presence of crystalline regions lead to improve the hardness, yield strength, chemical resistance, creep resistance and thermal stability. Nevertheless, during deformation, the restriction imposed by the hydrogen bonding in the mobile (-CH_2-) sections of the amorphous region contribute to limit the overall flow of molecular chains, thus leading to a good recovery after stress removal and good flexibility. The amorphous regions play an important role in stress elongation and impact resistance. Hence, nylons manifest high extension to break in combination with relatively high strength, resulting in high toughness.

Glass transition temperature (T_g) of Nylon 6 is related to the amorphous domains (mobility of -CH_2- sections) and to the inter and intra-molecular hydrogen bondings. An important parameter which affects the T_g in nylons is the moisture content. Polyamides are hygroscopic as water molecules lead to the formation of bridge-bonding between two carbonyl and amide groups of adjacent chains, as shown in Fig. 3.2.

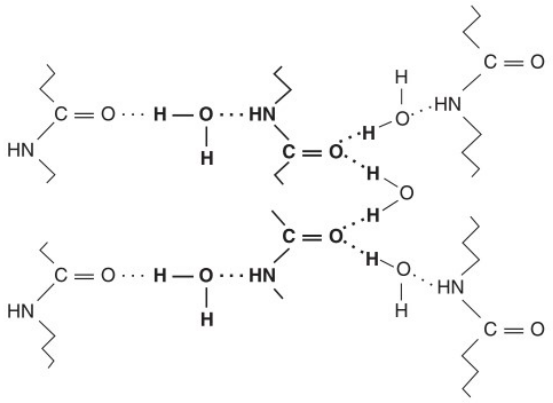

Fig. 3.2. *Effect of water interaction with nylon 6 [62].*

By acting as a plasticiser, water molecules affect the mechanical properties of polyamides leading to an increase in flexibility. Consequently, T_g tends to vary from -10 to 90°C in wet and dry conditions, respectively. T_g is also influenced by the number of CH_2 segments: with increasing content of CH_2 units the degree of flexibility in amorphous regions increases, along with T_g. Typically, T_g values for nylon 6 are in the range from 40 to 55°C [62]. Polyamides 6 shows high melting temperature due to the presence of the

strong hydrogen bondings in the crystalline domains. T_m of Nylon 6 varies in the range from 215 to 228°C and is related to the concentration of amide and CH_2 groups.

3.1.1 Applications of Nylon 6

Polyamides 6 can be used in several applications due to low density, good elastic recovery, good chemical resistance, high fracture and abrasion resistance. Moreover, the ability to tolerate high pressure, temperatures, and chemicals such as acids, alkalines and solvents make the polymer an extremely valued industrial material. All these characteristics make PA6 suitable for several applications such as fibre, film and injection mouldings components for engineering application. In order to achieve a low-weight and less expensive substitute for traditional materials like steel, brass, aluminium etc., further improvements have been obtained by introducing reinforcing fillers in Nylon 6 structure, thus creating a nanocomposite with additional features than the polymer itself. A first example of nanocomposite application can be found with the creation of Nylon 6- clay hybrid automotive components, by Toyota Motor Company [63]. The introduction of montmorillonite fillers led to Young's modulus enhancement (from 1.1 to 2.1 GPa) and coefficient of thermal expansion reduction with respect the virgin polymer. In situ-ring polymerisation was also adopted by Xu *et al.* [64] for producing Nylon 6- graphene oxide (GO) composites. The good compatibility between the constituents lead to an improvement in Young's modulus and tensile strength of PA6. Recent studies have been focus on the preparation and characterisation of Nylon 6/carbon-filled composites, with the aim to achieve improvements in thermal stability, thermal conductivity, mechanical properties, electrical conductivity and gas barrier properties. The incorporation of carbon based material such as graphene and its derivatives into engineering thermoplastic polymers such as Nylon 6, represents a potential solution in the production of light-weight and high-strength automotive and aerospace components, as well as electronics and heat-dissipative devices. Electrically conductive nylon 6/graphite nanocomposites have been made by Pan *et al.* [65] with a reached conductivity value equal to 10^{-4} S/cm at a graphite content of 2.0 vol%. Liu *et al*. [66] were able to incorporate small amount of MWNTs into PA6 matrix obtaining significant improvement of Young's modulus, strength the hardness by about 214%, 162%, and 83%, respectively, with less than 2 wt% CNTs.

3.2 Graphene

Graphene is a monoatomic layer of sp_2 hybridized carbon atoms, organized according to a hexagonal cell crystal structure. This basic structure has a planar conformation and therefore the monoatomic layer is presented as a two-dimensional material (2D). Until the early 2000s, it was believed that this material was not thermodynamically stable due to its tendency to bend and form structures such as fullerenes and nanotubes. In 2004, Novesolov and Geim scientists succeeded in isolating a layer of graphene by means of a *scotch-tape* technique, which consists in the mechanical exfoliation from graphite on silicon wafers through a piece of adhesive tape [67]. This discovery led them to win the Nobel Prize in Physics six years later. Over the years, various methods have been developed for the production of graphene, which can be divided according to the chemical or physical process [68]. The properties of graphene are necessarily linked to the 2D structure of the material itself and a complete physical and chemical characterisation is still ongoing as its discovery is relatively recent.

Graphene is characterised by the presence of three σ bonds in every lattice which provide a stable hexagonal structure. The electrical conductivity of graphene is associated with the π bond located perpendicularly with respect to the lattice plane. The high stability of graphene is attributed to its tightly packed sp_2 hybridised carbon atoms, which bonding derived from a combination of orbitals s, p_x, and p_y. The final p_z electron contribute to the formation of the π-bond, which in turn hybridises with the other π-electrons in order to form the so-called π-band and π*-bands. Most of the electronic properties of graphene are related to these bands, which enable free-moving electrons to flow.

Graphene is considered as the basic structural constituent of other carbon allotropes such as graphite, carbon nanotubes, fullerene, as well as aromatic molecules with indefinite size, i.e. planar polycyclic aromatic hydrocarbons. More specifically, graphene is constituted of a strictly packed single layer of carbon atoms, creating a 2D honeycomb plane framework. In single-layer graphene, carbon atoms are bound with the adjacent carbon atoms through sp_2 hybridization, thus making a benzene ring in which each atom provides an unpaired electron.

3.2.1 Electric Properties

One of the most important features of graphene is it that of being a zero-energy gap semiconductor (where both holes and electrons are the charge carriers) with very high electrical conductivity. The carbon atoms contain a total of 6 electrons: 2 in the internal valence shell and 4 in the outermost shell. The 4 outer shell electrons in each distinct carbon atom, have the possibility to create chemical bonds, but in graphene each carbon atom is bound to 3 others in the same xy plane, leaving a free electron in the third dimension (z). The orbitals of these electrons, which are called as "π electrons", are positioned above and below each graphene sheet, overlapping and strengthening carbon-carbon bonds. Electronic properties of graphene depend on the bonding and anti-bonding (the valence and the conduction bands) of these π-orbitals. It has been shown that at the Dirac point of graphene (energy spectrum near the maximum of the valence band and the minimum of the conduction band) holes and electrons are characterised by a zero-effective mass. This happens because of the linear relationship between the energy and the wave vector of electrons of π-orbitals, at low energies near the Brillouin area. In this area electrons and holes are defined as "Dirac fermions" and the 6 vertices are called as "Dirac points". Due to the zero density of state at the Dirac points, electron conductivity of graphene is very low. However, the Fermi level can be varied through the doping of graphene (with the introduction of electrons or holes), in order to create a material that is potentially more electrically conductive than copper, at room temperature [69-71].

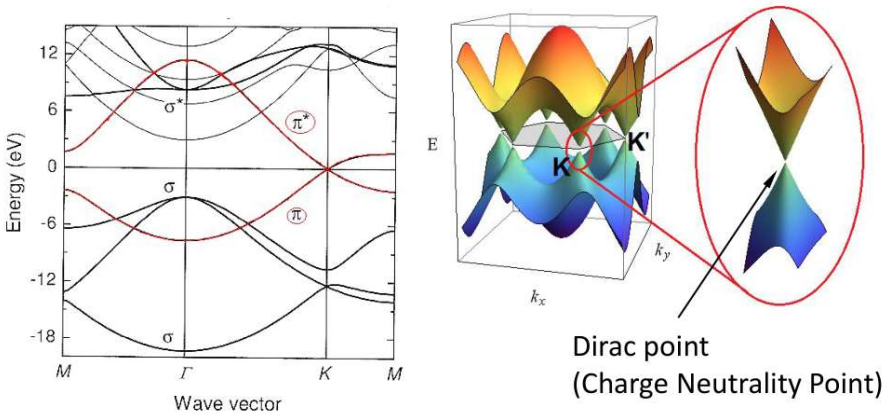

Fig. 3.3. *Zero effective mass of fermions at Dirac points of graphene [72].*

Several tests have demonstrated the high mobility of the graphene electronic cloud, with results between 15000 and 200000 $cm^2 \cdot V^{-1} \cdot s^{-1}$ (limit due to the acoustic scattering of photons). Generally, the most limiting factors in electrical conductivity of the material are related the quality of graphene itself and the substrate used during the measurement. Given that graphene is just one atom thick, all the carbon atoms are entirely exposed to the surrounding environment, thus the electrical properties can change in presence of external atoms or molecules absorbed on the graphene surface. Graphene is the material known so far with the lowest electrical volume resistivity, equal to $1.0 \cdot 10^{-8}$ Ωm. This resistivity value is lower than that of most conductive metallic materials, such as silver ($1.59 \cdot 10^{-8}$ Ωm), and it is possible to obtain current densities even higher than 10^8 A/cm^2 which are about six orders of magnitude higher than those which can flow in silver [69-73].

3.2.2 Mechanical Properties

The impressive mechanical properties of monolayer defect-free graphene make it highly suitable for using as reinforcement filler in composite materials. With a measured Young's modulus of 1 TPa and tensile strength of 130 GPa, graphene is considered as the "strongest material ever tested". The reason of these properties is due to the presence of strong and very stable sp_2 in-plane bonds (or sigma bonds) which contribute to the formation of a fully resistant hexagonal lattice. The Young's modulus of graphene is much higher than the one of steel A36 (200 GPa) or that of Kevlar (170 GPa), and its density is particularly low ($0.77 \text{ mg} \cdot m^3$)

3.2.3 Thermal Properties

Graphene is a perfect thermal conductor due to the high velocity of phonons through strong in plain sigma bonds. Its thermal conductivity, around 5000 $W\ m^{-1}\ K^{-1}$, has been recently measured at room temperature and is much higher than all the values observed for carbon structures such as, nanotubes, graphite and diamond.

3.2.4 Production Methods

Graphene derived by the crystalline structure of graphite which consists of overlapping layers of the monoatomic material, held together by weak van der Waals inter-layer bonds with energies of about 2 eV · nm^2. The inter-layer bonds nature makes the graphite easily flaking in the direction parallel to the crystalline plane, by applying forces of about 300 nN/mm^2. This characteristic enables the use of different techniques to separate the graphene layers, but no ideal methods and cost for producing high graphene quality have been found yet. The most commonly used methods for producing graphene in laboratory and industrial scale are listed below

- *Physical mechanical exfoliation*, in which a sample of graphite is subjected to repeated exfoliation through "scotch tape method" and subsequently transported to a substrate.
- *Chemical vapor deposition* (CVD, in which graphene is obtained through the nucleation and growth of carbon atoms over a metallic substrate, starting from the decomposition of gaseous hydrocarbons, such as methane or ethylene.
- *Liquid phase exfoliation*, in which graphite flakes are exfoliated in a suitable solvent and then a purification process is held in order to separate the exfoliated material from the non-exfoliated one.
- *Chemical reduction of graphene oxide (GO)*, where single-layer GO sheets are obtained by exfoliation of GO and subsequently subjected to in-situ reduction process for producing single-layer graphene.
- *Bottom up synthesis,* where molecules of graphene are synthesised at high temperature starting from atomically well-defined building blocks.

3.2.4 Graphene Nanoplatelets (GNPs)

Graphene nanoplatelets (GNPs) are constituted of small stacks of parallel graphene sheets, with an average thickness ranging from 5 to 10 nanometers and diameters up to 50 microns. Because of its 2D structure, high aspect ratio and high surface area, GNPs can be exploited to enhance the properties of a wide range of polymer materials such as thermoplastics, natural or synthetic rubber, thermoplastic elastomers etc. High barrier and

mechanical properties (stiffness, strength) along with enhancement in thermal and electrical conductivity can be induced in polymers, whilst maintaining light weight and transparency. However, properties of GNPs filled composites is strictly related to the degree of dispersion and interaction of fillers with the polymer matrix. Specifically, size and shape variations of GNPs during composites processing can alter the intrinsic properties of the carbon-based material.

Chapter 4

Experimental

The following chapter deals with the description of the principal processing methods and characterisation techniques used to produce and analyse Nylon 6 – Graphene nanocomposites.

4.1 Processing Techniques

This first section is concerned with the instruments used for the production and sample preparation of PA6/GNPs nanocomposites. The composites have been fabricated via melt-blending, using a co-rotating twin extruder and subsequently shaped in several samples of different geometries by mean of injection and compressing moulding.

4.1.1 Melt-Blending: Co-Rotating Twin Extruder

Extrusion is a processing technique in which a compression stress is applied on a molten state material in order to force it to flow through an orifice and to assume a specific cross-sectional shape [74]. Thermoplastic polymers are typically subjected to extrusion because of their high related to the pseudoplastic nature. High strain rate levels lead to the so-called shear thinning behaviour of molten polymers which manifest a decrease in viscosity, also affected by the increasing temperature during the process. Extrusion consists in a continuous process which lasts as long as the material is supplied. Generally, polymer in form of pellets or powder is fed into an extrusion barrel by using a hooper and subsequently heated, melted and induced to flow into a die.

In this study, a EuroLab 16 XL Twin-Screw Extruder (Thermo Scientific) have been used for the melt mixing process of PA6/GNPs composites.

The 16-mm extruder structure can be divided in three main subsystems:

1) *Feeding system*, which is constituted by a hooper located at the end of the barrel, opposite to the die. The polymer in form of pellets or powder is fed into the hooper and is transported by two co-rotating screws which lies at the bottom of the hooper itself. The rotational speed of these screws can be regulated in order to have a better control on the material's flow. In addition, this system provides a pre-mixing of the polymer with the additives in case of composite materials extrusion. The screws transport the pellets (or powders) through a tube which connects the hooper's bottom to the barrel. The tube ends in correspondence of a second hooper of smaller size which is located on the opened barrel surface, and the pellets are fed by gravity into the extruder (as shown in Fig. 4.1).

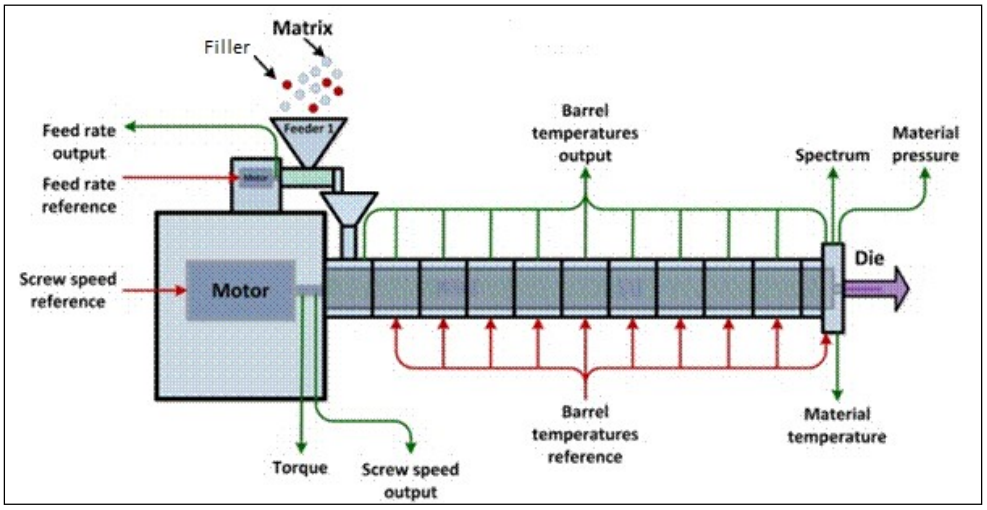

Fig. 4.1. *General schematic of a feeding and extruder system [75].*

2) *Extruder system*, which is composed by two co-rotating screws with a specific geometry and configuration, and the barrel in which they lie. The barrel is constituted by a series of steel blocks, heating elements and thermocouples for controlling the temperature profile of the extruder. The screws are connected to an engine for suppling the rotational power. Temperature profile, screws speed rate and feeder rate can be regulated by using a Thermo Scientific software.

3) *Cooling system and pelletiser.* This system allows the extrudate (extruded product) to be cooled while is being pulled through a water bath. The solid polymer in form of filament is cut in pellets by the pelletiser though a system of rotating blades and then collected in a plastic bag. The blade rotational speed can be regulated in order to vary the pellets production rate. By controlling the screw speed, it is also possible to change the extrudate flux and increase or decrease the pellets dimensions.

In the feeding zone the polymer pellets are still solid and are transported towards the central section of the extruder called compression or fusion zone. In this part, thanks to the synergy of the heating elements and mechanical stresses developed on the polymer by the motion of the screw, the material gradually starts to melt. Once completely melted, the polymer is transported and homogenizes into the so-called metering section, and subsequently pumped through the die opening. Extrusion is largely used for melt compounding processes which enable to create composites formulations by mixing polymers with specific additives in the molten state. In order to achieve good results in the dispersion of additives in polymer melts, it is necessary to design a specific screw configuration based on the materials to be extruded. A screw geometry that allows high mixing and transmission of materials stresses involves the presence of elements of different shape which are, specifically: conveying and kneading elements [76] (see Fig. 4.2). Conveying elements represents the largest volume fraction of the screws and their aim is to push the polymer forward along the barrel starting from the feeding zone, as shown in Fig. 4.2. Once the solid polymer bed is fully compacted a back pressure is exercised by the material towards the screws, thus slowing down the entire extrusion process. In order to cope with this problem, the presence of kneading elements is required to accelerate the polymer melting, along with the heating elements of the barrel. Kneading block are made up of several stacked disks of varying thickness and positioned at one angle to another. By varying the angle between the elements, it is possible to obtain different effects of mixing and melting on the material. Generally, kneading blocks provide intense shearing and has a chopping effect on the material flow, thus making these parts of the screw the most effective at filler dispersive mixing and polymer melting. A difference in orientation of the kneading elements equal to 90° can be observed in the

screw configuration used for the melt-compounding process of PA6/GNPs composites (see Fig. 1.2). The greater is the angle difference, the more intense is the action of the elements on the extruded material. A mid-zone kneading block composed by 0-degree oriented elements is also present in the used screw configuration, in order to favour the polymer melting while balancing the chopping action.

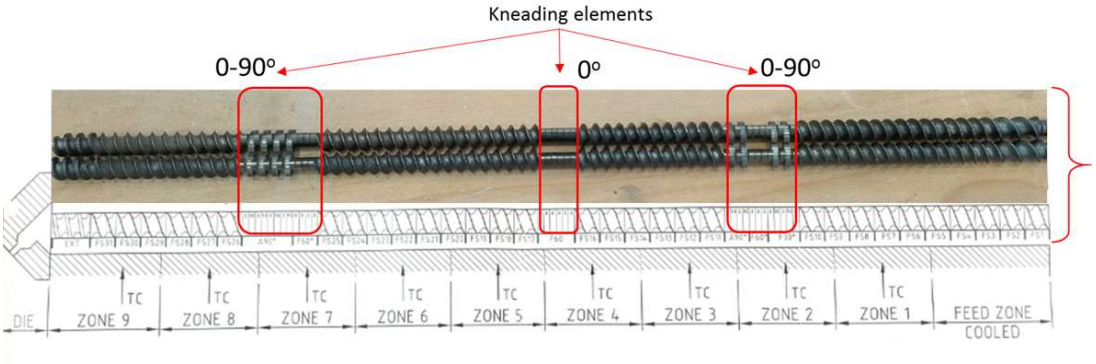

Fig. 4.2. *16-mm co-rotating twin screws configuration.*

Extruders are divided in two main categories: single screw extruders and twin-screw extruders. Twin-screw extruders contain two screws of equal diameter, which rotate side by side within the extruder barrel, at the same speed. This type of configuration is commonly used for melt compounding of thermoplastics polymers with additives, and provides a higher control on the residence time, degree of dispersion and mixing, with respect that of single screw extruder. Twin screw extruders are in turn subdivided in corotating intermeshing, counter rotating intermeshing and counter rotating non-intermeshing extruders [77] (see Fig. 4.3). Corotating intermeshing twin extruders are the most used for the synthesis of nanocomposites materials.

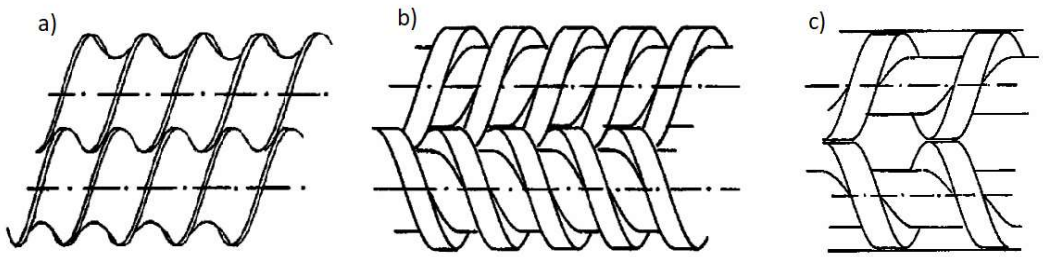

Fig. 4.3. *Different twin screw extruder types: a) corotating intermeshing, b) counter rotating intermeshing, c) counter rotating non-intermeshing [77].*

In co-rotating screw systems, the polymer develops an 'eight' shaped path around the screws themselves, allowing a high and continuous contact with the cylinder walls, which enable the material to be heated efficiently. Instead, in counter-rotating screw systems the material tends to accumulate in the two contact areas above and below the screws themselves. These clusters are pushed forward by means of the threading of the screws. In the part between the two screws very high mechanical stress values are obtained but not all the accumulated material is subjected to the forces. The overall shear stress effect is therefore lower than the co-rotating twin screw extruders and similar to the single screw: much of the material does not undergo mechanical action and is only transported through the cylinder. The extruder co-rotating twin-screw also guarantees greater residence time to the material.

4.1.2 Injection Moulding

Injection moulding is a manufacturing process in which the material is heated beyond its melting temperature and forced to flow under high pressure into a mould cavity [78]. The material quickly solidifies when in contact with the internal walls of the mould and, it is thus possible to remove the moulded part (moulding) from the cavity. For this research, a HAAKE™ MiniJet Pro Piston Injection Moulding System was used to make several specimens of small dimensions and different shapes (e.g. dumb bell samples, rheology disks, dma bars etc.) in order to perform characterisation analysis of the compounded nanocomposites. The apparatus (shown in Fig. 4.4) consists in three well defined parts which are listed below:

- *Heated cylinder*, which is the part where the material in form of pellets/powder is fed into a cylindrical cavity and then heated until fusion. The inner hollow portion (barrel) of the heated cylinder is surrounded by heating elements for reaching the temperature and provide a homogeneous melting. The heated cylinder is equipped with a sprue at the opposite side of the feeding gate, in which the material can flow with a specific pressure and can be injected into the mould.
- *Pneumatic cylinder,* which consists in a stainless steel piston that fit in the cylindrical cavity of the heated cylinder and provide the compression stress at the

material in order to force it to flow through the sprue and then into the mould. The level of injection pressure exercised by the cylinder and can be regulated by the instrument, as well as the time of pressing.

- *Mould,* which is made up of a cast iron holder that can be heated separately from the cylinder and the mould itself that is inserted into the holder for reaching the desired temperature. Moulds are interchangeable depending on the shape of moulding that is to be obtained. Generally, moulds are made up of two separate parts: a bottom half that contains an internal cavity of specific shape, and a top half that has no cavities and allows to close the moulding system.

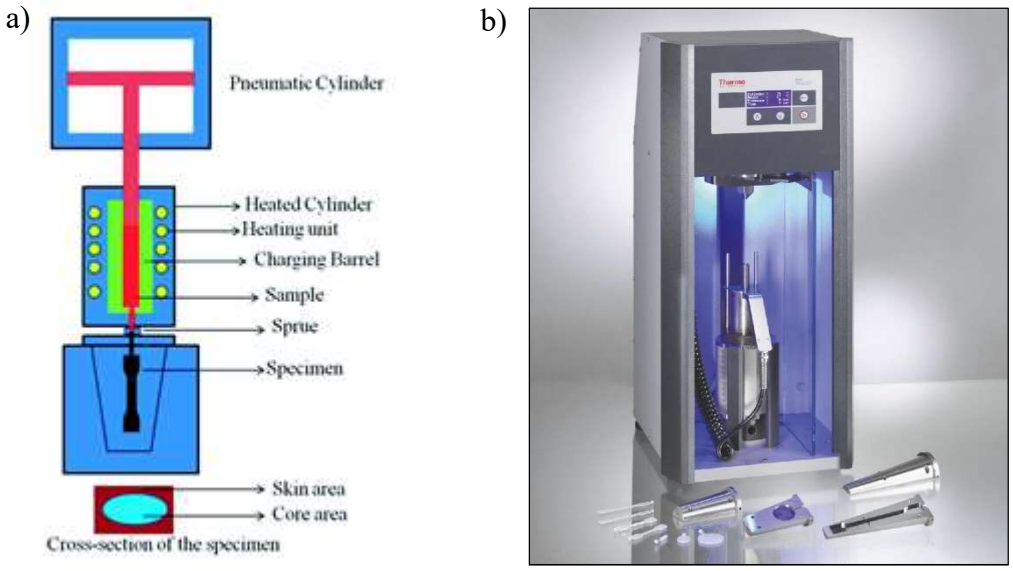

Fig. 4.4. *Mini-injection moulding system: a) Schematic [79] and, b) HAAKE™ MiniJet Pro Piston Injection Moulding System (adapted from Thermo Fisher scientific website).*

Through the use of the MiniJet Injection Moulding System a maximum of 3.5 grams of material can be fed into the barrel. When the feeding is completed, the movable piston is inserted into the cavity in order to close the chamber and allows the material to be melted completely. After the fusion time, the movable heated cylinder along with the piston is placed in an appropriate support below the pneumatic press. Once the system is assembled, the automatic press is activated and a compression forced is exerted on the piston which in turn injects the polymer into the mould. The material is left to solidify for few seconds and then the part is removed from the cavity.

4.1.3 Compression Moulding

Hot compression moulding is a technique which is useful to produce variety of composites specimens, by applying a specific pressure on the material while it is being heated at high temperatures. The material, in form of pellets or powders, is placed between two thermos-stated plates (the base plate is movable and the upper plate is stationary) which have been preheated to specific temperature. As the plates contact each other, the material is melted by heat and consequently shaped due to the pressure generated by the press, thus taking the shape and dimensions of the sample to be produced. For this study, a Collin P 200 P/M hot press was used (see. Fig 4.5).

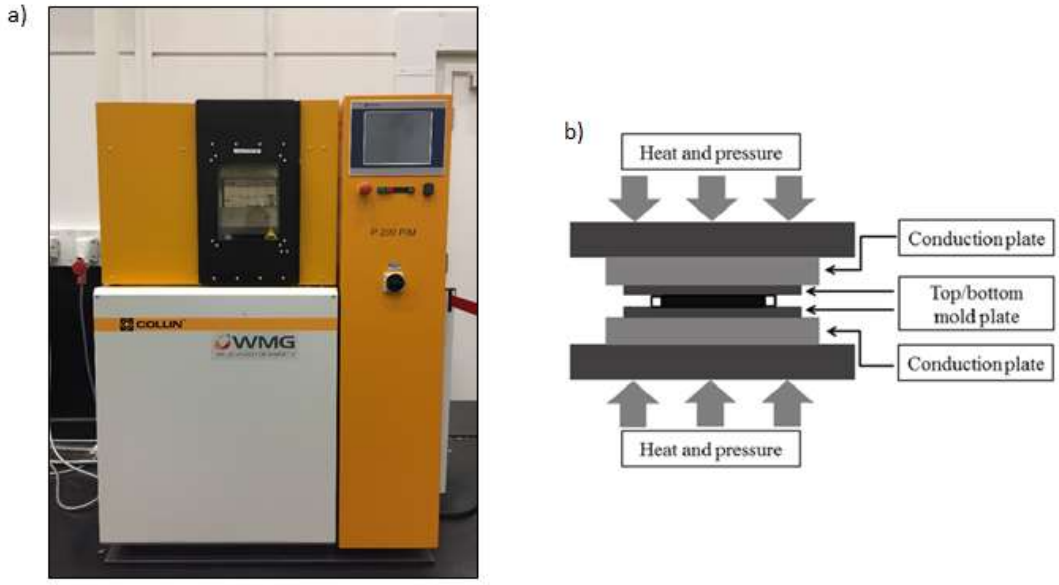

Fig. 4.5. *a) Collin P 200 P/M hot press and, b) schematic of hot pressing system [80].*

Prior to pressing, it is possible to set up a molding program divided in several phases in which temperature, pressure and time of application can be specified. All these three parameters are critical and should be optimized efficiently to achieve good characteristics of composite products. Generally, interfacial adhesion between matrix and fillers depends on the applied pressure: if is not sufficient a poor adhesion is obtained whilst, if too high, damaging or breakage of the filler can occur [81]. Temperature and time needs to be regulate effectively in order to avoid matrix degradation in case of too high temperature and exposition time, and to avoid poor dispersion of the filler in case the temperature is not sufficiently high to promote a good viscosity reduction. Thickness and shape of the

specimens can be controlled by inserting a metallic profile with fixed geometry between the plates. Collin P 200 P/M hot press can work in a temperature range from 20 to 450°C, with a cooling/heating limit rate of 30 °C/min. The instrument is equipped with a hydraulic mechanism which provides a pressure of 200 bar.

4.2 Characterisation Techniques

This section presents a description of the characterisation techniques and instruments used for analysing mechanical, thermal, rheological, electrical, chemical and physical properties of Nylon 6 – Graphene nanocomposites.

4.2.1 Mechanical Characterisation

4.2.1.1 Tensile Testing

Mechanical tests are generally performed to verify which kind of physical response the material manifests when subjected to a specific stress. This allows to evaluate how and if the material can resist to the load under conditions similar to those of exercise. Every material tends to react at the stress by manifesting a deformation which can be different according to the structural and chemical characteristic of the matter. Polymer materials exhibit three different form of deformation when subjected to an external force. A spontaneous elastic deformation occurs at low strain and stress level, when the material tends to completely recover the original shape and size once the stress is removed. In this type of deformation, all the energy involved in the process is accumulated by the material and then released when the stress is removed. Elastic deformation is related to the change of atoms spacing and valence angle shifts. In this regime, the stress (σ) can be expressed as a function of the strain (ε) through the following relation:

$$\sigma = E\varepsilon \tag{4.1}$$

where σ is given by the ratio between the applied force and the cross-sectional area of the sample. The strain is calculated as the ratio between the length variation (ΔL) and the initial length (L_0) of the sample tested. The Young's Modulus (E) represents the slope of

the stress- strain curve shown in Fig. 4.6, and it is a measure of the "rigidity" of the material. The higher is the slope of the elastic region, the stiffer it is the material.

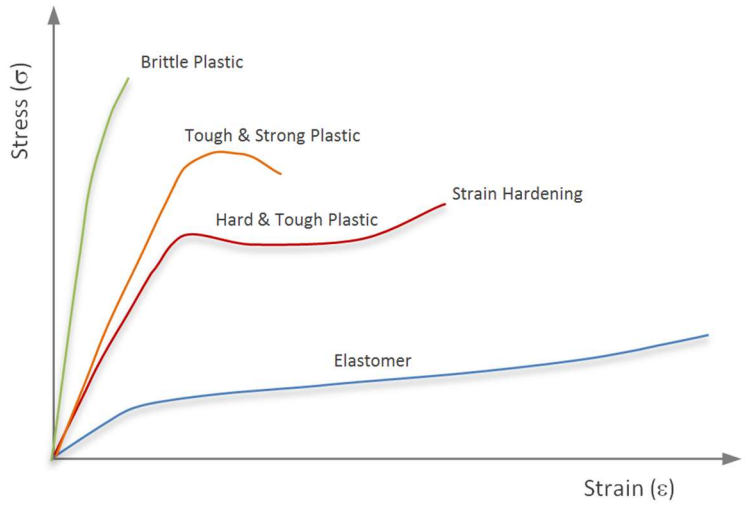

Fig. 4.6. *Stress/strain curve for different type of polymers [82].*

In operation conditions it is difficult that the material manifests an ideally elastic mechanical behaviour, at high loading levels. In general, polymers exhibit other two kinds of deformations, which are time-dependent [83]. On one hand, a viscoelastic deformation occurs when the polymer chains react to the applied stress within a certain period of time. The deformation is recovered completely but it needs again a certain length of time to be resumed. On the other hand, an irreversible time-dependent viscous deformation behaviour occurs when the polymer is subjected to high level of strain, and the material starts to undergo plastic deformation. In this case, the energy involved in the process is not completely recovered, as well as the strain occurring in the material. The transition from the linear elastic behaviour and the irreversible non-linear deformation can be recognised from the stress-strain curve, by identifying the so-called *Yield Point*, which corresponds to the level of stress at which the slope of the stress-strain curve reaches a zero value. Other important points can be identified form the stress-stress curve, as listed below:

- *Proportional limit,* which is the maximum stress up to which the stress and strain remain proportional;

- *Tensile stress at break*, which is the tensile stress at which the failure of the part occurs;
- *Tensile strain at break,* which is the level of strain corresponding to the tensile stress at break;
- *Toughness,* which is represented by the area under the stress-strain curve. A high area indicates a high capacity of the material to absorb energy and higher ductility.

The elasto-plastic behaviour of polymers can be explained by referring to the structure and molecular organisation of the material. In the elastic region, the deformation is related to the reversible mobility of the amorphous domains. A disentanglement process of the macromolecules in the direction of the applied force occur, whilst the ordered crystalline structure remains intact. Once the yield point is overcome, a more marked movement of the chains occur, leading to the breakage of the polymer entanglements and craze formation. These regions are characterised by a lower density and can turn into cracks with a further increase of the loading. The mechanical behaviour of polymer strictly depends on the temperature. Below the glass transition temperature (T_g) the polymer tends to be brittle and the failure occurs at very low strain rate level. At higher temperature, a brittle-ductile transition behaviour tends to develop and the yield point start to be visible. Semi-crystalline polymers such as polyamide typically show a yield point in tensile stress/strain curves [84]. After this point, there is a decreasing of the stress level associated with the so-called “necking behaviour”, for which a reduction of the cross-section of the sample occurs in a specific region of the material. The curve ends with a new increase of the stress because of the alignment of polymer chains in the stretch direction which increases the strength of the plastic part. Subsequently, a gradually breakage of the secondary bonds and molecular disentanglement lead to the final failure of the material.

In order to verify the effect of the addiction of nanofillers on the mechanical properties of the polymer (Polyamide 6), static tensile tests have been performed by using a Shimadzu AGS – X series tensile tester (see Fig. 4.7) with a load cell of 10 kN. Through this test, the applied force and elongation of the material were constantly monitored while the specimen underwent a longitudinally elongation until fracture. Tests were carried out

in order to determine the Young's modulus, the tensile strain at break, the tensile strength at break and the yield strength of the composites samples.

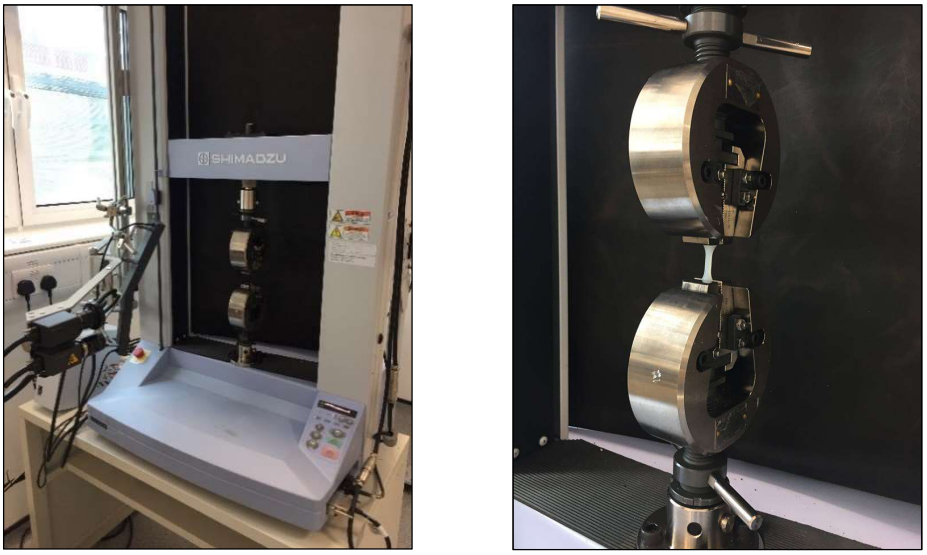

Fig. 4.7. *Shimadzu AGS – X series tensile tester equipped with video extensometer.*

4.2.1.2 Dynamic Mechanical Thermal Analysis (DMTA)

Dynamic Mechanical Thermal analysis is useful for studying the viscoelastic properties of polymers, such as the storage modulus, and to identify the thermal transition associated with the mobility of the polymer chains. As mentioned in the preceding section, polymer materials are characterised by a time-dependent viscoelastic deformation behaviour when subjected to a stress over an extended period of time and/or temperature variation. Viscoelasticity is typical of thermoplastics polymers which exhibit both viscous and elastic behaviour when an external force is applied [85]. The elastic behaviour is characteristics of materials which completely recover the deformation (see previous section). In contrast, purely viscous material undergoes completely irreversible deformations: in other words, the whole energy spent to impose the deformation is dissipated in form of heat and cannot be recovered by removing the applied force. Polymer chains possess high mobility and they can slide past each other because of weak inter-chain interactions. This molecular rearrangement (called creep) represents the viscous contribute of the deformation. Polymers remain a solid even if the chains

rearrange in order to reach an equilibrium state with the stress applied. This needs a certain time to occur, as well as the recovery of the deformation once the stress is removed, which represents the elastic response of the material. Viscoelasticity can be detected by monitoring the evolution of the strain of the material. If a polymer is placed under constant stress for a long period of time, a progressive increase in strain will be observe. Consequently, since the elastic modulus is defined as the applied stress divided by the strain, the value of the modulus after a certain length of time will show a decrease. A similar result is observed within plastic materials as the temperature is increased. In this way, it is possible to detect a sensible variation of the viscoelastic properties of a polymer by applying a stress under a specific range of temperature. Specifically, DMTA is useful to apply a sinusoidal stress to a polymer at a fixed frequency, and observe the material change as temperature varies.

In this research, a Tritec 2000 DMA (Triton technology, UK) was used and the sample was tested under a flexural stress. The apparatus is shown in Fig. 4.8.

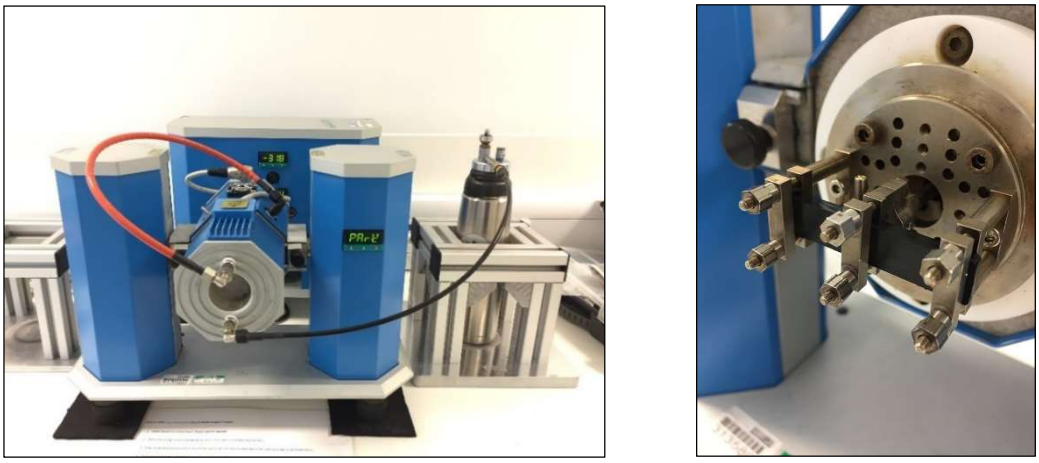

Fig. 4.8. *Tritec 2000 DMA (on the left) and dual cantilever apparatus (on the right).*

The DMTA apparatus consists of two stationary clamps which hold the bar-shaped sample in horizontal position, while a movable clamp applies the linear displacement at the center of the specimen. A movable furnace is applied on the sample and the furnace chamber is equipped with a connector for nitrogen alimentation. This system enables to vary the temperature at which the material is exposed. The sample is subjected to a

controlled strain (fixed displacement) and the variation of the stress is measured. Generally, when a material undergoes a sinusoidal strain in the form:

$$\varepsilon(t) = \varepsilon_0 \sin(\omega t) \tag{4.2}$$

the related stress manifests a phase lag (δ) of a specific angle, with respect the imposed deformation, as shown below:

$$\sigma(t) = \sigma_0 \sin(\omega t + \delta) \tag{4.3}$$

where the ω is the strain oscillation frequency, t is the time and ε_0 and σ_0 are the maximum strain and stress amplitude, respectively. According to the characteristic of the material, a different phase angle between stress and strain can be present (see Fig 4.9):

- $\delta = 0°$, which means that the strain and the stress are perfectly in phase. This is characteristic of perfectly elastic solids.
- $\delta = 90°$, which means that the strain is 90° out-of-phase with respect the stress. This is characteristic of viscous fluids.
- $0° < \delta < 90°$, which is typical of polymer materials that exhibit a viscoelastic behaviour.

Equation (4.3) can be transformed by using the trigonometric relations, as follows:

$$\sigma(t) = \sigma_0 \sin(\omega t)\cos(\delta) + \sigma_0 \sin(\omega t)\sin(\delta) \tag{4.4}$$

The final relation for the stress as a function of time is shown below:

$$\sigma(t) = \varepsilon_0[E' sin(\omega t) + E'' cos(\omega t)] \tag{4.5}$$

where:

$$E' = \frac{\sigma_0}{\varepsilon_0} cos(\delta) \qquad E'' = \frac{\sigma_0}{\varepsilon_0} sin(\delta) \tag{4.6}$$

E' is called as the *Storage Modulus* and is the measure of the sample's elasticity, hence the ability of the material to store energy. E'' is defined as *Loss Modulus* and is related to the viscous behaviour of the material. It represents the energy loss as heat.

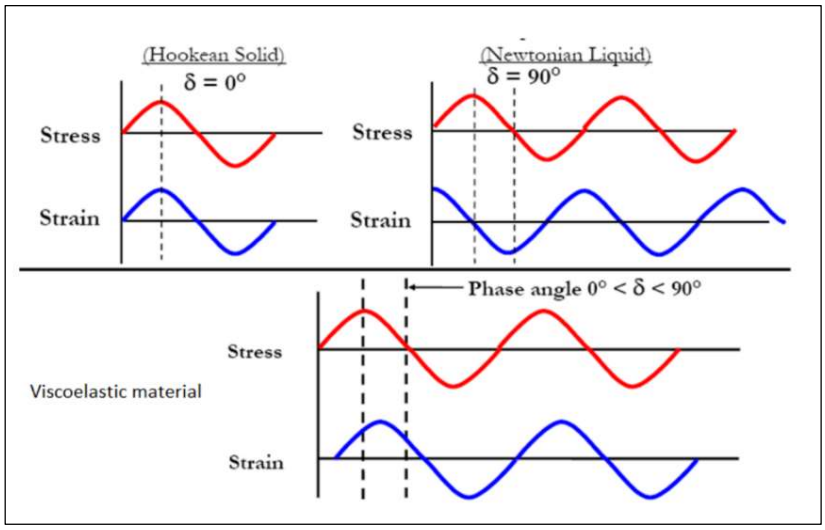

Fig. 4.9. *Phase difference between strain and stress sinusoidal curves [86].*

Another important parameter is given as follows:

$$\tan(\delta) = \frac{E''}{E'} \tag{4.7}$$

DMTA measurements provide the value of the storage modulus, the loss modulus and of $\tan(\delta)$ which represents a measure of the material damping (energy absorbance capacity). All these properties can be plotted as a function of the temperature and important information regarding the viscoelastic behaviour of the polymer can be extrapolated. The change in the storage modulus is a detector for the abovementioned molecular rearrangement that occurs in the polymer structure. During heating, the polymer chains are subjected to a series of movements that take the name of thermal transitions [87]. The most important thermal transition is related to the glass transition temperature (T_g) which is the minimum temperature at which coordinated movements of the chain terminals are possible. Macroscopically, a sensible change of the properties of the polymer occurs at this temperature, and the material passes from a rigid state to a rubbery and easily deformable one. The techniques for determining the value of the T_g from the trend of the parameters detected by the instrument are multiple: normally the value is retrieved at the peak of the $\tan(\delta)$ curve or in the temperature range in which the storage modulus abruptly decreases.

4.2.3 Thermal Characterisation

4.2.3.1 Differential Scanning Calorimetry (DSC)

Differential scanning calorimetry is a technique which is used to investigate physical property changes of a material, such as thermal transitions in polymers. In this work, a Mettler Toledo DSC 3+ (see Fig. 4.10b) has been utilized and the result's evaluation has been performed through the Star Software evaluation system. This instrument worked through a heat flux operational mode which is based on the difference between the heat fluxes of an empty reference pan and of another pan which contain the material to be investigated. Each pan is heated up by a heating element and both are subjected to the same thermal cycle, with a heating rate typically equal to 10 °C/min. This enables the machine to detect enthalpy changes in the sample due to variations in its physical properties as a function of temperature. Specifically, the measurement is possible because the pan containing the sample will require a different amount of heat to ensure that both the pans are subjected to the same temperature program. The difference in heat between the two systems is given as the output of the instrument and represents the thermal fingerprint of the material [88]. Due to the transitions occurring in the material as the temperature varies, the crucible containing the material generates endothermic (heat flowing out of the sample) or exothermic heat flow (heat flowing into the sample). For instance, as the sample undergoes exothermic process, such as crystallisation, less heat is required to increase the sample temperature. The instrument is able to record the heat flux variations and to plot them as a function of temperature or time. A schematic of the DSC mechanism is shown in Fig. 4.10a.

The tests were carried out in an inert atmosphere (100% nitrogen), in order to avoid any possible oxidative reaction that could distort signal detection of transient phenomena. The samples were inserted in hermetic aluminium capsules. DSC can detect important information regarding thermal transitions in polymers, such as the T_g, the onset and peak temperatures for both endothermic melting and exothermic crystallisation, in addition to the enthalpies of crystalline melting and fusion. The latter enables the determination of the degree of crystallinity, (X_c) to be calculated using the 100% crystalline enthalpy (ΔH_m^0) of the pure polymer.

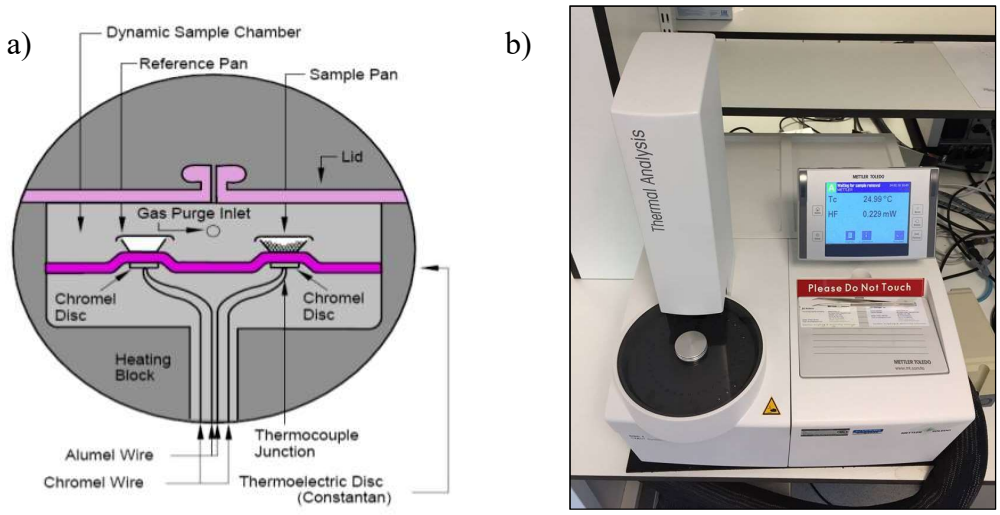

Fig. 4.10. *Schematic representation of DSC functioning (a) and Mettler Toledo DSC 3+ (b).*

4.2.3.2 Thermal Gravimetric Analysis (TGA)

Thermal gravimetric analysis is method in which the weight variation of a sample can be examined as a function of temperature or time, when the specimen is exposed to a specific temperature range and controlled atmosphere [89]. The instrument used for this research was a Mettler Toledo TGA 2 (see Fig. 4.41a) equipped with Star Evaluation Software. The apparatus consists of a sample holder connected to a precision balance and surrounded by a furnace which can be heated or cooled during the experiments. The temperature is generally increased at a constant rate (10 °C/min) and an inert or reactive gas can be blown into the heating chamber and flow over the sample. Through this technique, a TGA thermal curve is obtained which provides the trend of the weight of the sample as the temperature increases. This is useful for studying thermal decomposition and determining the presence of any inorganic residue, indices of thermal stability of the material. Alumina crucible are generally used for the measurement. Firstly, an empty crucible is heated up to obtain a blank curve (as a reference sample). The sample is then inserted into the crucible and exposed at the same temperature range and heating rate of the empty reference sample. The computer records the weigh variation of the specimen with respect to the reference sample, through the software. The thermogravimetric data collected from the experiment are represented into a plot of weight loss percentage versus either temperature or time (TGA curve). The first derivative of the TGA curve (the DTA

curve) with respect to temperature, is plotted to determine the so-called inflection point, which corresponds to the peak of the derivative curve. This peak enables the determination of the temperature at which the maximum rate of material's decomposition takes place. Another parameter that can be extrapolated is the onset temperature which is the temperature at which the degradation begins.

a) b)

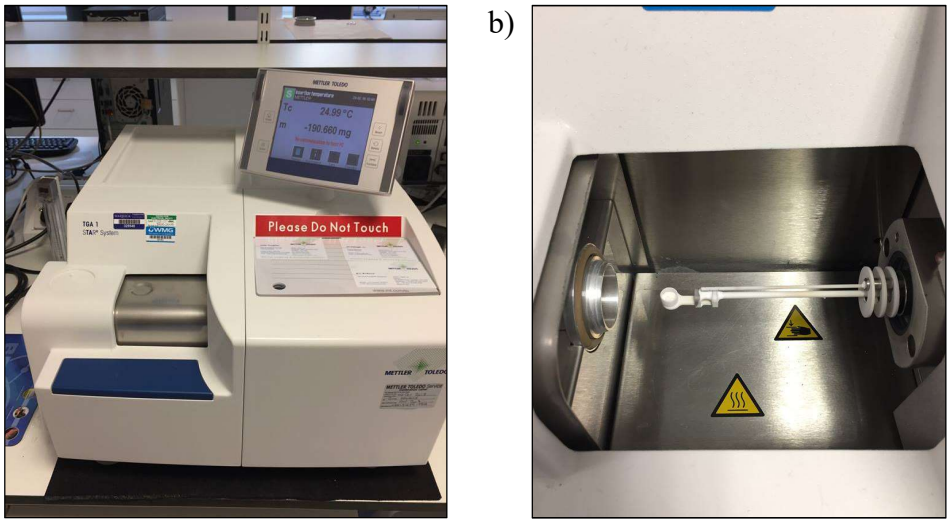

Fig. 4.11. *Mettler Toledo TGA 2 (a) and furnace equipped with sample holder and scale (b).*

4.2.4 Rheological Characterisation

Rheology is the study of the flow and deformation of material both in the molten state and in a particular type of solid state which responds to the applied force by flowing plastically rather than deforming elastically. Thermoplastic polymers belong to this category also defined as "soft materials" and are characterised by a viscoelastic behavior, which means that their mechanical properties fall between that of a perfectly elastic solid and that of a viscous liquid. A good knowledge of the behavior of molten thermoplastic polymers is fundamental for an accurate design of the operating conditions in many modern industrial manufacturing processes. Through oscillatory rheology analysis it is possible to quantify both the viscous-like and the elastic-like properties of a material as a function of the frequency. During this test, a disk-shaped sample is subjected to an oscillating preset shear stress, and the resultant time-dependent strain response is

determined. In this research, a Haake Mars Modular Advanced rheometer equipped with a plate-plate geometry was used (see Fig. 4.12a).

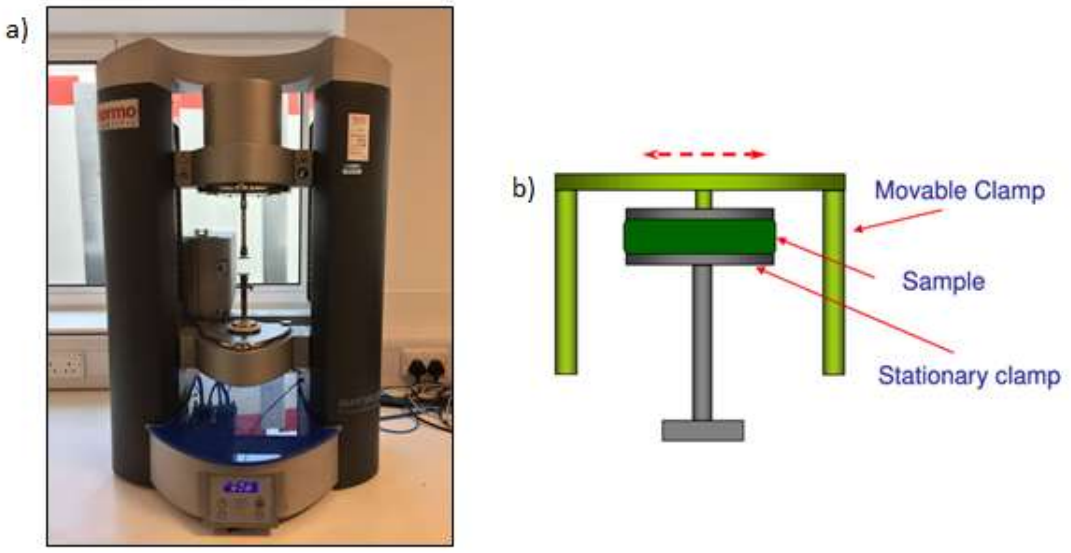

Fig. 4.12. *Haake Mars Modular Advanced rheometer (a) and plate-plate geometry (b).*

Typically, the sample is placed between two circular plates (one movable and one stationary) and an oscillating shear stress is applied on it, within a specific frequency (ω) range. As already mentioned in the previous chapter, the sinusoidal time-dependent shear strain (γ) manifested by the material can be expressed as follows:

$$\gamma(t) = \gamma_0 \sin(\omega t) \tag{4.8}$$

The strain is the result of an oscillatory shear stress apply on the sample, in the form:

$$\tau(t) = \gamma_0[G' \, sin(\omega t) + G'' \, cos(\omega t)] \tag{4.9}$$

where:

$$G' = \frac{\tau_0}{\gamma_0} cos(\delta) \qquad G'' = \frac{\tau_0}{\gamma_0} sin(\delta) \tag{4.10}$$

As seen before, G' and G'' are the Storage and Loss modulus of the material, in shear stress conditions. In a rheological experiment, these two parameters can be quantified as a function of the frequency. This permits to identity whether the polymer exhibits a liquid-

like or solid-like behaviour during the stress application. Other properties can be determined by the oscillatory rheology analysis. One of them is $\tan(\delta)$ which is the ratio between G'' and G', and is useful quantify the balance between the energy loss and storage by the polymer. Nevertheless, viscosity changes can be determined as a function of the frequency.

Melt polymers are characterised by a non-Newtonian behaviour, which means that they deviate from the Newton law, expressed as:

$$\tau = \eta \frac{d\gamma}{dt} = \eta\dot{\gamma} \tag{4.11}$$

where τ is the applied shear stress, $\dot{\gamma}$ is the shear strain rate and η is the viscosity. Specifically, polymers can be classified as *pseudoplastic* materials [90], for which melt viscosity decreases as shear rate increases (phenomenon called shear thinning). From a technological point of view this behaviour represents an advantage because high shear rate levels tend to speed up material flow and to reduce heat generation and energy consumption during processing. The viscosity drop can be explained by the increasing orientation of macromolecules with the flow and by the reciprocal slippage of chains that are normally interlaced (breaking of the entanglements). The viscosity changes can be monitored during an oscillatory frequency sweep measurement, by plotting the complex viscosity ($|\eta^*|$) as a function of the angular frequency. This is possible thanks to the so-called Cox-Merx rule [91], for which it has been detected that for several polymer systems a correspondence exists between the steady viscosity, η, plotted against strain shear rate $\dot{\gamma}$, and the profile of the complex viscosity, |η*|, plotted against angular frequency, ω. The complex viscosity is defined as follows:

$$\eta^* = \frac{G^*}{i\omega} \tag{4.12}$$

where G^* is the complex shear modulus, given by:

$$G^* = G' + iG'' \tag{4.13}$$

Thus, complex viscosity can be also expressed as:

$$\eta^* = \frac{G'}{i\omega} + \frac{G''}{\omega} \rightarrow |\eta^*| = \frac{|G^*|}{\omega} \tag{4.14}$$

where the first term is defined as imaginary viscosity (η''), while the second term represents the real viscosity (η'). The complex shear modulus represents a measure of the materials overall opposition to deformation, regardless of whether the deformation is recoverable (elastic) or non-recoverable (viscous). Phase angle can be plotted as a function of the complex modulus ($|G^*|$) in order to have a measure of the size of the elastic behaviour in a melt polymer.

4.2.5 Raman Spectroscopy

Raman spectroscopy is one of the main spectroscopic technique used for determining the vibration frequencies of a molecule. In general, spectroscopy is based on the interaction of electromagnetic radiation with the matter, which can lead to various effect including the absorption and the scattering by molecules. In the first case, an infrared absorption spectrum is obtained while in the second case a Raman scattering spectrum is achieved. Particularly, in Raman spectroscopy, the radiation emitted by a laser beam interacts with the roto-vibrational motions of the molecules of the sample with the consequent re-emission of light at different wavelengths than the incident one. The spectrum that is obtained from the analysis (called Raman spectrum) provides a sort of digital fingerprint of the molecules under examination, allowing their identification [92]. When a monochromatic radiation impacts on the sample surface different effects can take place:

- Part of the incident radiation passes through the sample and no scattering phenomena occurs;
- Part of the incident radiation is elastically scattered in all the directions. This process, also called Rayleigh scattering, do not involve any energy change which means that both incident light and scattered light have the same wavelength;
- A small percentage of the incident light is subjected to inelastic scattering which occurs in two different modes. On one hand a process called as Stokes Raman

scattering occurs and it involves energy absorption of the incident light by the molecules with subsequent emission of light with less energy (longer wavelength). On the other hand, the molecules are already in an excited state and a transfer of energy to the incident photon occurs, thus leading to the emission of a higher energy level radiation with respect the incident one (anti-Stoke Raman scattering).

The different mechanisms of scattering are shown in the figure below.

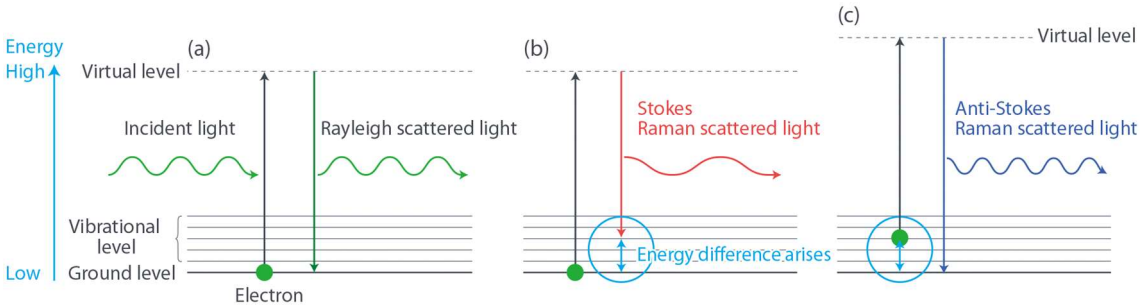

Fig. 4.13. *Schematic of Rayleigh and Raman scattering processes.*

From Fig. 4.13 it is apparent that the external electric field of the laser beam interacts with the electron cloud of the sample. This interaction creates an induce dipole moment within the molecule based on its polarizability and leads to the distortion of the electron cloud to form a sort of "virtual state". The instability of this state caused the photon to be re-emitted as scattered light. Generally, at room temperature, the number of molecule that are already in an excited state is smaller than the molecule with electrons at the ground vibrational level. Thus, the intensity of anti-Stokes Raman scattered light is lower than the Raman-stoke one, which is the one used for analytical purpose.

Raman technique can be used for studying polymers and identify their molecules and chemical bonding. Every peak appearing in the Raman spectrum is related to a specific molecular or lattice vibration. Hence, the determination of the peak position permits to identify which molecular functional group is included in the material. Moreover, Raman spectroscopy is used to better understand the structure and defects of inorganic material such as graphene. Raman spectrum of graphene and PA6/GNPs composites has been obtained by using a Renishaw inVia Reflex Raman Microscope with 633 nm laser, shown in Fig. 4.14.

Fig. 4.14. *Renishaw inVia Reflex Raman Microscope.*

4.2.6 Scanning Electron Microscopy (SEM)

Scanning electric microscopy is a technique which is useful to analyse the surface and topography of a material. SEM functioning is based on the possibility to detect the effects produced by the interaction of electrons with the matter [93]. Typically, a beam of accelerated free electrons, called primary electrons, is focused on the sample by a system of lenses. The interaction between the electrons and the matter lead to different signals which can be treated and amplified in order to produce a pixel in the screen and create an image. SEM apparatus consists of an electron source, an accelerator system, electromagnetic lenses for beam focusing, detectors, electronic system for data conversion and vacuum system (see schematic in Fig. 4.15). The main form of signals that are produced by the electronic scansion of the sample are listed below:

- Electronic emission (secondary electrons, back-scattered electrons, Auger electrons);
- Photonic emission (infrared and visible);
- X-ray emission.

Each of these forms of signal provides indications on composition and morphology of the material but the most commonly exploited source is the emission of secondary electrons.

Secondary electrons have lower energy (< 50 eV) than back-scattered electrons and they are the result of the interaction between the primary beam and the electron cloud of the material's surface. This interaction leads to the ejection of electrons from the valence band of the specimen's atoms (inelastic scattering). Non-conductive materials like polymers must be coated with high atomic number conductive materials (like gold) in order to prevent the accumulation of static electric charges on the surface of the sample. The presence of static charges on the surface causes interference with the signals carried by the secondary electrons and deteriorates the image formation. Secondary electrons provide information about the morphological characteristics of the sample surface. The identification of the tridimensional details of the specimen's surface is due to the so-called edge effect. A difference in contrast is revealed by the detector when the secondary electrons are scattered form different areas of the sample surface. Signal brightness is proportional to the number of secondary electrons which tend to change from flat areas to sharp surfaces and edges on the material. When the electron beam impacts the sample perpendicular to the surface a narrow area is irradiated and few electrons escapes. As the angle of incidence increases, a larger area interacts with incident beam, resulting in more electrons being emitted from the sample.

In this study, a Zeiss Gemini Field Emission Scanning Electron Microscopy (FE-SEM) was used, with an operating voltage of 5 kV.

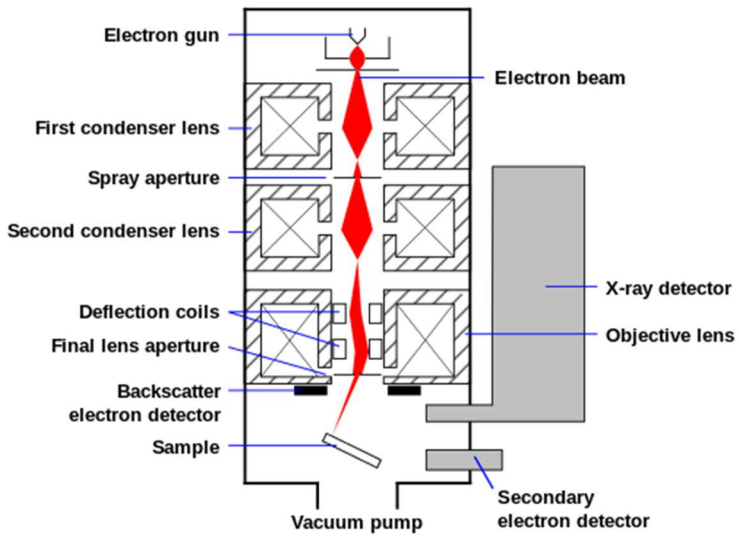

Fig. 4.15 *Schematic of a SEM.*

4.2.7 X-Ray Photoelectron Spectroscopy (XPS)

X-ray photoelectron spectroscopy is a quantitative spectroscopic method which is utilized to analyse the surface chemistry of a material. XPS can detect the chemical elements which compose the material surface and determine the bonding state. The analysis is performed by irradiating the material surface with an X-ray beam and by measuring the kinetic energy of the emitted photoelectrons. From the measurement, a photoelectron spectrum is obtained by calculating the number of ejected electrons over a range of kinetic energies. Each atom is characterised by a specific energy of emitted electron, thus enabling the identification and quantification of all surface elements of the material. The operating principle of XPS is the so-called photoelectric effect (see Fig. 4.16a) which is one of the response modalities related to the interaction of photons with the surface of a solid material [94]. The direct transfer of energy from the photons to the core-level of electrons of material atoms surface leads electrons to be expelled from the surface. The kinetic energy (KE) of the expelled electrons is related to their binding energy (BE) which is the energy required to overcome the Coulomb attraction of electrons to the nucleus. Electrons binding energy can be determined by means of the following equation:

$$E_{binding} = E_{photo} - (E_{kinetic} + \phi) \tag{4.15}$$

where E_{photo} is the energy of the X-ray photons which are used for the experiment; $E_{kinetic}$ is the kinetic energy of the expelled electrons and ϕ is the work function which is related to the instrument.

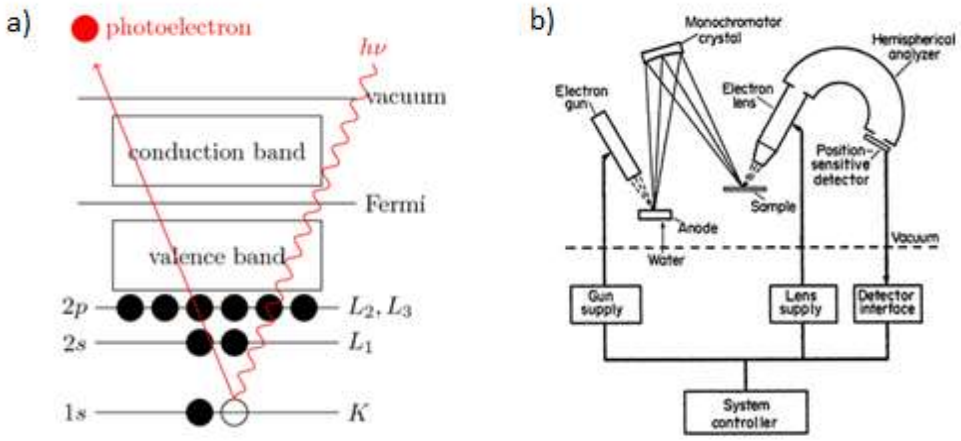

Fig. 4.16. *Photoelectric effect (a) and schematic of XPS system (b).*

X-rays are typically produced by the interaction of accelerated electrons, which are emitted from a heated filament (cathode), with the surface of a solid anode (Mg or Al). The energy of the produced X-ray can be measured (e.g. for Al K_α X-rays, E_{photon} = 1486.7 eV) as well as the emitted electron's kinetic energies during a XPS analysis. Hence, this information along with the work function (ϕ), enables the determination of the binding energy of the electrons through eq. 4.15. For this study, a Scienta Omicron X-ray photoelectron spectroscopy was used.

4.2.8 Electrical Characterisation

In this research, electrical resistivity measurements have been carried out through the use of a Keithley 6517B High resistance meter (electrometer). The instrument is equipped with an electric generator which supplies an alternating voltage in order to eliminate the effect of residual charges that can be accumulated by the material surface. The method consists in the application of a sufficient large voltage to the sample, while the current circulating in the material is detected by the picoammeter inside the instrument. The Ohm's law (R=V/I) is then applied in order to determine the resistance value. The instrument is able to provide the value of the volume resistivity of the sample, by converting the resistance value according to the following equation:

$$\rho = \frac{A}{L} R \tag{4.16}$$

where A is the cross-sectional area perpendicular to the current flow, L is the distance between the two electrodes and R is the resistance (in Ohm).

The Electrometer is equipped with a model 8009 resistivity chamber which contains to circular-shaped electrodes where the sample can be introduced. This device is able to maintain good sample contact with uniform pressure and is suitable for sheet specimens from 64 to 102 mm of diameter and up to 3.2 mm of thickness.

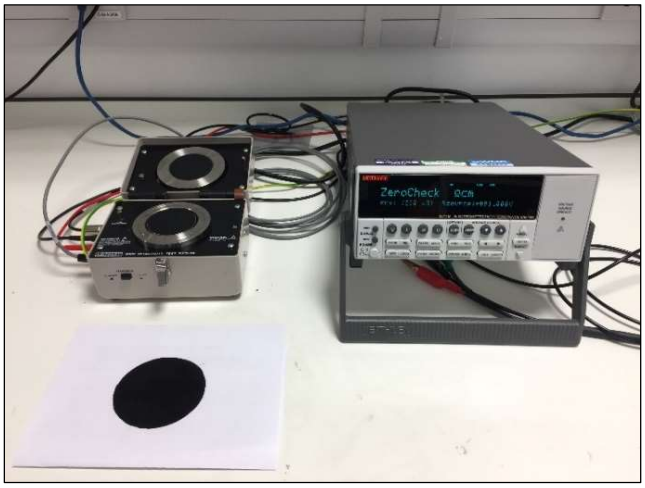

Fig. 4.17. *Keithley resistivity chamber (on the left), and Keithley 6517B electrometer (on the right).*

4.2.9 Fourier Transform Infrared Spectrometer (FTIR)

Infrared spectroscopy is a technique used to examine the electromagnetic radiations related to transitions between vibrational or rotational energy states of a molecule. When an infrared radiation is shined onto a material surface, the sample molecules tend to absorb specific radiation wavelengths which lead to a net change of their dipole moment [95]. These bond vibrations consist in different type of molecule movements such as bending, twisting and stretching (symmetric and asymmetric), and their frequency is related to the nature of functional groups from which they derived. The energy which corresponds to the vibrational state of the molecules can be described by the following equation:

$$E = \left(v + \frac{1}{2}\right) h v_m \tag{4.17}$$

FTIR technique measures the fraction of incident radiation absorbed by the sample at a specific energy, obtaining an infrared spectrum of absorption of the material. The energy related to each peak of an absorption spectrum corresponds to the frequency of a vibration of a part of a sample molecule. Moreover, the number of peaks is associated with the number of vibrational freedom of the molecule. From the spectrum, it is possible to obtain several structure information of a molecule. The infrared spectrum includes radiation with

wavenumbers ranging from 14000 to 20 cm^{-1}. Generally, this region is divided in three sub-ranges: near-infrared region (14000 ~ 4000 cm^{-1}), mid-infrared region (4000 ~ 200 cm^{-1}) and far-infrared region (50 ~ 1000 cm^{-1}). The mid-infrared region is the most commonly used for the analysis of polymer samples.

A Bruker Tensor 27 FTIR instrument was used for this research, in order to detect functional groups and chemical bond nature in the structure of Nylon 6.

Fig. 4.18. *Bruker Tensor 27 FTIR system.*

4.2.10 Modified Transient Plane Source Method (MTPS)

Modified Transient Plane Source technique is used for measuring the thermal effusivity and thermal conductivity of complex materials such as nanocomposites. The advantages of this method are the high accuracy, easy sample preparation, non-destructive measurements, high range of thermal conductivity measurable (0.005 – 500 W/m K) and high versatility in term of material type to be analysed [96]. MTPS measurements are performed through the use of a transiently heated plane sensor, which consists of an electrically conducting pattern with the shape of a double spiral, which is obtained from a thin metal foil. A C-Therm TCi Thermal Conductivity Analyser was used in this research to quantify the thermal conductivity of PA6/GNPs composites samples.

The operational procedure of the C-Therm TCi system is described as follows:

- The apparatus is constituted of a one-sided interfacial sensor, controller electronics and computer software (Fig. 4.19 a).
- The transiently heated plane sensor (Fig. 4.19 b) is delimited by a guard ring which produces heat in addition to the spiral heater. Hence, a one-dimensional heat flow occurs from the sensor into the material under examination in contact with the device. The difference between this system and traditional transient plane source method is that the heating element is maintained on a support, which provides mechanical backing, electrical insulation and thermal insulation.
- The voltage gradient on the spiral heater is measured before and during the transient. The voltage data is then converted into the effusivity value of the tested material.
- The thermal conductivity is determinate from the slope of the voltage data.

During the measurement, the sensor applies a constant current to the sample in order to heat the material (approximately of 1-3°C). The sample absorbs a specific amount of heat depending on its thermal conductivity, and the rest leads to a temperature increase at the sensor interface. The rate of the increment in temperature at the sensor surface is inversely proportional to the capacity of the sample to dissipate heat. Thermal conductivity and effusivity are obtained directly, providing an exhaustive indication of the thermal nature of the sample material.

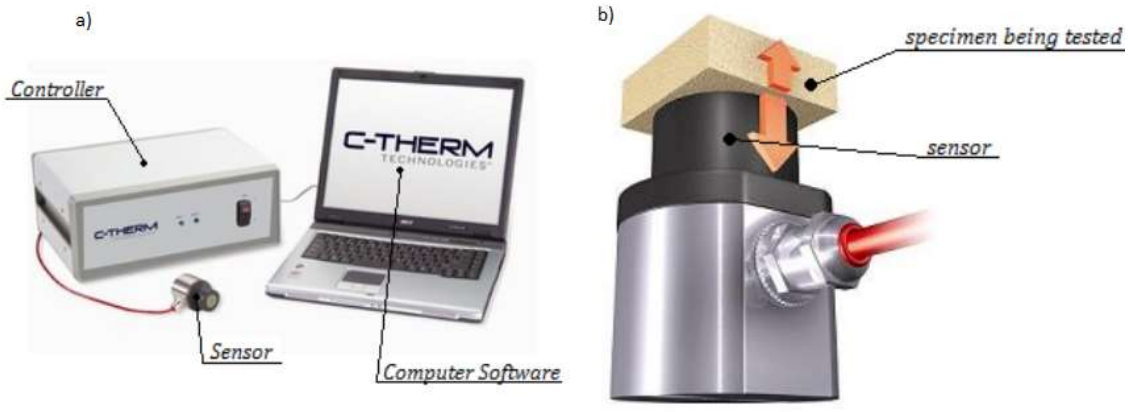

Fig. 4.19. *Schematic of C-Therm TCi Thermal Conductivity Analyzer: (a) C-Therm TCi apparatus and (b) Sensor in use.*

Chapter 5

Production of Nylon 6 – Graphene Nanocomposites

In this chapter, the constituents of the produced composites material are listed and a description of the processing parameters and production procedures is given. Several specimens of different geometries have been made in accordance with the characterisation techniques, by the use of injection moulding and hot-pressing processes.

5.1 Materials

In this study, Nylon 6-graphene nanocomposites were formulated and produced via melt-compounding process, using a co-rotating twin extruder. The basic materials of the produced composites consist of two types of Nylon 6, each characterised by a specific melt flow index (MFI), and graphene nanoplatelets (GNPs). The materials used and related properties (extracted by the datasheets) are listed as follows:

- PA6 Icorene™ N9602 (A. Schulman Specialty Powders)

Tab. 5.1. *Characteristics of Icorene™ N9602.*

Physical	Nominal Value (English)	Nominal Value (SI)	Test Method
Density	1.14 g/cm³	1.14 g/cm³	ISO 1183
Mechanical	**Nominal Value (English)**	**Nominal Value (SI)**	**Test Method**
Tensile Strength (Yield)	11600 psi	80.0 MPa	ASTM D638
Tensile Elongation			ASTM D638
Yield	20 %	20 %	
Break	75 %	75 %	
Flexural Modulus	392000 psi	2700 MPa	ASTM D790
Impact	**Nominal Value (English)**	**Nominal Value (SI)**	**Test Method**
Charpy Notched Impact Strength (73°F (23°C))	9.5 ft·lb/in²	20 kJ/m²	ISO 179
Thermal	**Nominal Value (English)**	**Nominal Value (SI)**	**Test Method**
Heat Deflection Temperature			ISO 75-2/B
66 psi (0.45 MPa), Unannealed	347 °F	175 °C	
Vicat Softening Temperature	415 °F	213 °C	ISO 306
Melting Temperature (DSC)	432 °F	222 °C	ISO 3146

- PA6 Grilon® BS/2 (EMS Grivory)

Tab. 5.2. *General characteristics of Grilon® BS/2.*

General Properties					
Density		ISO 1183	g/cm³	dry	1.14
Flammability (UL94)	0.8 mm	ISO 1210	rating	-	HB
Water absorption	23°C/sat.	ISO 62	%	-	9
Moisture absorption	23°C/50% RH	ISO 62	%	-	3
Linear mould shrinkage	long.	ISO 294	%	dry	1.05
Linear mould shrinkage	trans.	ISO 294	%	dry	1.05

Tab. 5.3. *Specific characteristics of Grilon® BS/2.*

	Grilon BS/2	
Mechanical properties	**dry / cond**	**Unit**
Tensile Modulus	**3300 / 1100**	MPa
Yield stress	**90 / 45**	MPa
Yield strain	**3 / 15**	%
Nominal strain at break	**5 / >50**	%
Stress at break	**70 / 55**	MPa
Charpy impact strength (+23°C)	**N / N**	kJ/m²
Charpy impact strength (-30°C)	**N / 30**	kJ/m²
Charpy notched impact strength (+23°C)	**4 / 20**	kJ/m²
Charpy notched impact strength (-30°C)	**4 / 3**	kJ/m²
Mechanical properties (TPE)	**dry / cond**	**Unit**
Ball indentation hardness	**140 / 60**	MPa
Thermal properties	**dry / cond**	**Unit**
Melting temperature (10°C/min)	**222 / -**	°C
Temp. of deflection under load (1.80 MPa)	**55 / -**	°C
Temp. of deflection under load (0.45 MPa)	**170 / -**	°C
Coeff. of linear therm. expansion (parallel)	**70 / -**	E-6/K
Coeff. of linear therm. expansion (normal)	**100 / -**	E-6/K
Burning Behav. at thickness h	**HB / -**	class
Thickness tested	**0.8 / -**	mm
Max. usage temperature (long term)	**70 - 90**	°C
Max. usage temperature (short term)	**180**	°C
Electrical properties	**dry / cond**	**Unit**
Volume resistivity	**1E12 / 1E11**	Ohm*m
Surface resistivity	**- / 1E12**	Ohm
Electric strength	**30 / 28**	kV/mm
Comparative tracking index	**- / 600**	-

- Graphene nanoplatelets (GNPs) SE1233 (The Sixth Element)

Tab. 5.4. *Characteristics of GNPs SE1233.*

Appearance	pH	Tap density (g/cm^3)	Specific surface area (m^2/g)	H_2O (wt%)	Particle size (μm)		Non-metal content (wt%)			Fe (ppm)	Surface resistance of PAA (2% loading, Ω)	DBP absorption (ml/100g)
					D_{50}	D_{99}	C	O	S			
Black powder	6.0~8.0	<0.025	≥450	<1.0	<10.0	≤ 20.0	> 97.0	<1.0	<0.2	<50	$<10^6$	>1700

Unfunctionalised graphene nanoplatelets in powder form (with specific surface area of 468.65 m^2/g) was supplied by Haydale Composite Solutions Ltd. for research purposes. Nylon 6 Icorene™ N9602 was provided in powder form while Grilon® BS/2 was received in pellets form.

5.2 Processing Parameters

In order to obtain a good pre-mixing between the filler and the polymer matrix, cryo-grinding of Nylon 6 (Grilon® BS/2) pellets was performed through the use of a Spex SamplePrep 6870 Freezer Mill which cooled the polymer down at -196°C. The polymer pellets were closed into a plastic cylinder along with a steel milling element and all the system were poured into a liquid nitrogen bath. The cooling process enable the polymer to become highly brittle and to be easily grinded in form of powder. The ground PA6 (Grilon®) powder and the Icorene™ powder (as received) were dried at 80°C for 12 hours in order to remove the moisture content of the polymer which was absorbed due to its hydrophilic nature. Dried PA6 and GNPs powders were subsequently hand-mixed in plastic bags at specific filler concentration: 0.1 wt%, 0.5 wt%, 1 wt%, 3 wt% and 5 wt%. Nylon 6-GNPs composites were obtained by means of a melt-blending process, which began with the introduction of the pre-mixed compounds into the extruder's hooper. Before and after the cryo-grinding process FTIR analysis was carried out in order to verify the chemical integrity of the polymer. Moreover, TGA measurements were performed on both types of polymers in order to determine the degradation temperature of the material

which is useful to define the upper temperature for the extrusion process. The temperature of each of the heating element located along the 9 barrel's zones was selected for each formulation of composite to be produced. Thus, an operating temperature profile was set by considering a range of values which are comprised between the melting temperature of the neat polymer and a value well below its degradation temperature. The melting temperatures of the neat polymers were taken by the material datasheets and confirmed by DSC measurements. Initial extrusion attempts have been carried out in order to adjust the temperature profile in according to the characteristics of the extrudate (viscosity, in particular). The processing parameters for the extrusion of the PAG/GNPs composites are tabulated in the tables below.

Tab. 5.5. *Extrusion processing parameters for PA6 Grilon® /GNPs composites.*

GNPs (wt%)	T_1 (°C)	T_2 (°C)	T_3 (°C)	T_4 (°C)	T_5 (°C)	T_6 (°C)	T_7 (°C)	T_8 (°C)	T_9 (°C)
0	220	225	230	235	240	245	250	250	250
0.1	220	225	230	235	240	245	250	250	250
0.5	220	225	230	235	240	245	250	250	250
1	225	230	235	245	250	250	250	245	245
3	225	230	235	245	250	250	255	250	250
5	235	240	245	250	255	255	260	260	260

Tab. 5.6. *Extrusion processing parameters for PA6 Icorene™/GNPs composites.*

GNPs (wt%)	T_1 (°C)	T_2 (°C)	T_3 (°C)	T_4 (°C)	T_5 (°C)	T_6 (°C)	T_7 (°C)	T_8 (°C)	T_9 (°C)
0	235	240	245	250	250	250	255	255	255
0.1	235	240	245	250	250	250	250	255	255
0.5	235	240	245	250	250	250	250	255	255
1	235	240	245	250	250	250	255	255	255
3	235	240	245	250	250	250	255	255	255
5	235	240	245	250	255	255	260	260	255

From the processing parameters it can be observed that the temperature profile was slightly modified by increasing the temperature with higher GNP loading, in order to contrast the increase in viscosity due to the presence of the nanofillers. By working at

higher temperature, the viscosity of the polymer is lower as well as the shear stress impressed by the screws on the material. This is important in order to facilitate a more homogeneous mixing of the filler and to preserve its structural integrity. In fact, the outlet pressure (at the die) and the amount of energy transferred to the material by the screws are both depending on the viscosity. It has also been noticed that working at higher screw speed leads to a decrease of the residence time of the material into the barrel, but at the same time it provides a higher level of stress on the composites, thus determining more enhanced damage of the filler. The real temperature at which the material is exposed during the extrusion process depends not only on the level of current provided to the heating elements but also on the shear stress which occurs between the material and the extruder body (barrel and screws). A friction effects arises due to the forces at work, thus exposing the polymer to possible degradation. The screw speed was maintained at a constant value of 50 rpm (revolutions per minute) in order to exercise comparable shear stresses on the different composite formulations.

The composites pellets produced from the extrusion process have been dried for at least 10 hours at 80°C before proceeding with injection moulding and hot pressing processes. MiniJet Injection moulding was set at the conditions listed in Table 5.6, for all the formulations.

Tab. 5.6. *Injection moulding processing parameters for all composites.*

$T_{cylinder}$ (°C)	T_{mould} (°C)	Inj. P (bar)	P.Inj. P (bar)	Time (s)
250	90	650	200	5

*Inj. P: Injection pressure; P. Inj. P: Post-Injection pressure.

The same processing conditions have been maintained to produce the samples required for the characterisation analysis. Different moulds were used in order to produce dumb-bell samples for tensile tests, bar-shaped specimens for DMTA analysis, disk-shaped samples for rheology and thermal conductivity measurements. Difficulties have been observed during the fabrication of disk-shaped samples of the neat Nylon 6 (Icorene™). Specifically, the presence of air bubbles and degraded parts inside the material have been identified. FTIR analysis was performed in order to detect the chemical integrity of the specimens.

Compression moulding through hot pressing was carried out in order to produce disk-shaped sheet samples for electrical resistivity measurements. Few grams of extruded composite pellets have been introduced between two aluminium plates which were previously covered with PTFE tape in order to facilitate moulding removal. The hot-pressing processing parameters (listed in Table 5.7) have been maintained constant for all the composites formulations.

Tab. 5.7. *Compression moulding processing parameters for all composites.*

Step	Time (s)	Temperature (°C)	Pressure (bar)
1	120	240	5
2	10	240	5
3	240	240	100
4	650	30	100

Chapter 6

Results and Discussion

The following chapter deals with the description and interpretation of the experimental results obtained by the thermal, rheological, mechanical, morphological, electrical and chemical characterisation of Nylon 6 – Graphene nanocomposites.

6.1 Fourier Transform Infrared Spectrometer (FTIR)

FTIR analysis was performed on neat Nylon 6 in order to investigate functional groups and possible chemical modification of the polymer after the cryo-grinding treatment and high temperature processing for the production of the nanocomposites. Several previous researches have been carried out in order to better understand chemical and physical changes occurring in the material during degradation. Do *et al.* [97] noticed an increase of non-hydrogen bonded amine group and formation of different type of carboxylic groups during the thermal-oxidation of Nylon 6 samples. Svoboda *et al*. [98] found nitrile and vinyl ends group as result of the characterisation of the degradation products. FTIR investigation was performed on injected-moulded samples of Nylon 6 Icorene™ to verity the nature of visible brown zones in the section of disk-shaped and bar-shaped samples, after the process. The presence of these regions suggested that a degradation phenomenon could take place during the injection moulding performed at high temperature (250 °C) due to the oxidation of the polymer. The FTIR spectrum of PA6 samples (after and before injection moulding) is shown in Fig. 6.1. From this figure a most noticeable variation in the spectra of the two samples can be observed in the wavelength range between 1700 and 1800 cm^{-1}, with the appearance of an additive peak in the processed sample. This band is associated with the increment of carbonyl groups in the polymer structure, such as aldehydes, ketones, carboxylic acids etc. The result demonstrated that an oxidative

process occurred during the thermal process. A similar result was obtained also by Grigg (2006) [99]. In order to detect possible oxidative degradation during cryo-grinding, FTIR spectrometry was performed on the milled as well as the original Nylon 6 (Grilon®).

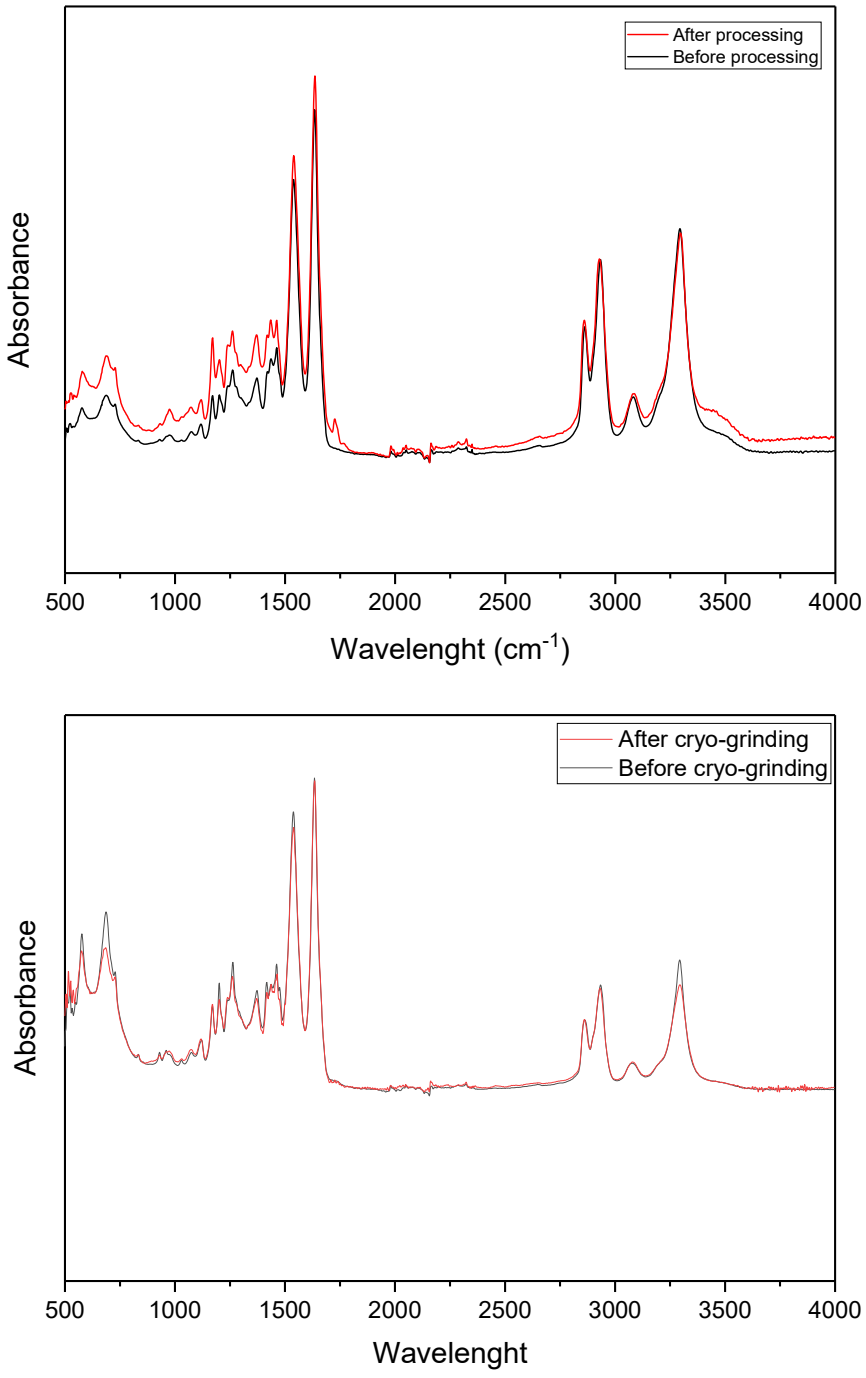

Fig. 6.1. *FTIR spectra comparison between (a) neat PA6 (Icorene™) before and after injection-moulding, and (b) neat PA6 (Grilon®) before and after cryo-grinding.*

From Fig. 6.1b it can be observed that no significant changes occurred after the cryo-grinding process, except for the reduction of the amine group (N-H) peak intensity (3300 cm^{-1}). This variation could be related to a different content of humidity into the two samples which affect the peak intensity related to the stretching of O-H functional group, which wavelength ranges from 3200 to 3350 cm^{-1}, thus overlapping with that of amine group.

6.2 X-ray Photoelectron Spectroscopy (XPS)

XPS measurements were performed on the filler (GNPs SE1233, in form of powder) in order to analyse the surface chemistry of the material. An immediate identification of the chemical composition of the material surface was obtained. In addition, chemical bonding information were determined from detailed analysis. The results are shown in the figures below.

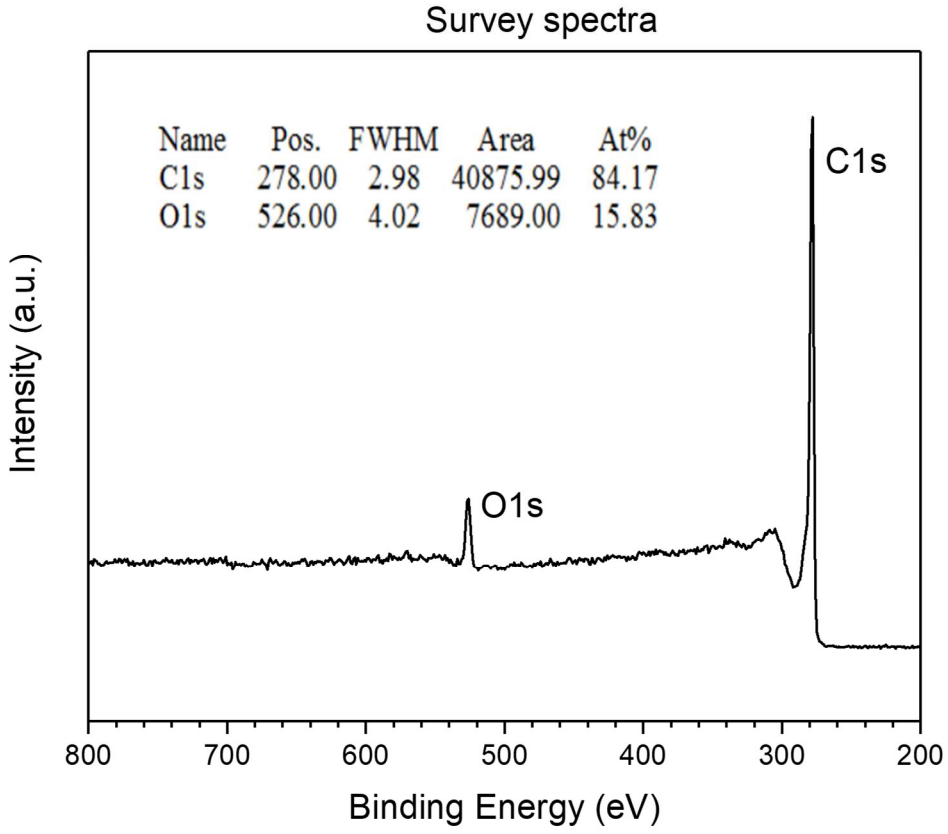

Fig. 6.2. *XPS general spectra of GNP powder.*

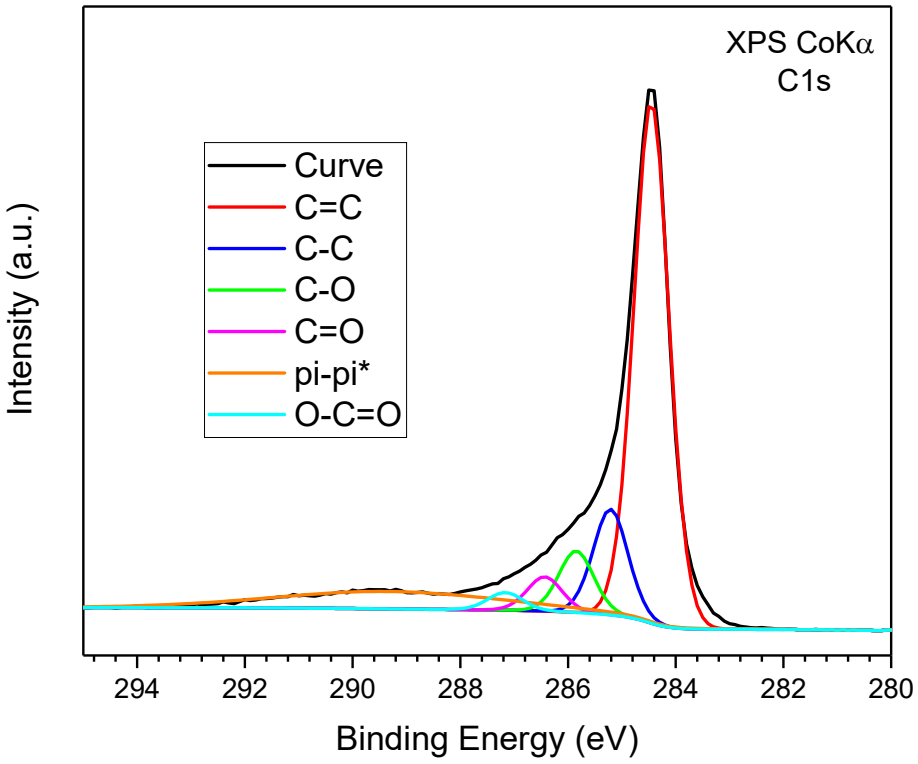

Fig. 6.3. *C1s XPS core level spectra of GNP powder.*

The general XPS spectra (Fig. 6.2) showed a C1s peak at 278 eV related to the graphene carbon based bonds (C=C and C-C) and a minor O1s peak which can be associated with physical oxygen adsorption in air from the filler's surface [100]. The oxygen and carbon concentrations of GNPs are equal to 15.83% and 84.17%, respectively, with a O/C ratio of 0.19. A considerable high level of oxidation is also indicated by the deconvoluted C1s spectrum of GNPs (Fig. 6.3). Oxygen adsorption manifested through the generation of oxygenated functional groups, such as epoxide, hydroxyl, carbonyl and carboxyl groups, which derived from the C=C (or sp^2 bond) bond-breakage and led to the formation of single C-C or sp^3 bonds.

Tab. 6.1. *Functional groups obtained from curve fitting of C1s XPS spectra.*

	C=C	**C-C**	**C-O**	**C=O**	**O-C=O**	**$\pi - \pi^*$**
B. E (eV)	284.5	285.2	285.9	286.4	287.2	289.5
%	61.00	12.36	7.21	4.02	2.06	13.35

Table. 6.1 shows the percentage distribution of the functional groups attached to GNPs. Carbonyl carbon (C=O), carboxylate carbon (O-C=O) and hydroxyl and epoxide groups (C-O) are present in not negligible quantities when compared with other studies on GNPs [101, 102]. This characteristic can affect the properties of graphene and make the material more electrically insulating, as stated by Mkhoyan *et al*. [103]. Moreover, a structural modification of graphene occurred due to the presence of functional groups, leading to an increase of disorder as in accordance with the graphene Raman Spectra, which is characterised by a large D/G band ratio. G band is associated with the relative motion of sp^2 carbon atoms, which in turn have been affected by the oxidation and converted in sp^3 atoms.

6.3 Raman Spectroscopy

Raman spectroscopy is a non-destructive technique commonly used for the chemical investigation of the material surface. By the use of a Renishaw inVia Confocal Raman Microscope, the PA6/GNPs composites samples were irradiated by a laser beam at 633 nm, with 1800 l/mm grating and 50x objecting lens. The analysis results provide a structural fingerprint from which it is possible to identify different molecules and study chemical bonding. The interest of this study was to detect the typical peaks of the graphene structure, by exploiting the response of sp^2 bonded carbons characteristics of this material. Fig. 6.4 shows the Raman spectra of graphene. The characteristic peaks of graphene structure are listed below:

- D band at ~1350 cm^{-1}, is related to the expansion and contraction of sp^2 carbon atoms in rings, although the rings must be adjacent to the edge or defect to be active [104]. When it is pronounced it means that the material contains a large number of defects both of chemical type (presence of functional groups unrelated to the graphitic structure) and of physical type (for example the curled edges).
- G band at ~1582 cm^{-1}, is representative of in-plane vibrational mode of sp^2 hybridized carbon atoms of graphene. The position of the band is quite independent with respect to the frequency of the incident laser, while it varies according to the height of the graphene analysed: the more layers are, the more the peak moves to lower levels of energy.

- 2D band: ~ 2700 cm^{-1}, also called G ', is due to the vibrational process and the consequent emission of two phonons of the lattice, but unlike the D band it is active not only near the defects. The shape and position of this peak are the most studied aspects for the identification of the graphene height. It has been shown that the more the layers of the material increase, the greater the characteristic wave number, while the shape of the peak assumes a shoulder shape, typical of graphite, since the band is no longer constituted by a single component as in the ideal case of a monolayer.

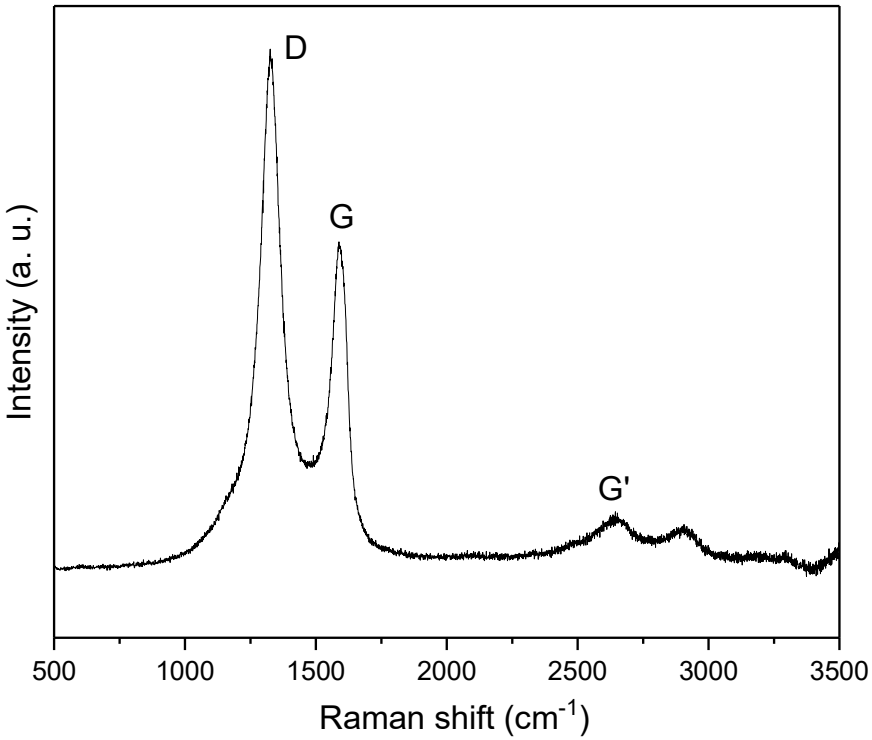

Fig. 6.4. *Raman spectra of GNPs in form of powder.*

The peak position in the Raman spectra of the sample of Graphene SE1233 are listed in Tab. 6.2.

Tab. 6.2. *Data from Raman spectra of graphene.*

Peak type	Peak position (cm^{-1})
D	1325.4
G	1588
G’	2647.2

Moreover, the ratio between the intensity of 2D and G peak (I_{2D}/I_G) and the ratio between the intensity of D and G peak (I_D/I_G) were calculated and shown in Tab. 6.3.

Tab. 6.3. *Data from Raman spectra of graphene.*

Ratio type	Value
I_{2D}/I_G	0.15
I_D/I_G	1.57

The following graphs show a comparison between the Raman spectra of unfilled PA6 and its composites.

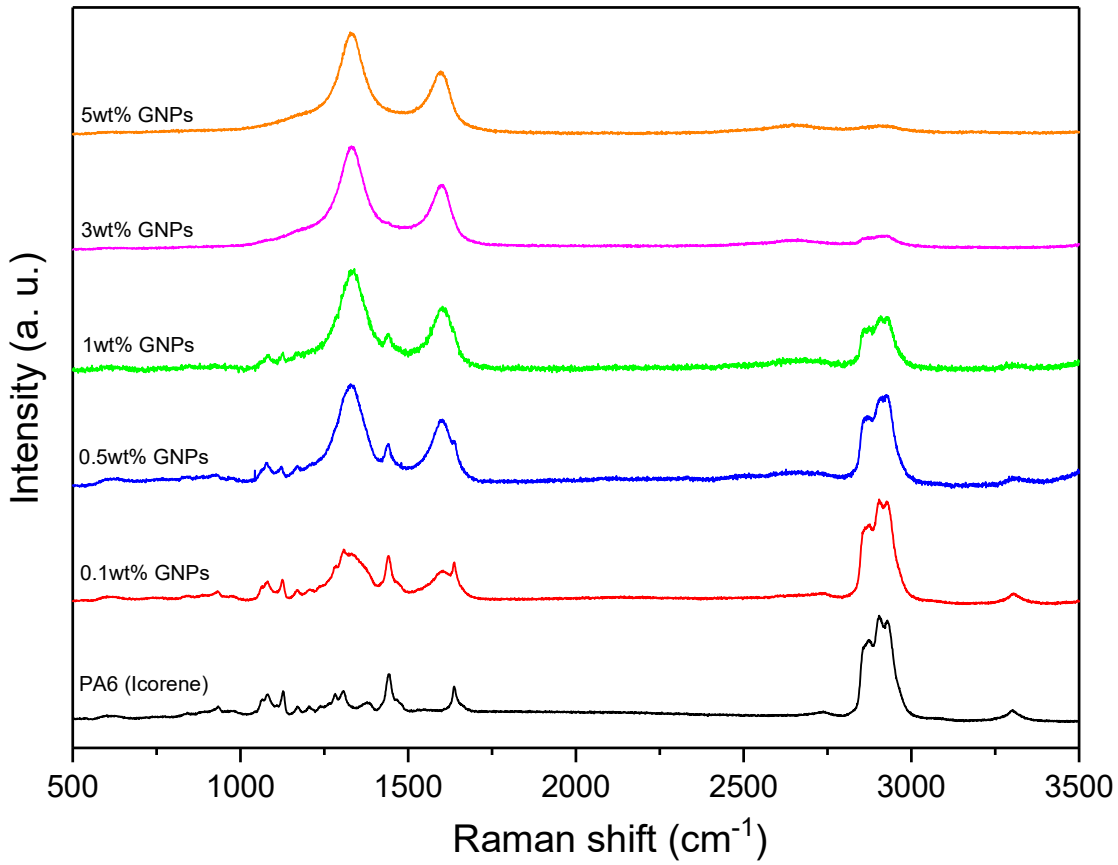

Fig. 6.5. *Raman spectra of unfilled PA6 and PA6/GNPs composites based on Icorene™.*

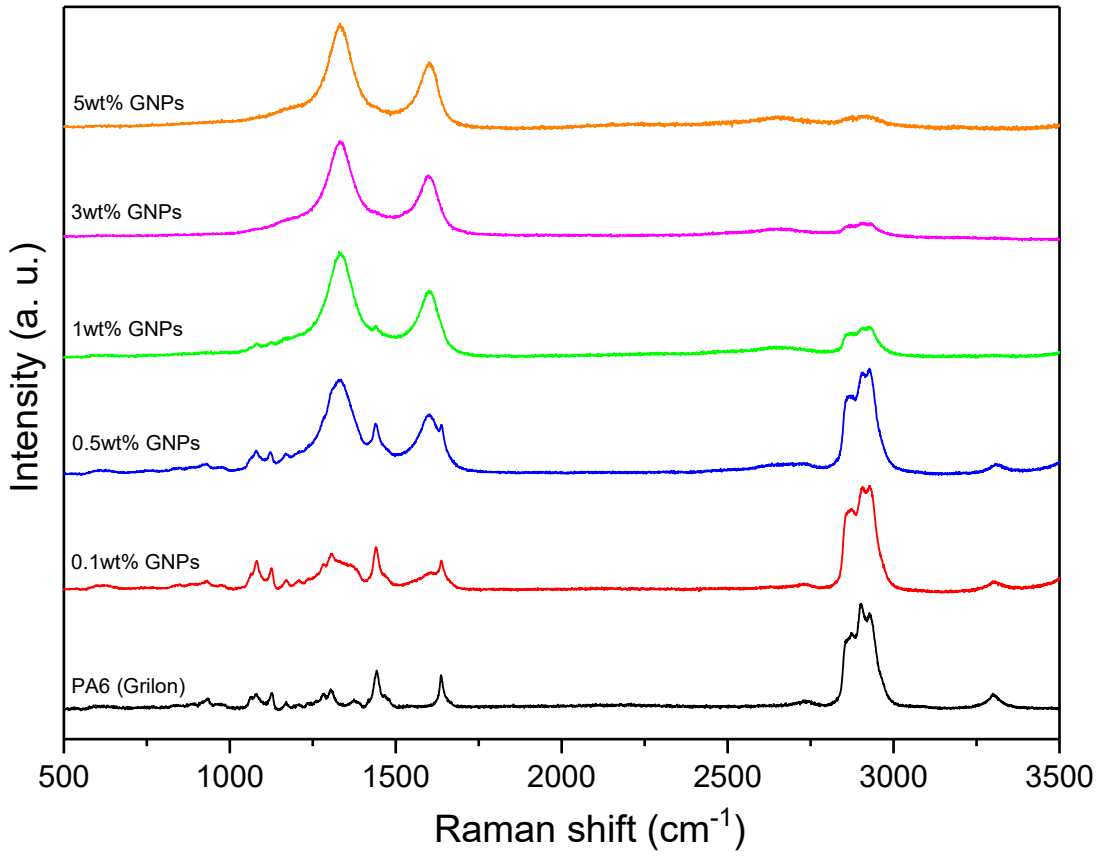

Fig. 6.6. *Raman spectra of unfilled PA6 and PA6/GNPs composites based on Grilon®.*

It is apparent from Fig. 6.4 that D band of Graphene SE1233 is particularly pronounced, which reflects that the material contains many defects. In addition, from the intensity ratio between 2D peak and G peak it is possible to obtain information regarding graphene layer thickness. Typically, for a high quality (no defect) single layer graphene the ratio I_{2D}/I_G is equal to 2, and tend to decrease with a higher number of graphene sheets. The test sample showed a ratio equal to 0.15, suggesting that more than 5-6 layers are present in the material structure. It is not possible to define the exact value of layers because after 5-6 of them, the value of the ratio does not decrease anymore. Similar spectra of carbon materials have been reported by Bokobza *et al*. [105]. The addition of successive layer of graphene lead to the formation of a broader and weaker 2D band than the one of a single layer graphene. Particularly, a significant variation of 2D shape was observed passing from single layer graphene to graphite which shows a double peak structure. It can be concluded that the Graphene SE1233 is characterised by a multilayer structure, given the

fact that with more than 5 layers, the shape of 2D band tend to be similar to that of graphite, characterised by two main components. The data related to the Raman spectra of PA6/GNPs composites are tabulated below.

Tab. 6.4. *Data from Raman spectra of PA6/GNPs composites (Icorene™).*

	D peak Position (cm^{-1})	G peak Position (cm^{-1})	2D peak Position (cm^{-1})	I_{2D}/I_G	I_D/I_G
PA6 (Icorene)	-	-	-	-	-
0.1wt% GNPs	1307.8	1604	2734.4	0.35	1.60
0.5wt% GNPs	1328.2	1596.9	2670.7	0.26	1.51
1wt% GNPs	1331	1604.9	2661.2	0.23	1.55
3wt% GNPs	1332.9	1603.1	2652.4	0.18	1.58
5wt% GNPs	1331.1	1596.2	2659.7	0.20	1.57

Tab. 6.5. *Data from Raman spectra of PA6/GNPs composites (Grilon®).*

	D peak Position (cm^{-1})	G peak Position (cm^{-1})	2D peak Position (cm^{-1})	I_{2D}/I_G	I_D/I_G
PA6 (Icorene)	-	-	-	-	-
0.1wt% GNPs	1304.9	1597.8	2730.1	0.52	1.89
0.5wt% GNPs	1331	1600.4	2705.1	0.22	1.55
1wt% GNPs	1335.7	1600.5	2655.3	0.19	1.54
3wt% GNPs	1330	1591.5	2653.1	0.28	1.48
5wt% GNPs	1331.9	1600.4	2658.2	0.21	1.56

6.4 Thermal Properties

6.4.1 Thermal Gravimetric Analysis (TGA)

Thermal gravimetric analysis is an experimental technique which is useful for measuring the thermal stability of a material and extrapolate its maximum operating temperature, above which degradation starts to take place. In this study, all tests were performed from

25 to 800 °C at a heating rate of 10 °C/min in air atmosphere, using alumina crucibles. Samples with a weight of less than 5 mg were prepared by cutting the edge of injection-moulded specimens. A comparison between the thermal responses of the unfilled PA6 (for both types of polyamides) and PA6/GNPs composites was carried out, by determining the temperatures at which a specific weight % loss occurred. The same procedure was repeated for the analysis of the filler itself, in powder form. Two kinds of graphs are typically represented in relation to the thermal gravimetric measurements, as shown in Fig. 6.7 and Fig. 6.8. The first graph displays the variation of the % weight loss as a function of the temperature (TGA curve). From this curve, the initial decomposition temperature (T_d) at which 5% of weight loss of the sample occurs can be determined, as well as $T_{10\ wt\%}$ and $T_{50\ wt\%}$ (10% and 50% weight loss, respectively). In addition, differential thermogravimetric thermograms (DTA) curves can be plotted by calculating the first derivative of weight loss curves. The temperature at which the maximum weight loss rate occurs (T_{max}) was determined from the peak value of the DTA thermograms, as well as the onset temperature (T_{onset}), which is determined by the intersection of the tangent of the peak with the baseline. Figure 6.7 and Fig. 6.8 shows TGA and DTA curves obtained for the two types of Nylon 6 (Icorene™ N9602 and Grilon® BS/2), respectively.

TGA/DTA curves for raw materials:

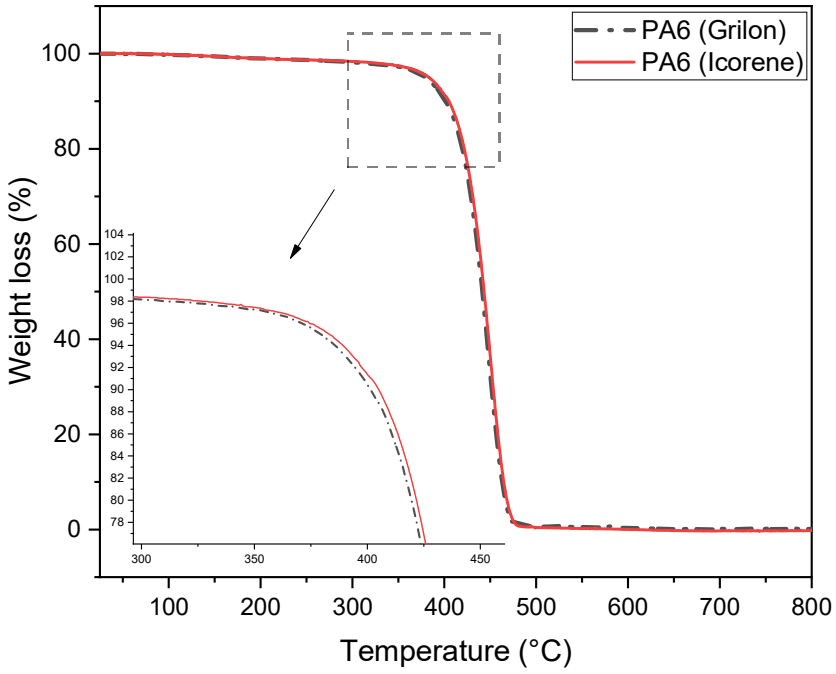

Fig. 6.7. *TGA curves of unfilled PA6 (both types).*

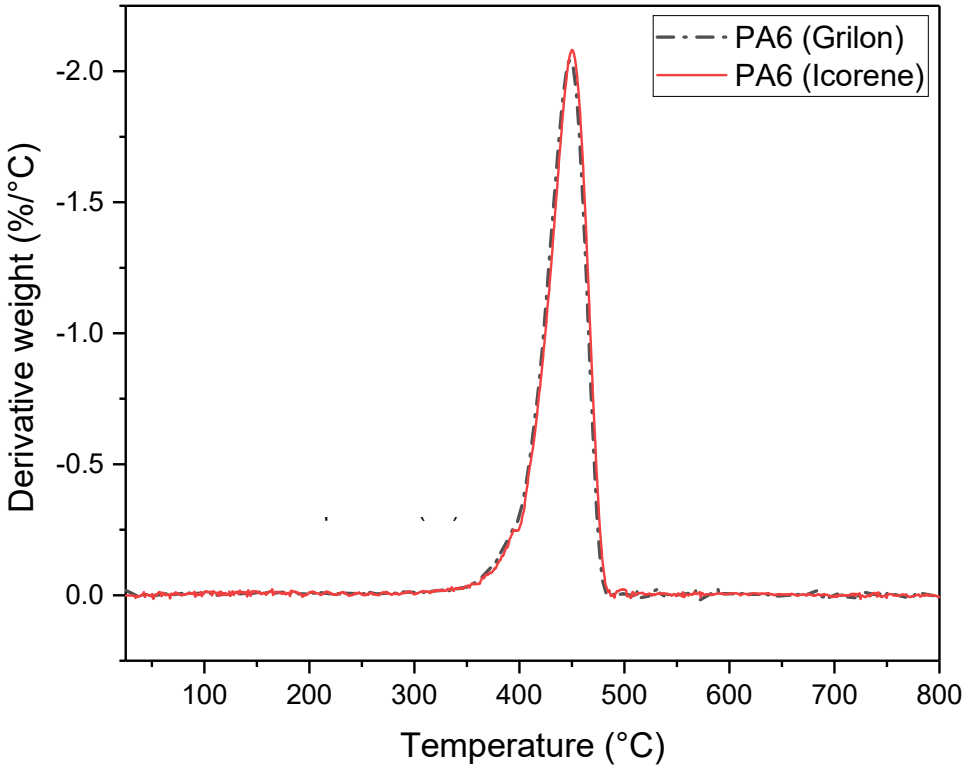

Fig. 6.8. *DTA curves of unfilled PA6 (both types).*

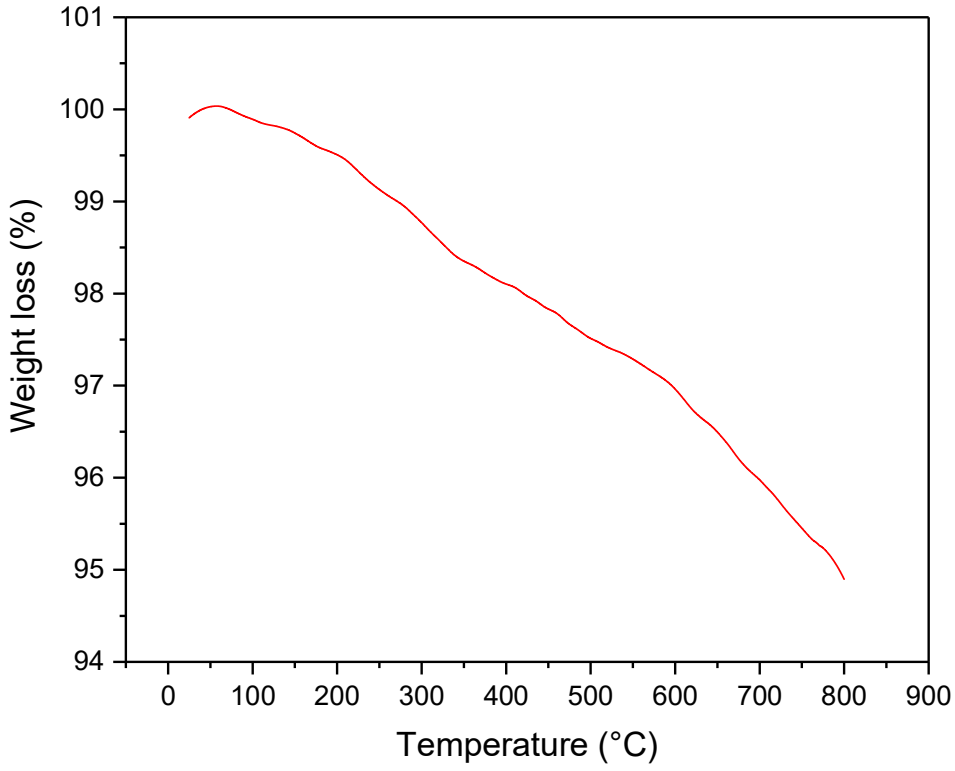

Fig. 6.9. *TGA curve of GNPs.*

TGA/DTA curves of PA6/GNPs composites:

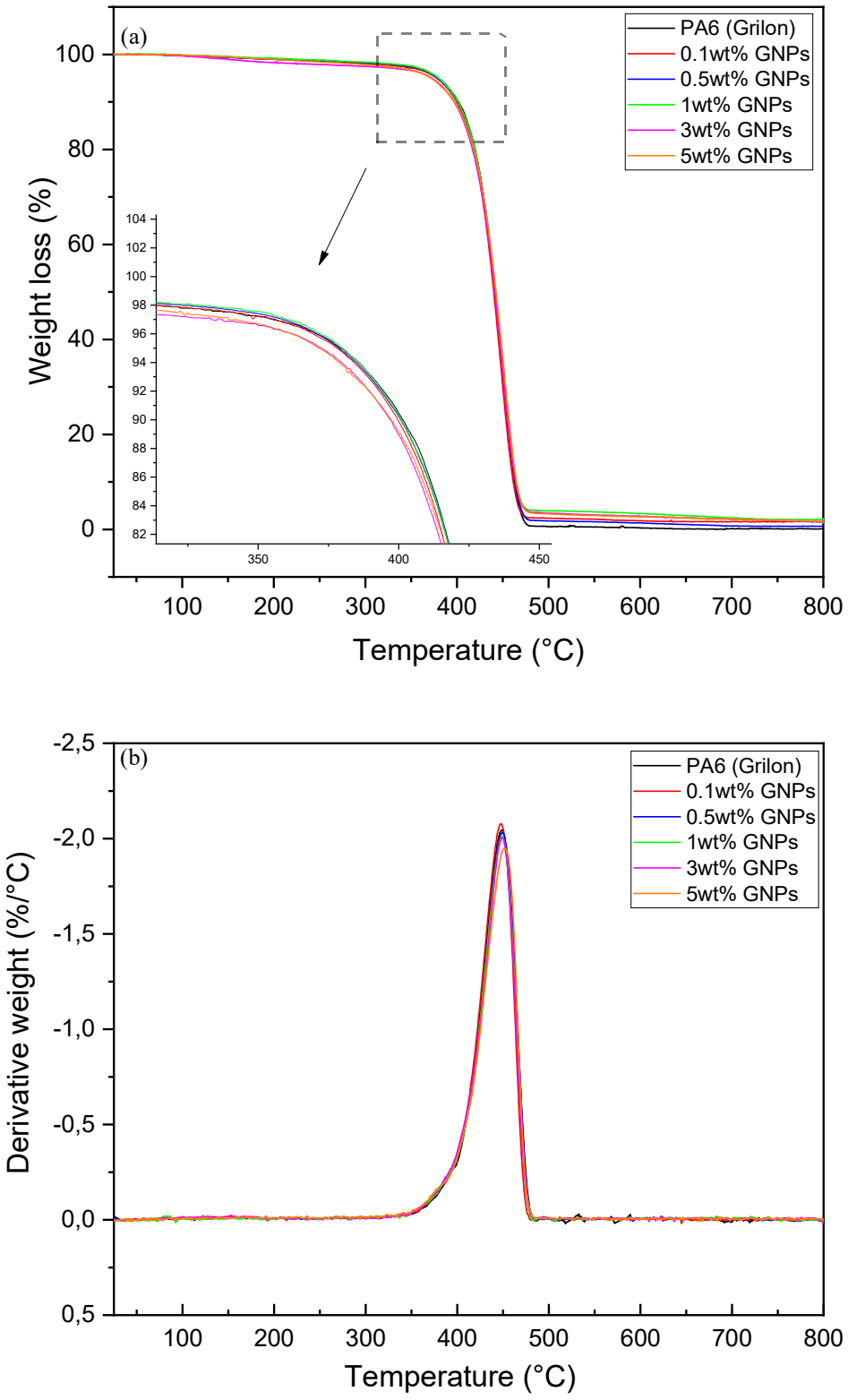

Fig. 6.10. *(a) TGA and (b) DTA curves of PA6 (Gilon®/GNPs composites.*

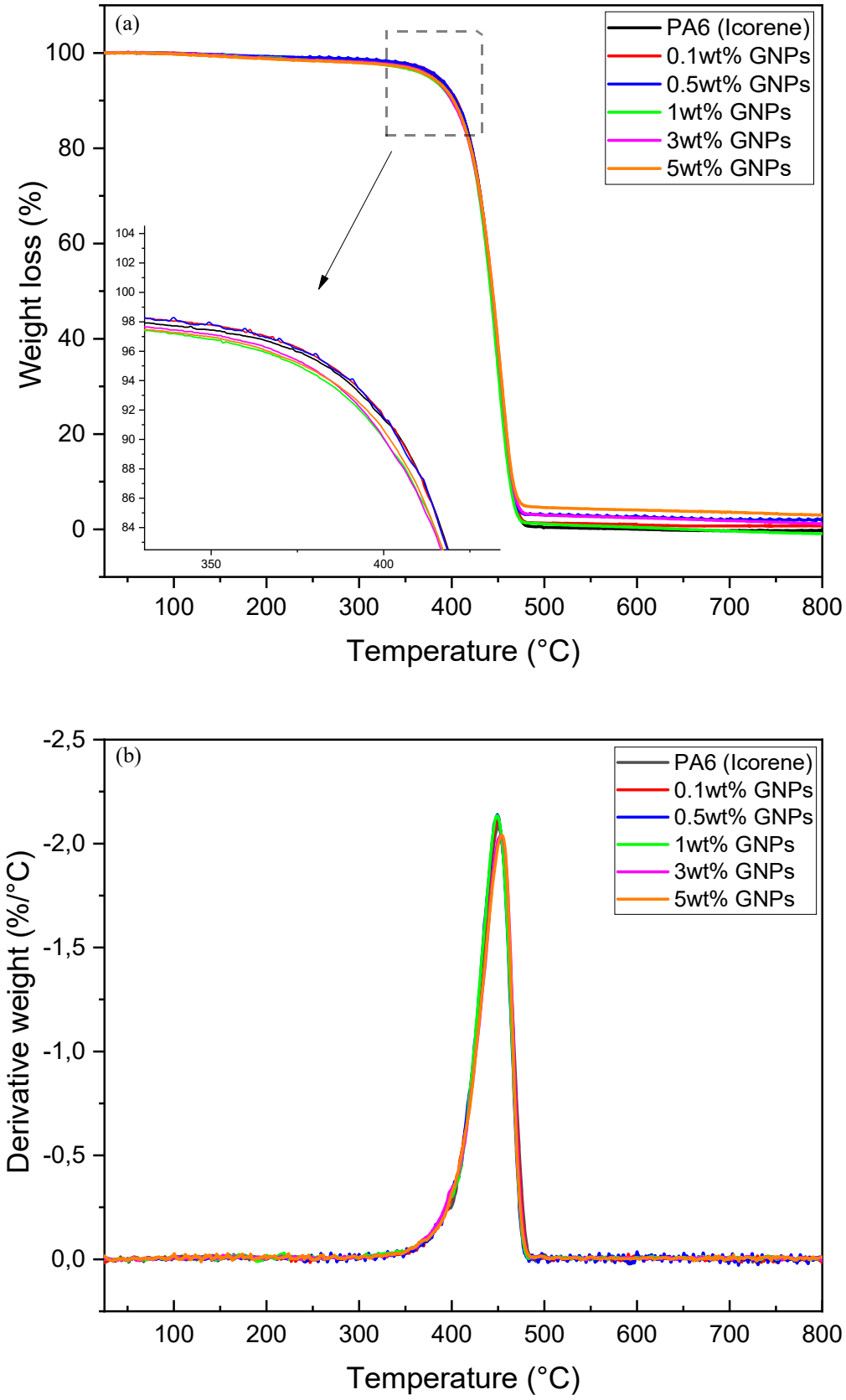

Fig. 6.11. *(a) TGA and (b) DTA curves of PA6 (Icorene™)/GNPs composites.*

In order to clarify the TGA graphs, all the data related to the abovementioned parameters are listed in the tables below.

Tab. 6.6. *Data obtained from TGA analysis.*

Samples	T_d (°C)	$T_{10\ wt\%}$ (°C)	$T_{50\ wt\%}$ (°C)	T_{max} (°C)	T_{onset} (°C)	Residue at 600 °C (wt%)
PA6 (Grilon)	379	402	441	449	399	0
0.1wt% GNPs	378	400	440	448	402	2
0.5wt% GNPs	379	401	442	449	402	1
1wt% GNPs	380	401	442	449	402	3
3wt% GNPs	372	397	441	449	403	3
5wt% GNPs	372	397	443	452	398	3

Samples	T_d (°C)	$T_{10\ wt\%}$ (°C)	$T_{50\ wt\%}$ (°C)	T_{max} (°C)	T_{onset} (°C)	Residue at 600 °C (wt%)
PA6 (Icorene)	383	405	443	450	403	0
0.1wt% GNPs	385	405	443	450	403	1
0.5wt% GNPs	384	404	443	449	401	3
1wt% GNPs	375	400	442	450	406	1
3wt% GNPs	378	400	444	453	403	2
5wt% GNPs	377	402	444	450	402	4

The TGA curves demonstrated that only one decomposition stage took place during the heating process, and that T_d slightly decreased as the graphene content increased (about 8 and 6 °C for Grilon® and Icorene™, respectively). The trend of TGA and DTA curves of the neat polyamide 6 (for both types) is similar to the one of the nanocomposites with different graphene content, as also confirmed by the T_{max} which has not changed significantly. This suggests that there was not a sensible variation of the thermal stability of the polymer even in the presence of the filler. From the TGA curves it can be also observed a difference in term of weight residue due to different concentration of GNPs in the polymer. The presence of a higher weight residue with increasing filler loading is justified by the high thermal stability of graphene, which undergoes just 5% of weight loss at about 800 °C, as shown in Fig. 6.9. Different authors stated that the presence of nanofillers inside a polymer helps to improve the thermal stability of the matrix, by

increasing the heat dissipation and by acting as a heat protective barrier for the polymer [106, 107]. This effect can take place if the nanofillers are well dispersed into the polymer matrix and have a high surface area which promotes a much better adhesion with the polymer chain. A possible reason why the thermal stability of the polyamide 6 has not been affected by the presence of the GNPs could be related to the weak adhesion between the polymer matrix and the additives as well as to the damaging of the graphene nanoplatelets caused by the strong shear forces involved in the extrusion process.

6.4.2 Differential Scanning Calorimetry (DSC)

Differential scanning calorimetry was carried out to measure the amount of heat absorbed or released by the material during phase transitions, in order to detect the crystallisation and melting behaviour of Nylon 6 and its composites. DSC analysis were conducted in accordance with a heating-cooling-heating cycle in order to remove the thermal history of the polymer. For this reason, the samples were firstly heated from 25 to 280 °C at a rate of 10 °C/min under an inert nitrogen atmosphere, and then held for 2 minutes in an isothermal state. Subsequently, the material was cooled at room temperature and re-heated at 280 °C at a rate of 10 °C/min. Samples have been obtained by cutting small portions of material from the injected-moulded specimens. Few grams (from 5 to 10 grams) of material were introduced in a pre-weighed aluminium crucible which was then subjected to the heating and cooling program. The following figures shows the crystallisation and melting peaks of neat PA6 and PA6/GNPs composites.

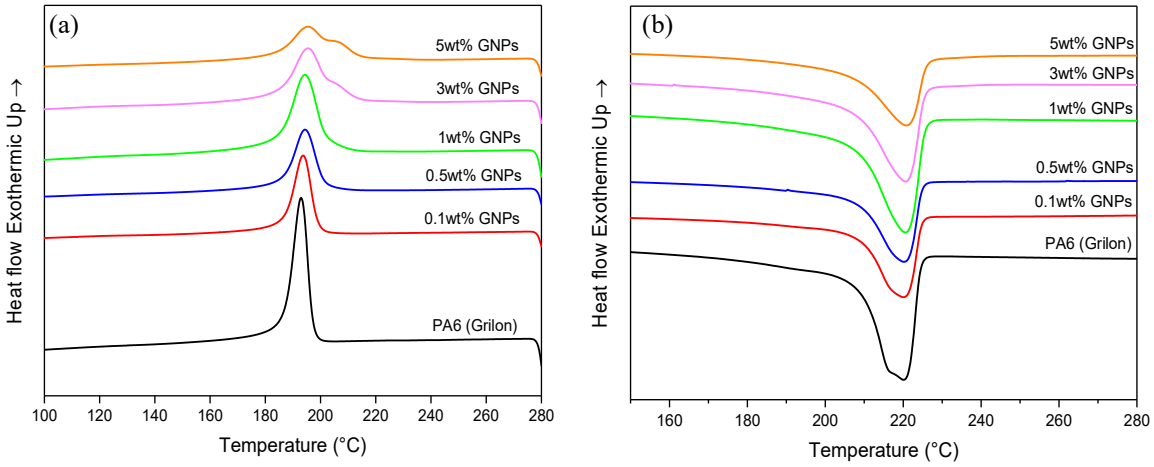

Fig. 6.12. *Crystallisation exotherms (a) and melting endotherms (b) of unfilled PA6 (Grilon®) and PA6/GNPs nanocomposites.*

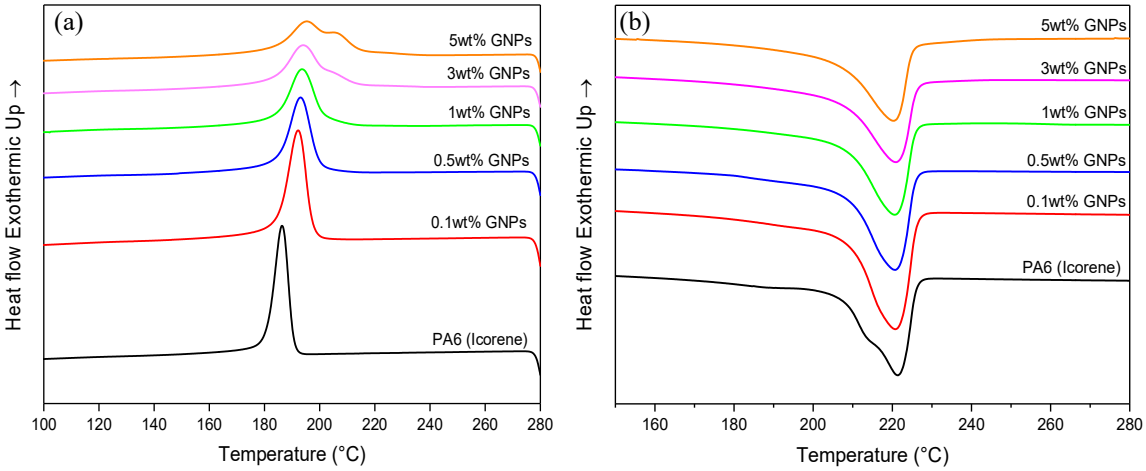

Fig. 6.13. *Crystallisation exotherms (a) and melting endotherms (b) of unfilled PA6 (Icorene™) and PA6/GNPs nanocomposites.*

From the crystallisation exotherms and the melting endotherms it is possible to determine several representative data for each sample. The crystallisation temperature (T_c) and the melting temperature (T_m) were obtained as the temperature corresponding to the crystallisation and melting peak, respectively. In addition, the onset temperature (T_{onset}) was derived as the intercept of the tangent of the peak with its baseline. Lastly, the enthalpy of fusion (ΔH_m) and the enthalpy of crystallisation (ΔH_c) were calculated from the integral of the area under the peak curve, normalized by the sample weight. The measurement of the degree of crystallinity of the sample was also performed by using the following equation.

$$X_c\,(\%) = \frac{\Delta H_m}{(1 - w_f)\Delta H_m^0} * 100 \qquad (6.1)$$

where $X_c(\%)$ is the percentage crystallinity, w_f is the filler weight fraction and the ΔH_m^0 is the melting enthalpy of a 100% crystalline PA6, the value of which is equal to 230 J/g, as proposed by Khanna and Kuhn [108]. All the representative data abovementioned are summarised in the following tables.

Tab. 6.7. *Data obtained from DSC analysis.*

	Cooling			Second heat				
	T_c onset (°C)	T_c peak (°C)	ΔH_c (J/g)	T_m onset (°C)	T_m peak (°C)	ΔH_m (J/g)	X_c (%)	Impr. * (%)
PA6 (Icorene)	191	187	66	206	221	68	30	-
0.1wt%	198	193	65	208	220	73	32	7
0.5wt%	200	194	64	207	220	71	31	3
1wt%	202	194	61	207	220	72	32	7
3wt%	205	194	66	205	221	73	33	10
5wt%	210	196	64	204	220	76	35	17
	Cooling			Second heat				
	T_c onset (°C)	T_c peak (°C)	ΔH_c (J/g)	T_m onset (°C)	T_m peak (°C)	ΔH_m (J/g)	X_c (%)	Impr. * (%)
PA6 (Grilon)	198	194	65	208	220	71	31	-
0.1wt%	199	194	61	208	220	72	31	0
0.5wt%	202	195	61	207	220	78	34	10
1wt%	203	195	61	207	220	72	32	3
3wt%	205	196	62	206	220	74	33	6
5wt%	208	196	61	204	221	75	34	10

*Impr. → percentage increase of X_c of the composite with respect to PA6 unfilled.

The variation of the melting and crystallisation temperature of the nanocomposites as a function of the filler concentration is shown in the figures below.

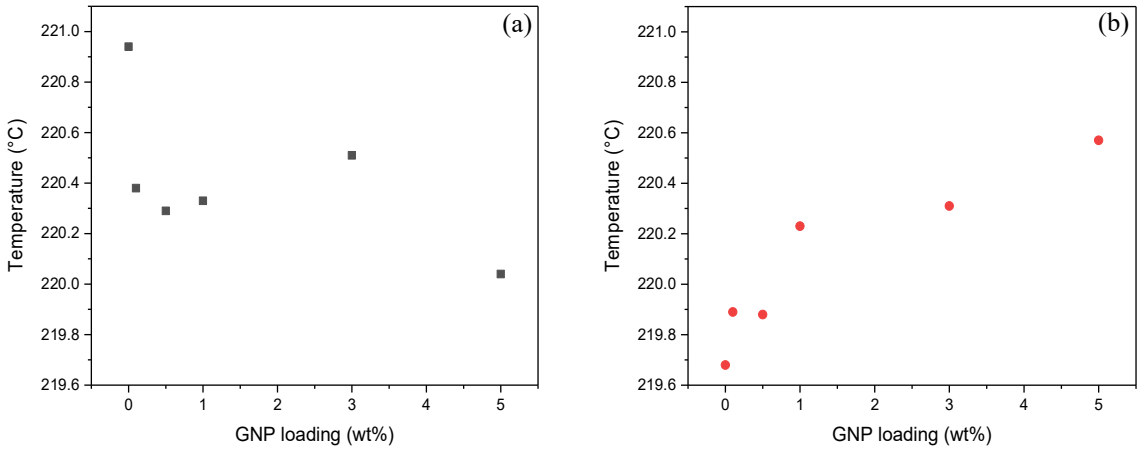

Fig. 6.14. *Effect of the %GNPs on the melting temperature (T_m) for PA6 (Grilon®)/GNPs composites (a) and PA6 (Icorene™)/GNPs composites (b).*

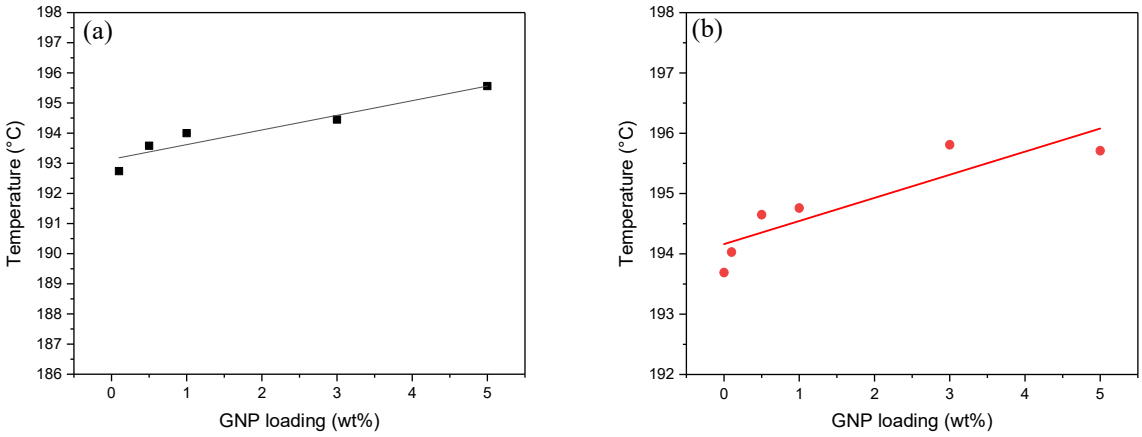

Fig. 6.15. *Effect of the %GNPs on the crystallisation temperature (T_c) for PA6 (Grilon™)/GNPs composites (a) and PA6 (Icorene®)/GNPs composites (b).*

The results in table 6.7 show that the melting temperature of both types of Polyamide 6 is not particularly affected by the addition of graphene nanoplatelets. The crystallisation temperature, in contrast, tends to increase with higher filler content, particularly for Icorene™ N9602. This effect is also visible in Fig. 6.13a, in which the crystallisation exotherms tend to shift on the right side of the graph. In addition, it can be observed a change in the shape of the crystallisation peaks, with a much broader and shorter peak for high filler content composites than the one of the unfilled polymer. Particularly, at 5 wt% of GNPs, the crystallisation curve manifests the formation of a double-peak, which indicates that the nanofillers act as nucleating agents. Similar results have been obtained with other fillers [109, 110]. Table 6.7 also shows an increase in the degree of crystallisation, which results higher for Icorene™ based composites. This suggests that the higher molecular weight (and therefore viscosity) of the Incorene™ unfilled PA6 with respect Grilon®, may have led to a better enhancement of the composite crystallisation.

Polyamide 6 is characterised by the presence of two different crystalline phases, called α and γ, and their formation is affected by the condition of crystallisation (such as the cooling rate) and the presence of nanofillers into the polymer matrix. Zhang and Wan [111] reported the results of DSC measurements on unfilled PA6 and MWCN reinforced PA6. XRD pattern exhibited the predominant presence of γ-form crystallites in neat PA6, whilst the composites showed an enhancement of α phase with increasing filler content. In the same way, a tendency to favour the crystallisation of α phase can be recognised in

PA6/GNPs composites by the formation of a second peak in the crystallisation exotherms at 5wt% of GNPs. Hence, a mixed crystalline structure began to form with increasing content of the filler. Particularly, the characteristic crystalline peak of unfilled PA6 showed a change with higher filler content, by becoming weaker and broader, suggesting that the complete formation of γ-form crystallite is limited by the filler presence. At the same time, the α-form crystallite was being favoured to form. Fig. 6.12b and 6.13b show that both types of unfilled PA6 present two melting peaks at about 214 and 221 °C. The second peak is associated with the melting process of γ-form crystallites which have a melting point below the one of α phase, as confirmed by Zhen Xu and Chao Gao [112]. With increasing content of GNPs, the peak at lower temperature tend to disappear, which suggests that the presence of the nanofillers prevented the formation of the γ-form crystallites and therefore, their fusion heat is not detectable.

6.5 Dynamic Mechanical Thermal Analysis (DMTA)

Dynamic mechanical thermal analysis was performed on melt processed PA6/GNPs nanocomposites in order to study the viscoelastic behavior of the unfilled polymer and its composites, as well as obtaining a location of the glass transition temperature (T_g) of the material. The analysis was carried out according to ASTM D-5418 by using bar-molded samples with a cross sectional area of 10 x 4 mm^2 and useful length equal to 17.50 mm. The instrument (Tritec 2000 DMA) operated in dual-cantilever mode at a fixed frequency of 1 Hz, at a temperature range from -50 to 200 °C, linear displacement at 0.015 mm and with cooling and heating rate of 3 °C min^{-1}.

The storage modulus obtained from the DMTA measurements was plotted in function on the temperature in order to investigate the effect of GNPs on both types of PA6. With the same purpose, tan δ (ratio between loss and storage modulus) is represented in function of the temperature to identify the glass transition temperature.

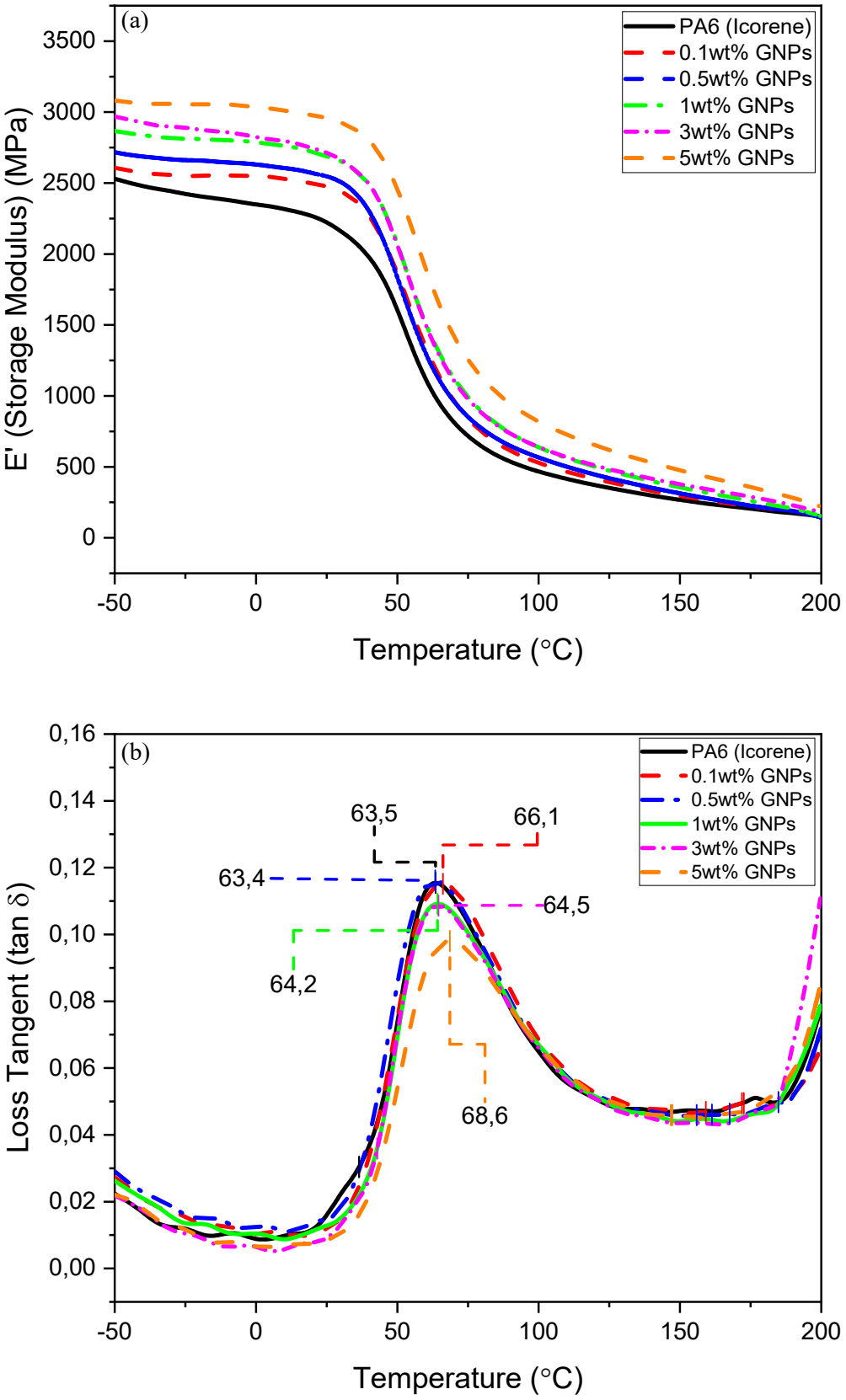

Fig. 6.14. *Variation of (a) Storage Modulus (E') and (b) Loss Tangent (tan δ) as a function of GNPs concentration, for PA6 (Icorene™)/GNPs composites.*

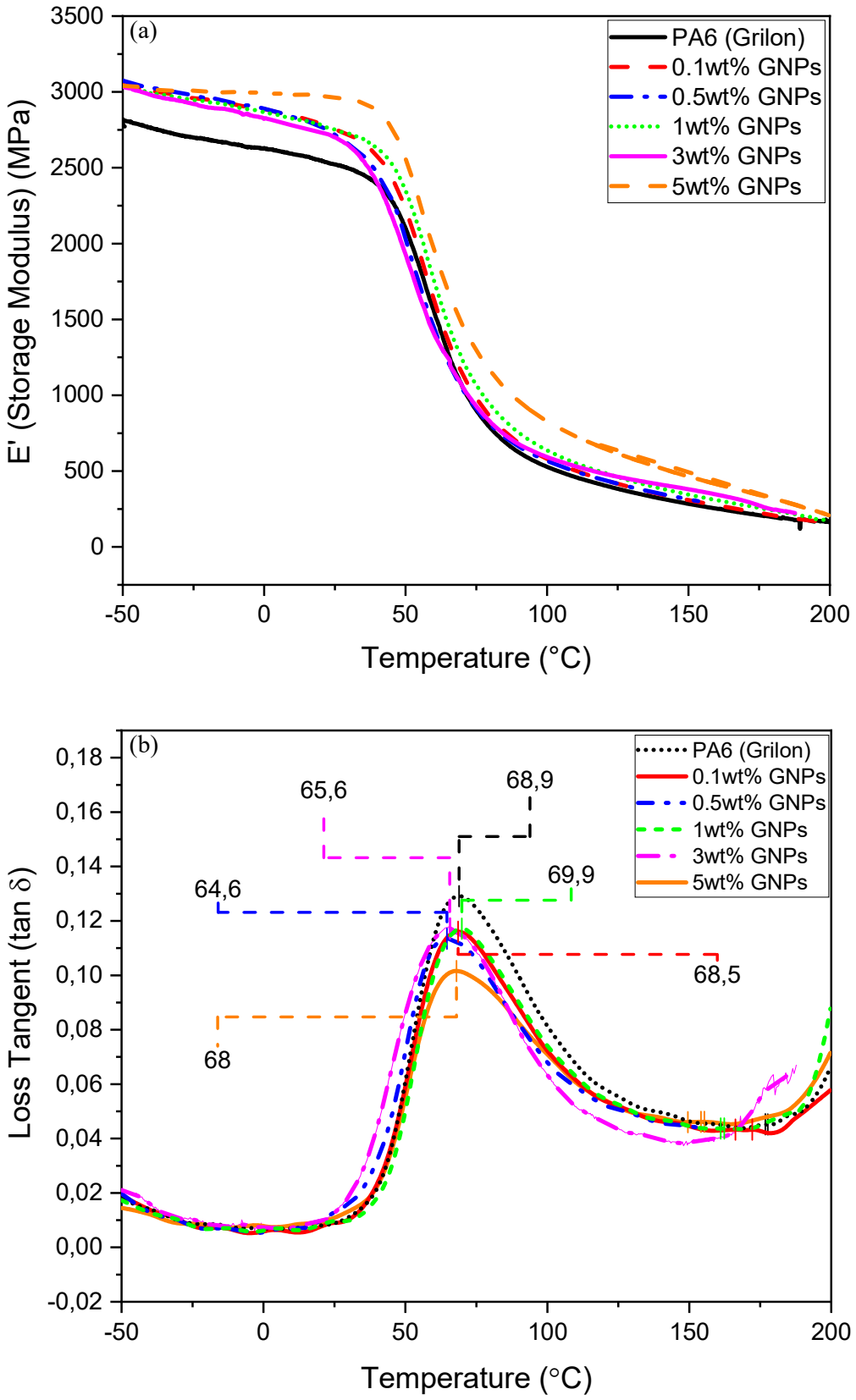

Fig. 6.15. *Variation of (a) Storage Modulus (E') and (b) Loss Tangent (tan δ) as a function of GNPs concentration, for PA6 (Grilon®)/GNPs composites.*

Figure 6.14a (and 6.15a) exhibits the profile of the storage modulus in function of the temperature. It is possible to notice a sharp variation of the mechanical response of the material with increasing temperature, and this is due to the overcoming of the glass transition temperature of the polymer. Above T_g the mobility of the polymer chains is enhanced and the material became less rigid, so that the elastic portion of the mechanical behaviour of the material is decreased. The storage modulus of the PA6 composites is slightly enhanced by the introduction of the graphene nanofillers. For instance, the modulus of PA6 (Grilon®) at 0 °C increased from 2627 to 2987 MPa (~ 14% of improvement) with a content of 5wt% of GNPs, whilst the modulus of PA6 (Icorene) increased from 2349 to 3035 MPa (~29%). This result is related to the constrained effect exercised by the graphene surface on the polymer chains which are present in the interphase zone around each platelet [113]. A good dispersion of the filler leads to an increase of the filler surface area in contact with the polymer chains, and to the consequent reduction of their mobility. This affect the storage modulus as well as the T_g which tends to shift to higher values. From the tan δ curves shown in Fig. 6.14b (and 6.15b) it is possible to conclude that the T_g is slightly affected by the presence of GNPs. A comparison of the T_g variation for the two polymer systems is shown in Fig. 6.16. It can be concluded that a greater improvement in terms of storage modulus and T_g occurred in Icorene™ based composites, with increasing filler loading. This difference was possibly due to the higher molecular weight (and therefore viscosity) of the unfilled PA6, than the Grilon® type, as in accordance with the DSC results.

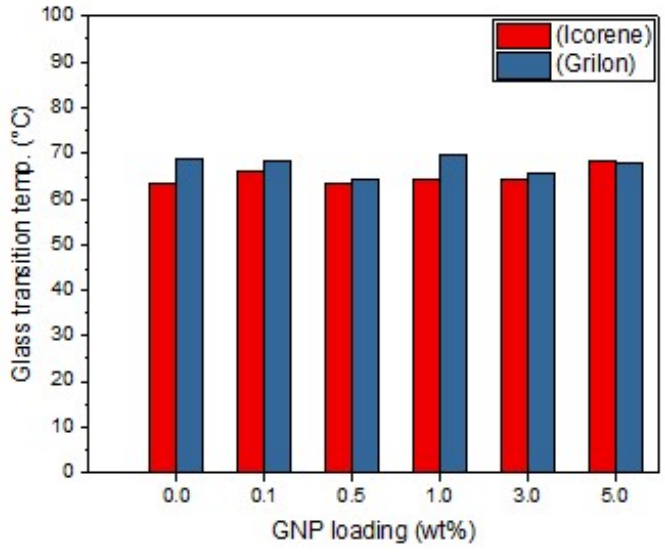

Fig. 6.16. *Variation of glass transition temperature as a function of GNPs loading.*

6.6 Rheological Properties

The rheological investigation of unfilled PA6 (both types) and PA6/GNPs nanocomposites have been performed using Haake Mars Modular Advanced rheometer. This machine in equipped with a plate-plate system (one stationary and one movable) surrounded by a movable oven. Injection-molded disk samples of 1.5 mm thick were inserted between the parallel circular plates (plate diameter of 25 mm and gap between them set to 1 mm). The first measurement was carried out in Oscillation Stress Sweep Mode (OSS) in order to identify the linear viscoelastic range of the material. The result of this first test are represented in Fig. 6.17.

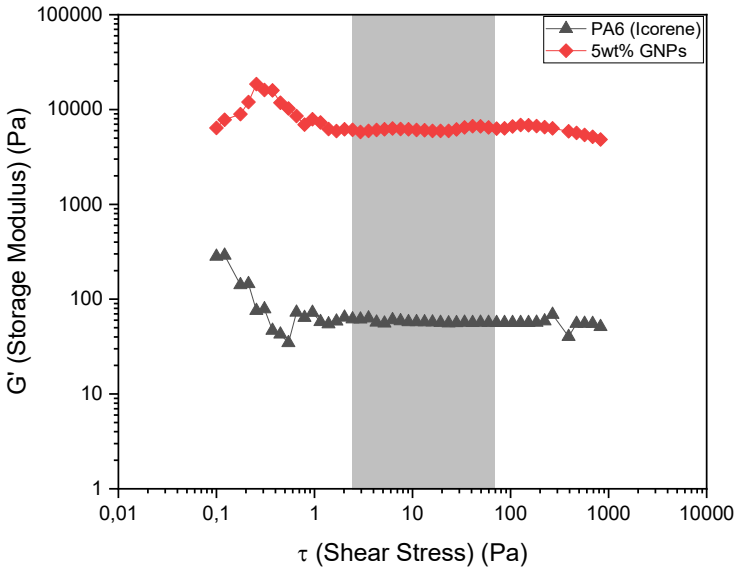

Fig. 6.17. *Result of oscillation stress sweep mode test.*

OSS experiments were performed over a shear stress range from 0.1 to 1000 Pa, at a fixed temperature and frequency of 240 °C and 1 Hz, respectively. The test was conducted for both types of PA6 and PA6/GNPs composites with 5wt% of GNPs, in order to detect the elastic region of the material. In this zone, the strain is small enough to prevent the storage modulus (G') to be dependent on the shear stress (τ) value. From the curve shown in Figure 6.17 it is possible to observe that the elastic region extends in the stress range close to 10 Pa. For this reason, the value of shear stress of 10 Pa has been selected for being used for Oscillation Frequency Sweep (OFS) experiments. Given the fact that 10 Pa was detected for both the neat polymer and the composite with highest GNPs content, it was

possible to assume the same value to be appropriate also for the other compositions. The OSS results regarding the second type of PA6 (Grilon®) have not been reported to avoid repetition. OFS experiments were performed by applying a constant shear stress (10 Pa) on the samples, in a frequency range from 0.01 to 100 Hz and again, at fixed temperature of 240 °C. The data experimental data were obtained by using the Thermo Scientific rheology data software. All the rheological properties of PA6 and PA6/GNPs composites are shown in the figures below.

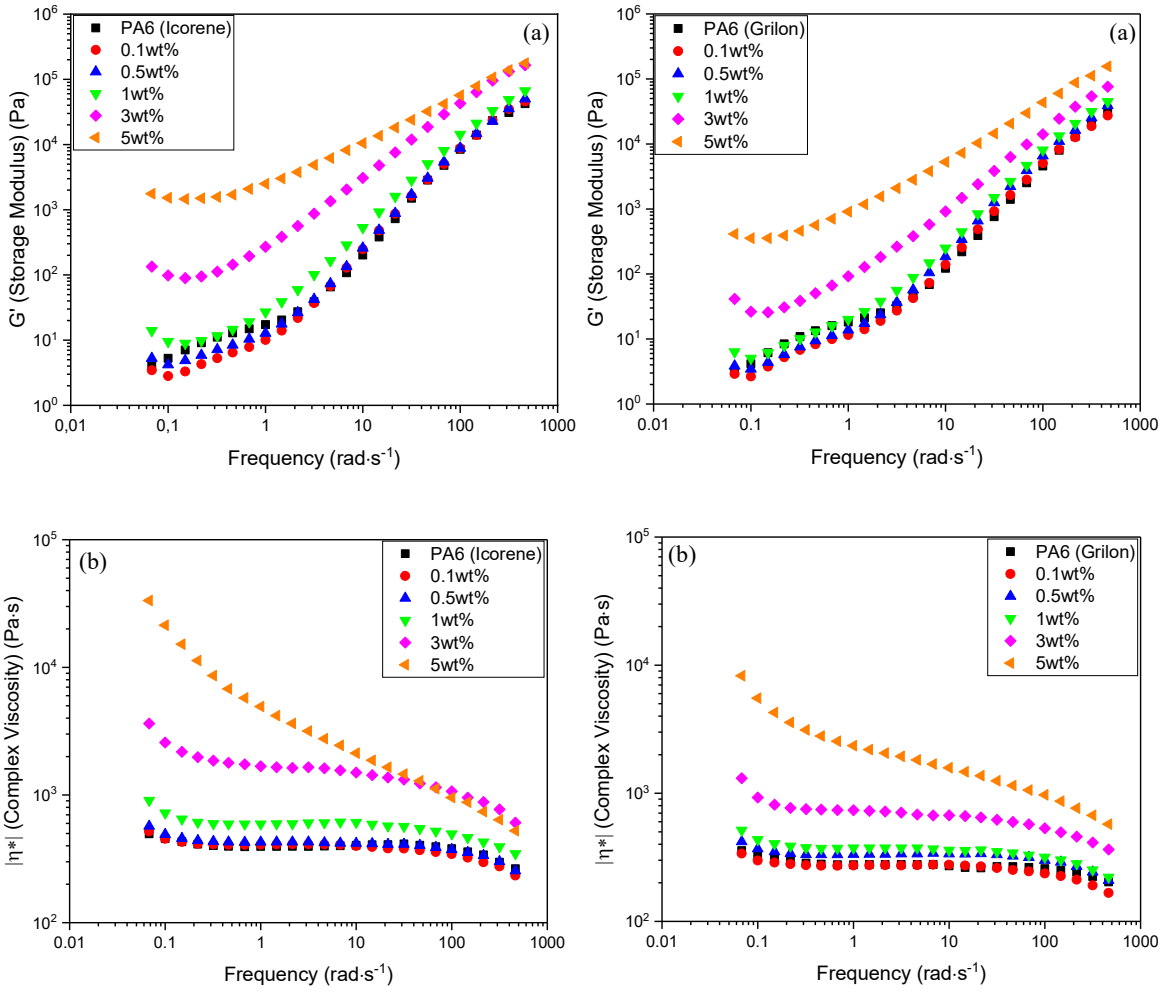

Fig. 6.18. *Variation of: (a) Storage modulus (G') and, (b) complex viscosity (|η*|) as a function of frequency for unfilled PA6 (Icorene™ and Grilon®) and PA6/GNPs composites.*

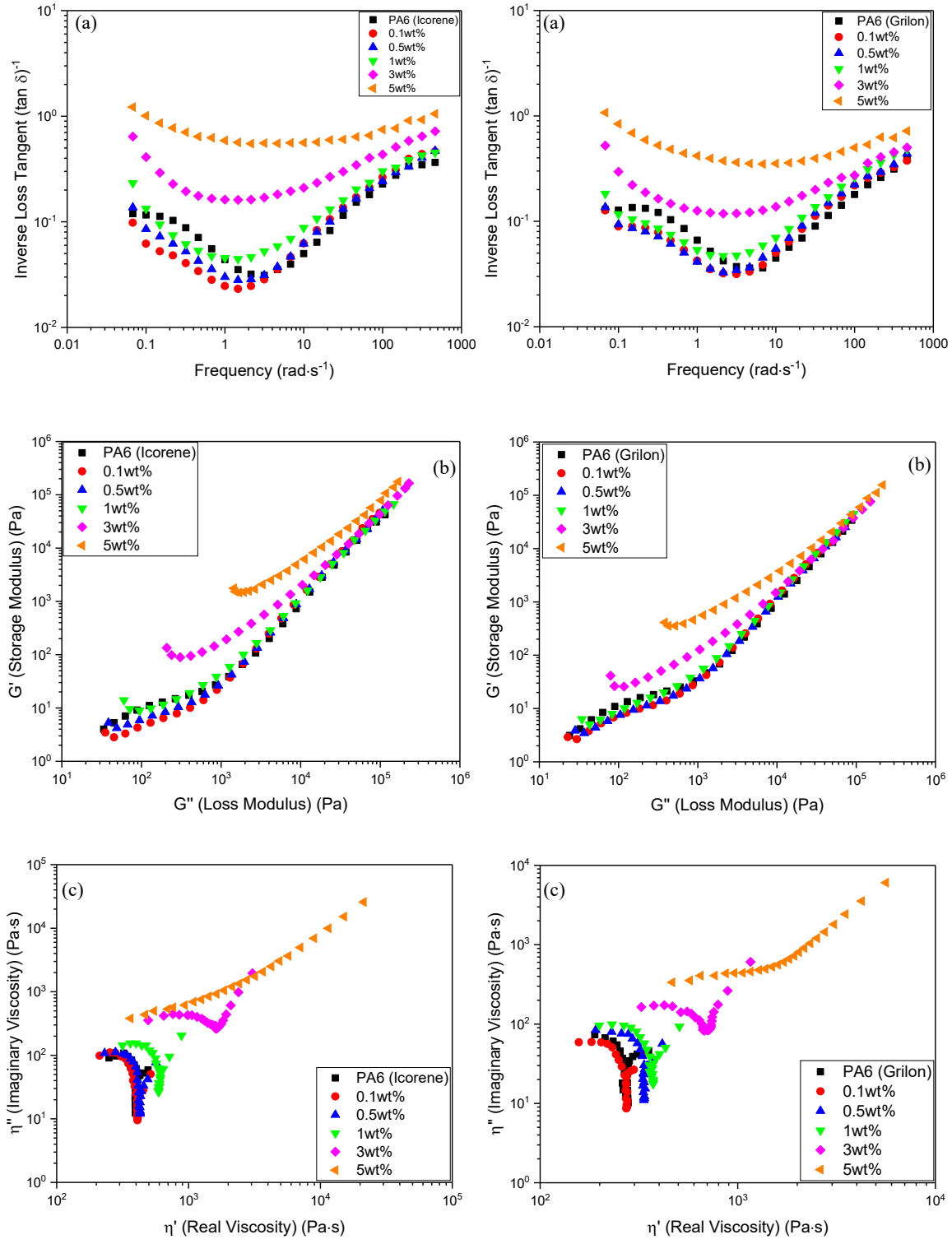

Fig. 6.19. *Variation of (a) reciprocal of loss tangent ((tan δ)$^{-1}$) as a function of frequency; (b) Cole-Cole plot (G' vs. G''); (c) Variation of imaginary viscosity (η'') with real viscosity (η') for unfilled PA6 (Icorene™ and Grilon®) and PA6/GNPs composites.*

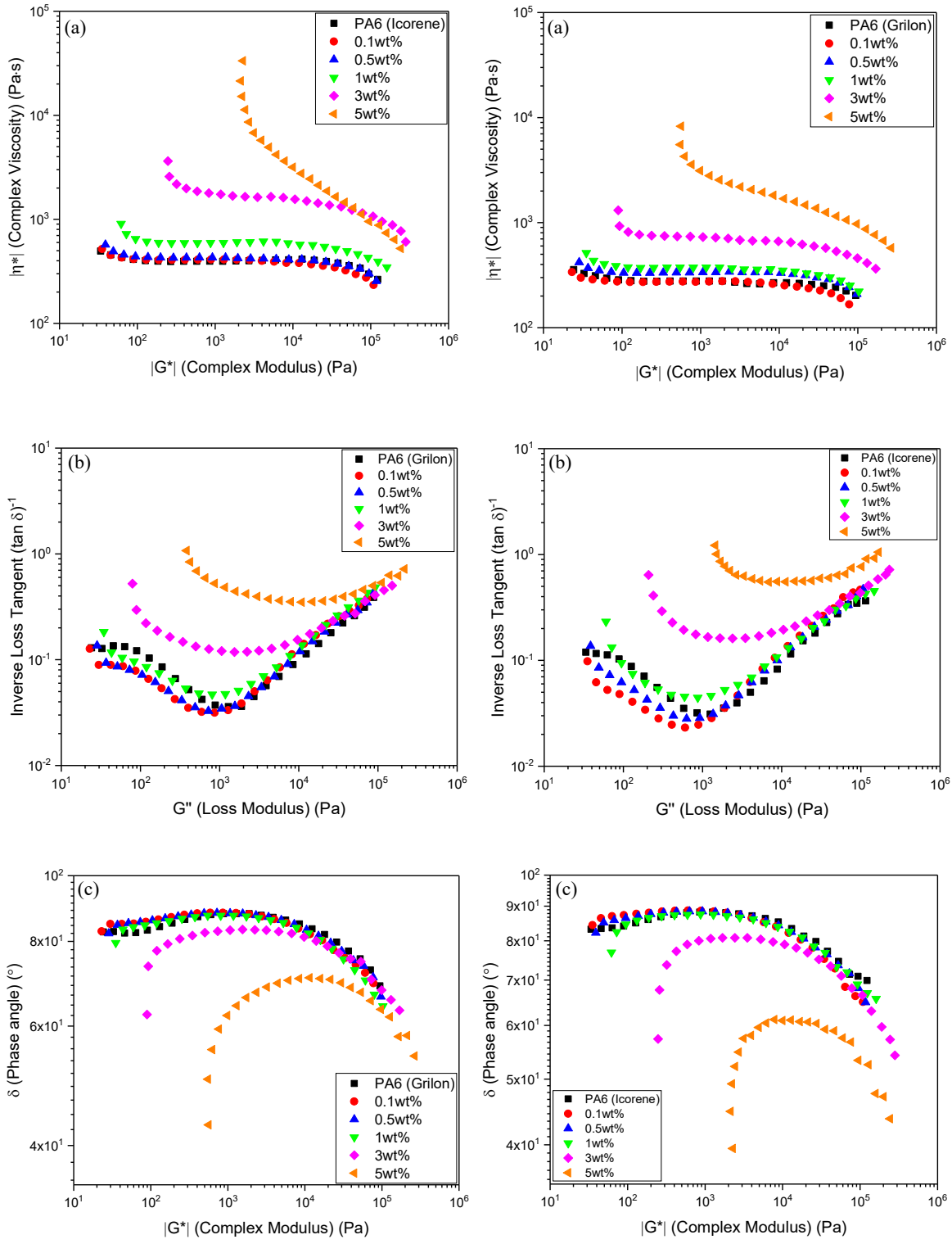

Fig. 6.20. *Variation of (a) complex viscosity (|η*|) with complex modulus (|G*|); (b) (tan δ)-1 with G'' and (c) phase angle with complex modulus (|G*|) (Van-Gurp Palmen plot) for unfilled PA6 (Icorene™ and Grilon®) and PA6/GNPs composites.*

The oscillatory melt rheology measurement was performed in order to investigate the extent of dispersion of GNPs in the polymer matrix and to study the level of interaction between the filler and the polymer chains. In addition, it was possible to detect if the nanofillers created a rheological percolated network inside the polymer matrix. Figure 6.18 shows that a significant variation of the storage modulus and complex viscosity occurred at low frequency, where the rheometer was more sensitive to detect changes in the visco-elastic behaviour of the material. At 240 °C and low frequencies, unfilled PA6 exhibits a viscous behaviour with fully relaxed chains and G' presents a power-law dependence on frequency which can be approximated as $G' \sim \omega^2$ [2]. With increasing filler content, the slope of G' curve started to decrease and the dependence of the storage modulus on the frequency became weaker. More specifically, it was possible to observe an increasing of G' and complex viscosity by one order of magnitude passing from 1wt% to 3wt% of GNPs. This distinct variation in the viscoelastic behaviour suggests that the formation of an interconnected network of GNPs occurred in this weight percentage range. The polymer chains long-range motion was restricted by the presence of the filler percolated structure and consequently, the visco-elastic nature of the material started to change by exhibiting a more pseudo-elastic behaviour. The rheological modifications caused by the GNPs can be attributed to a good dispersion of the filler into the polymer matrix. As reported by Du and Scogna, an intermediate or a good dispersion of the filler is sufficient to induce a non-terminal rheological behaviour of the polymer matrix [114]. A not well dispersion prevents the formation of a network because the nanofillers tend to create agglomerates into the matrix, thus enabling the polymer chains in the poor-filled domains to move more easily when the stress is applied.

It is apparent from a comparison between the behaviour of the two different composite systems (Fig. 6.18a-b) that Icorene™ based composites showed a higher increase of G' and η^* at low frequency than Grilon®. For instance, the first manifested an increase of G' from 5.3 to 1520 Pa (at 0.1 rad s^{-1}) passing from unfilled PA6 to 5wt% of GNPs, whilst G' of Grilon® composites increased from 4.2 to 355 Pa in the same conditions. This effect was due to the different molecular weight (and therefore viscosity) of the polyamides which affected the mobility of the polymer chains and their response towards the applied stress. However, both grades of PA6 achieved a rheological percolation at the same filler concentration, thus showing a good dispersion regardless of the matrix characteristics.

Further evidence of the formation of the percolated network is shown in Figure 6.19a, in which the inverse loss tangent $(\tan)^{-1}$ is plotted in function of frequency. At low frequency, an enhancement of $(\tan)^{-1}$ could be detected with increasing GNP content, suggesting a rise in the ratio of G' and G'' which explains a reduction of material damping effect and an increase of the elastic properties of the composite. Again, this property variation can be readily identified, at low frequency, between GNPs concentrations of 1wt% and 3wt%, while for concentrations below 1wt% the curves tend to overlap. Cole-Cole plot (log G' vs. log G'') in Fig. 6.19b, highlights a more enhanced deviation from the linear relation between storage modulus and loss modulus, at concentrations above 1wt% of GNPs. This effect confirms the abovementioned conclusions.

6.7 Mechanical Properties – Tensile Testing

Standard tensile tests were performed at room temperature in accordance to ASTM D638. A Shimadzu AGS – X series tensile tester was used for the measurements, with a load cell of 10kN and equipped with a video extensometer. Tensile properties of unfilled PA6 and PA6/GNPs composites were determined by applying a uniaxial stress on the specimens until the rupture point is reached. The dumbbell-shaped samples were prepared by injection-moulding and at least 5 specimens for each composition were tested. The measurement of the Young's modulus was carried out by determining the longitudinal strain through the use of a video extensometer which was able to detect in real time the distance between hand-made markers dots applied on the surface samples before the test. Modulus values were obtained from the slope of the stress-strain curve between 0.05 and 0.25% of strain. The instrument was calibrated before any measurement by setting the gauge length at 24.5 mm.

All the tests were performed at 10 mm/min crosshead rate. From the measurement it was possible to obtain the values of Young's modulus, yield stress, tensile stress at break and tensile strain at break for each sample. For each sample batch, the statistical average (with related standard deviation) of each of the abovementioned property was considered to interpret the results. A comparison of the stress-strain curve of unfilled PA6 (both types) and PA6/GNPs with different filler content was shown in Fig. 6.21.

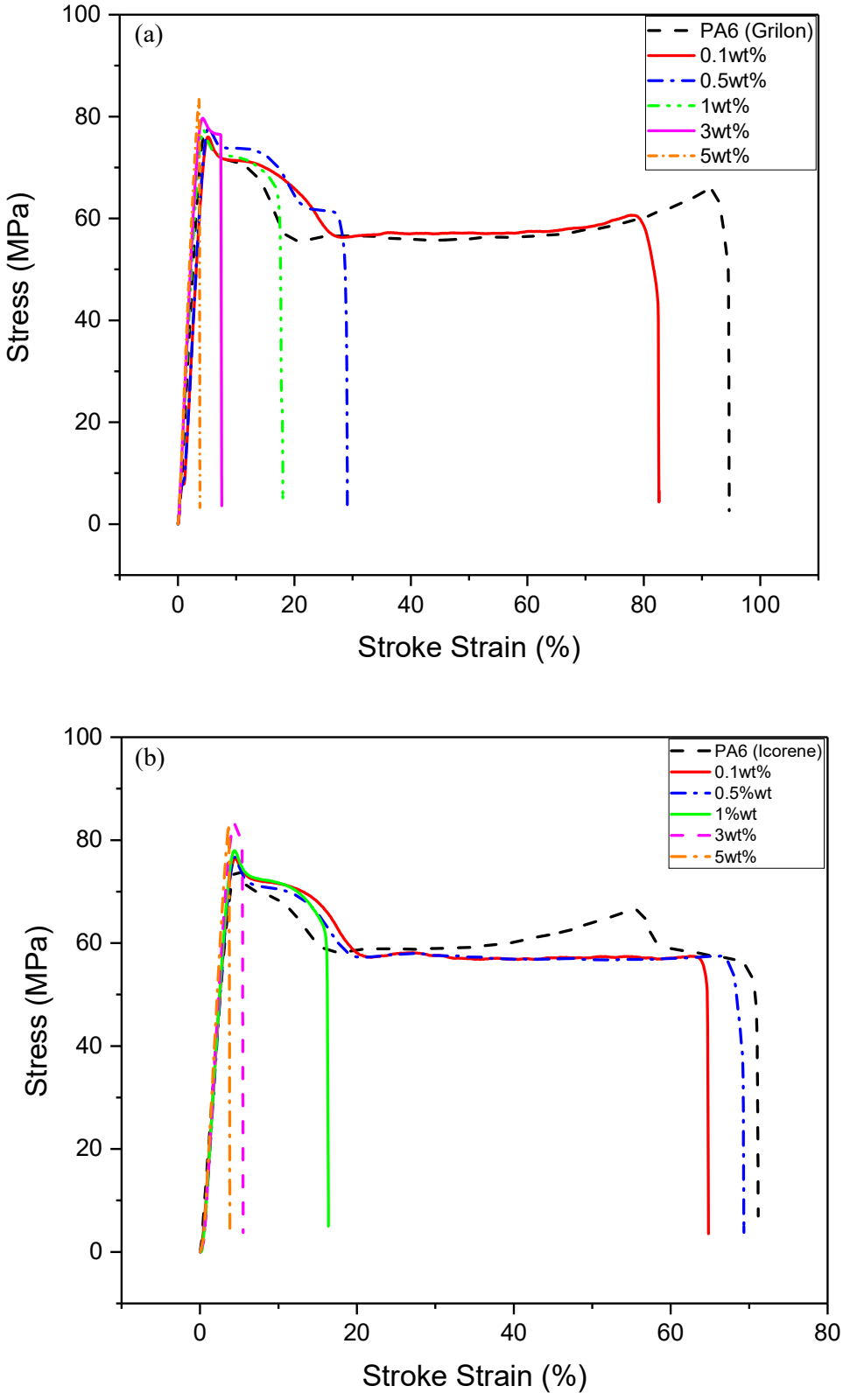

Fig. 6.21. *Variation of the stress-strain curve for (a) PA6 (Icorene™)/GNPs, and (b) PA6 (Grilon®)/GNPs composites, as a function of filler content.*

The stress-strain curves shown in Figure 6.21 indicate a variation of the mechanical response of the composites compared to unfilled PA6. Generally, all the curves manifest a linear elastic mechanical behaviour in the first region followed by the yield point which defines the beginning of the plastic deformation of the sample. Unfilled Icorene™ shows a second yield point which is typically associated to thermal treatment (such as injection moulding) and the crystallinity level of the polymer, as discussed by previous papers [115, 116]. This could justify the difference with the stress-strain curve of the second type of polyamide 6 tested. The difference in MFI and molecular weight affected the mechanical response of two unfilled polymers.

It is also apparent from Figure 6.21 that the presence of the nanofillers leads to a slight increase of the yield strength and to a significant decrease of the elongation at break of the composites. This behaviour, which was previously confirmed with other nanofilled materials [117] can be related to a weak polymer filler interface and/or poor dispersion of the filler whose agglomerates can act as failure point during the elongation test. The brittleness of the samples became more evident at higher filler loading (5 wt%), at which a homogeneous dispersion of the additive was more difficult to achieve. In order to give a better understanding of the effect of filler content on the mechanical response of PA6/GNPs composite, the Young's modulus, yield stress, tensile stress at break and tensile strain at break were plotted as function of GNPs content. Figure 6.22b does not report the data relating to the yield stress of PA6/GNPs composites with 5wt% of GNPs because the samples reached the failure in few seconds. This confirmed the brittle behaviour associated with the highest filler content among the composites tested. Specifically, PA6-GNPs cross-linkages limited the sliding of polymer chains.

All the plotted data are expressed as a mean of at least 5 samples, with the error bar representing the standard deviation. A lack of repeatability of the data was noticed when different specimens of the same composition were tested, resulting in quite high standard deviation values. A reason of that can be associated with the presence of defects due to the injection-moulding process, such as air bubbles and agglomerations of filler, which act as failure point.

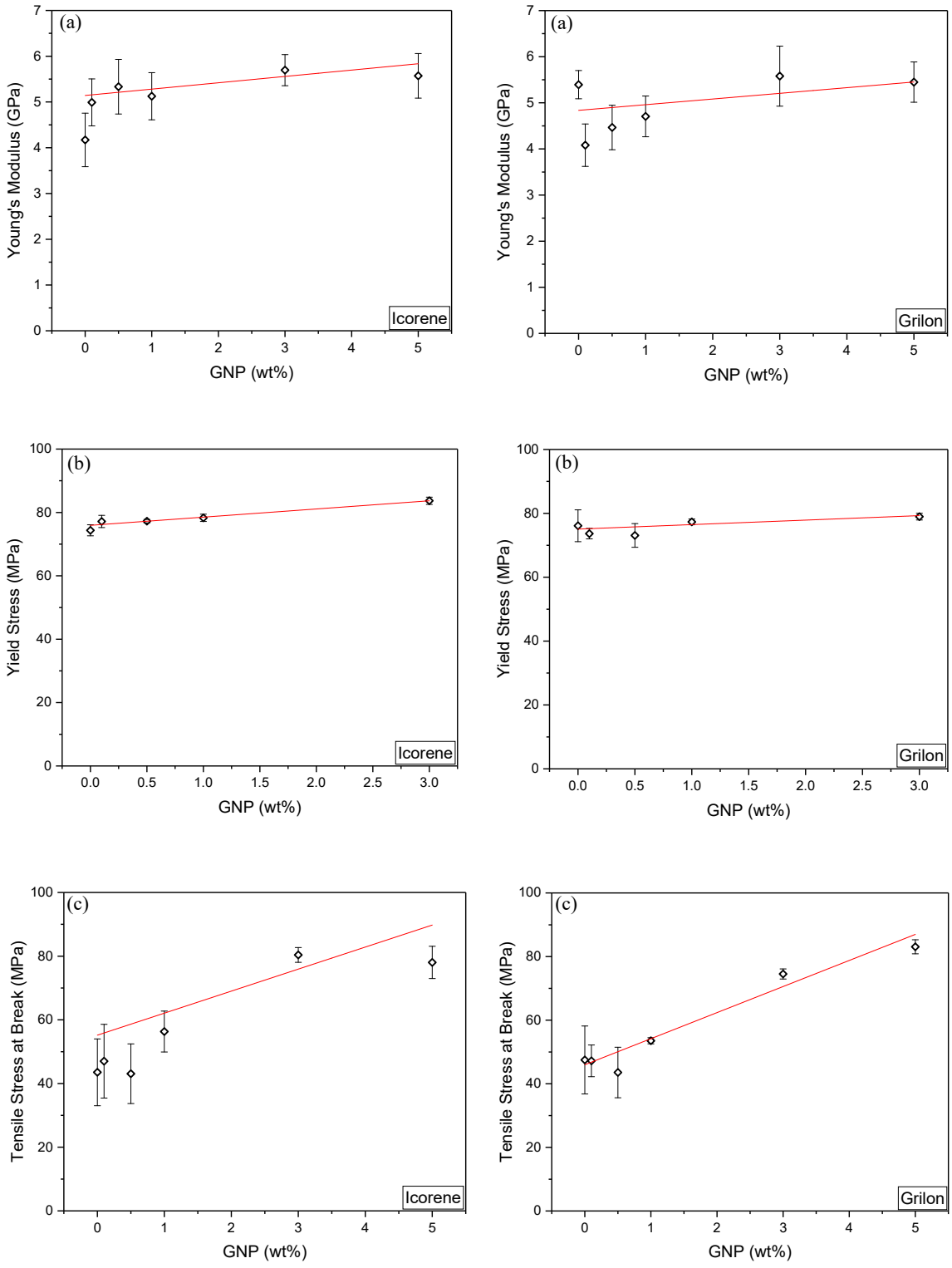

Fig. 6.22. *Variation of (a) Young' Modulus (b) Yield stress and (c) Tensile stress at break with GNPs content for unfilled PA6 (Icorene™ and Grilon®) and PA6/GNPs composites.*

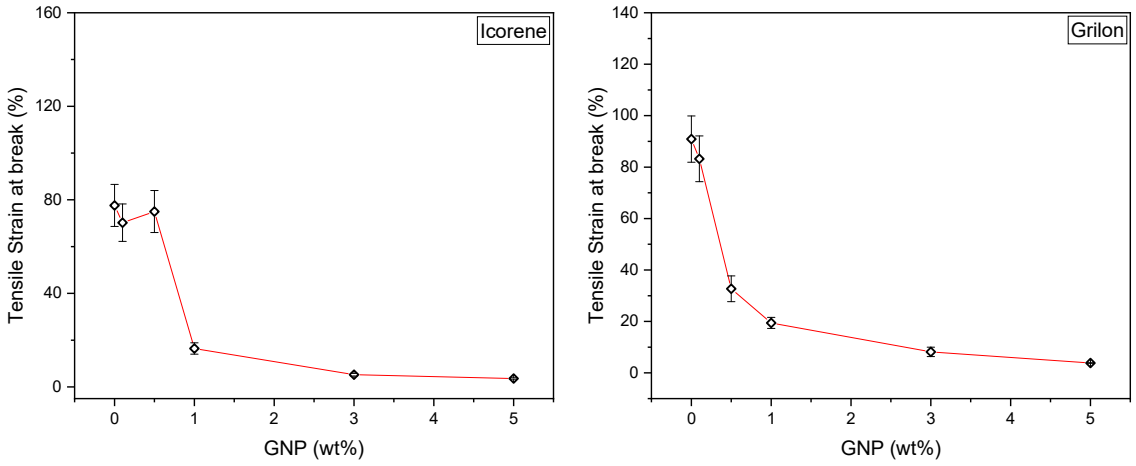

Fig. 6.23. *Variation of tensile strain at break with GNPs content for unfilled PA6 (Icorene™ and Grilon®) and PA6/GNPs composites.*

Tab. 6.8. *Data obtained from static tensile test measurements.*

GNP loading (wt%)	Young's Modulus (GPa)	Yield Stress (MPa)	Tensile Stress at Break (MPa)	Tensile Strain at Break (%)
PA6 (Icorene)	4.2 ± 0.5	75 ± 2	39 ± 13	77.6 ± 9.1
0.1	4.9 ± 0.5 (+17%)*	77 ± 1 (+3%)	53 ± 14 (+36%)	70.2 ± 8.3 (-10%)
0.5	5.3 ± 0.1 (+26%)	77 ± 1 (+3%)	46 ± 10 (+18%)	75.0 ± 9.2 (-3%)
1	5.1 ± 0.5 (+21%)	78 ± 1 (+4%)	56 ± 6 (+44%)	16.4 ± 2.4 (-79%)
3	5.7 ± 0.3 (+36%)	84 ± 1 (+12%)	80 ± 2 (+105%)	5.2 ± 0.5 (-93%)
5	5.6 ± 0.5 (+33%)	--	78 ± 5 (+100%)	3.6 ± 0.3 (-95%)
GNP loading (wt%)	**Young's Modulus (GPa)**	**Yield Stress (MPa)**	**Tensile Stress at Break (MPa)**	**Tensile Strain at Break (%)**
PA6 (Grilon)	5.4 ± 0.3	76 ± 5	47 ± 11	90.9 ± 9.2
0.1	4.1 ± 0.5 (-24%)*	74 ± 2 (-3%)	47 ± 5 (0%)	83.2 ± 8.9 (-8%)
0.5	4.5 ± 0.5 (-17%)	73 ± 4 (-4%)	44 ± 8 (-6%)	32.7 ± 5.1 (-64%)
1	4.7 ± 0.4 (-13%)	77 ± 1 (+1%)	54 ± 1 (+15%)	19.4 ± 2.1 (-79%)
3	5.6 ± 0.7 (+4%)	79 ± 1 (+4%)	75 ± 2 (+60%)	8.2 ± 1.8 (-91%)
5	5.5 ± 0.4 (+2%)	--	83 ± 2 (77%)	3.8 ± 0.1 (-96%)

*Percentage increase with respect to PA6 unfilled.

For greater clarity, all the measurement data are shown in Table 6.8 with the associated percentage of increase or decrease, with respect the unfilled PA6.

From Table 6.8 and from Figure 6.22a it can be observed that the addition of GNPs did not lead to a significant increase of the Young's modulus, especially if the standard deviation is considered in the evaluation. However, a greater increase was recorded for Icorene™ based composite, possibly due to the higher viscosity of the unfilled matrix. Ideal graphene nanoplatelets are characterised by a huge Young's modulus (1 TPa) parallel to the surface, and a fracture strength of 130 GPa, as reported from the literature [118]. The reason why these considerably high mechanical properties are not fully exploited when the inorganic filler is added to a thermoplastic matrix can be related to the defect density of the material as well as on the process method and conditions of the nanocomposites. The melt mixing procedure performed for the preparation of the PA6/GNPs nanocomposites can easily affect the orientation and shape of the graphene nanoplatelets through the application of high shear stresses in order to obtain an efficient mixing. This could cause the buckling or breakage of the filler and prevent it to elongate efficiently in the stress direction, thus justifying a reduction in the mechanical properties. No particular change in the Young' modulus of Grilon® Polyamide 6 was noticed with higher filler content. This effect can be again related to the different viscosity of the unfilled PA6, as confirmed by the rheological results. For the same reasons, the yield stress of Icorene™ tends to show a higher improvement than Grilon® with the addition of the filler, even if this increment is not as pronounced. An apparent enhancement of the tensile stress at break for both type of PA6 occurred with the addiction of the GNPs, whilst the elongation at break dramatically decrease. This denotes that the presence of GNPs contributes to make the nylon 6 stronger but less flexible.

6.8 Electrical Measurements

Electrical volume resistivity studies have been carried out on sheet samples using a Keithley 6517B Electrometer and a resistivity chamber (model N. 8009). The measurements were repeated 10 times by changing the polarity and by detecting the resistivity values after 60 seconds of electrification. The applied voltage was varied in

accordance to the conductance of the material, in a range from 1 V for high filler content to 30 V for less conductive samples. Volume resistivity was determined under DC current, at room temperature. Test specimens have been made by compression molding of the melt-compounded nanocomposite pellets. Disk-shaped thin samples were cut from the moulding products, with a diameter of 70 mm. The thickness of each sample was measured and used as input value for the electrometer. Table 6.9 shows the variation of the electrical resistivity values with increasing graphene loading, for both systems of PA6/GNPs nanocomposites.

Tab. 6.9. *Data from electrical volume resistivity measurements, for PA6 (Grilon®)/GNPs*

GNP (wt%)	Thickness (mm)	Voltage (V)	Vol. resistivity (Ωcm)	St. Dev. (Ωcm)
0	0.079	20	1.4E+16	6E+15
0.1	0.079	20	1.8E+16	9E+15
0.5	0.125	10	1.3E+16	8E+15
1	0.113	10	1.2E+16	9E+15
3	0.103	1	6.8E+8	2E+7
5	0.118	1	7.6E+6	3E+5

Tab. 6.10. *Data from electrical volume resistivity measurements, for PA6 (Icorene™)/GNPs*

GNP (wt%)	Thickness (mm)	Voltage (V)	Vol. resistivity (Ωcm)	St. Dev. (Ωcm)
0	0.132	30	1.1E+16	9E+15
0.1	0.091	30	1.4E+16	2E+15
0.5	0.111	30	1.1E+16	2E+15
1	0.107	30	1.3E+16	4E+15
3	0.102	10	3.9E+9	3E+8
5	0.136	1	6.8E+7	2E+6

Figure 6.24 shows the change of the electrical resistivity as a function of the filler concentration, with standard deviation as error bars. For both nanocomposites system (with different matrix in term of MFI) the electrical percolation threshold can be observed between 1 and 3 wt% GNPs. Percolation occurs through the interconnection between filler aggregated structures which lead to the formation of a phase-separate network into the polymer matrix [119]. A good degree of GNPs dispersion in the PA6 matrix is essential to promote the formation of a conductive network which also depends on the aspect ratio of the nanoparticles. The presence of a percolation threshold for concentration

above 1 wt% GNPs is in accordance with the rheological results which showed a marked enhancement of storage modulus and viscosity above the same filler concentration. This suggests that the melt-blending process have been useful to promote a sufficient dispersion of the filler through the PA6 matrix.

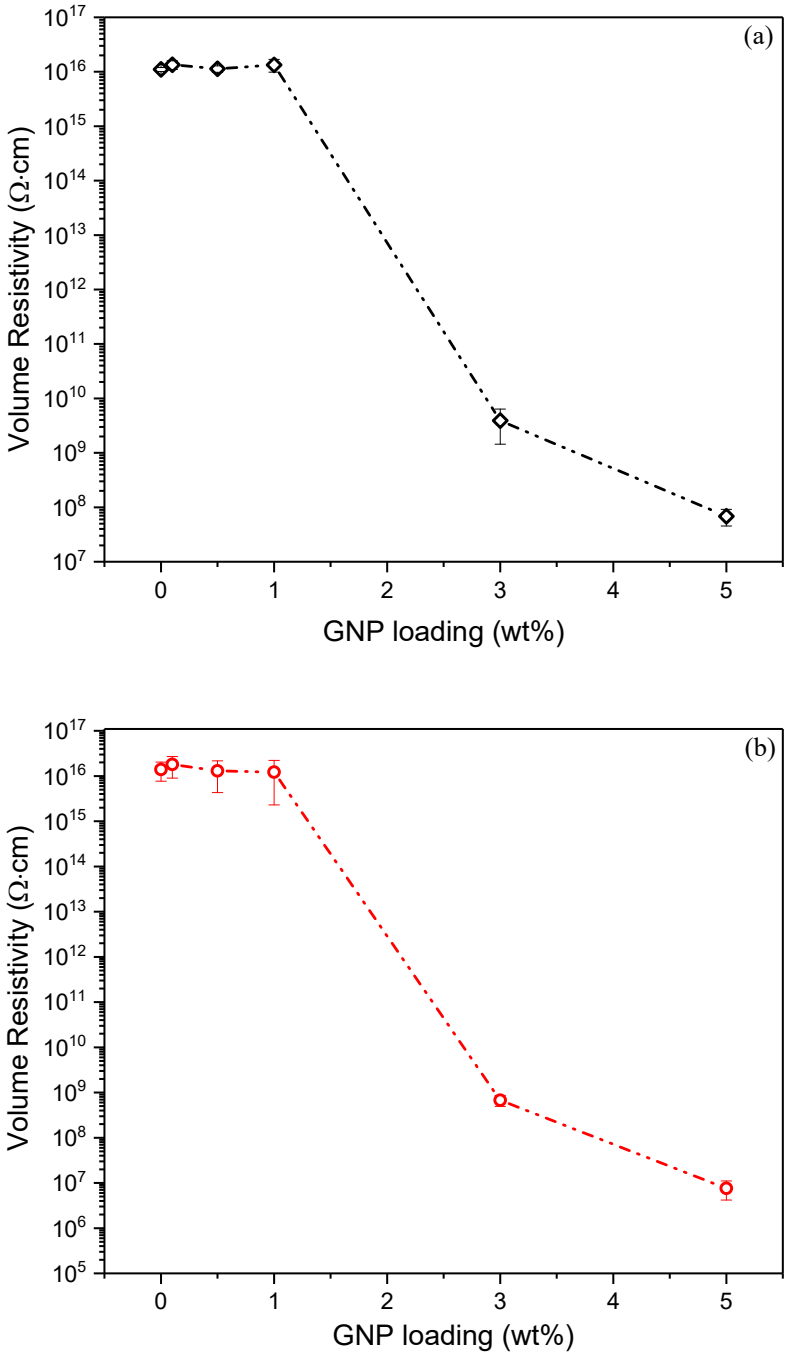

Fig. 6.24. *Variation of volume resistivity (log scale) as a function of filler content, for (a) PA6 (Icorene™)/GNPs composites, and (b) PA6 (Grilon®)/GNPs composites*

Previous studies on PA6/GNPs nanocomposites produced through melt-blending showed a percolation threshold around 2 wt% GNPs [120] and 0.1 wt% [121] while other authors have not identified a significance difference in term of electrical properties between 10 and 20 wt% GNPs [2]. The large discrepancy between these results can be explained by listing several parameters which tend to affect the electrical properties of nanocomposites:

- Aspect ratio of the filler, which consists in "the ratio between the length of the long axis to the length of the short axis" [7]. The higher is the aspect ratio, the lower is the percolation threshold. Specifically, higher aspect ratio provides an efficient point-point contact among the fillers thus promoting the conductive path formation.
- Polymer viscosity, which affects the degree of dispersion of the filler during the melt-compounding process. A too high viscosity prevents a well and homogeneous dispersion of the nanoparticles, and lead to increase the shear stress level exercised by the screws, thus affecting the structural integrity of the filler.
- Shear stress, which is a fundamental parameter to be controlled during extrusion of nanocomposites. A too low stress level is not sufficient to promote an effective disaggregation of GNPs agglomerates, thus slowing down the dispersion process of nanoplatelets into the matrix. A higher filler concentration is required to achieve the conductive network formation with the risk to make the material more brittle. A too high stress level leads to damage/break the filler structure and to reduce the aspect ratio and related properties.

6.9 Thermal Conductivity Measurements

Thermal conductivity measurements have been performed through Hot Disk method, using composites disks with a diameter of 3.4 cm and thickness of 5 mm. The variation of the thermal conductivity as a function of the GNPs loading for the two systems of Nylon 6 based composites is shown in Fig. 6.28. For the sake of clarity, the thermal conductivity results and related standard deviation are summarised in Table 6.11.

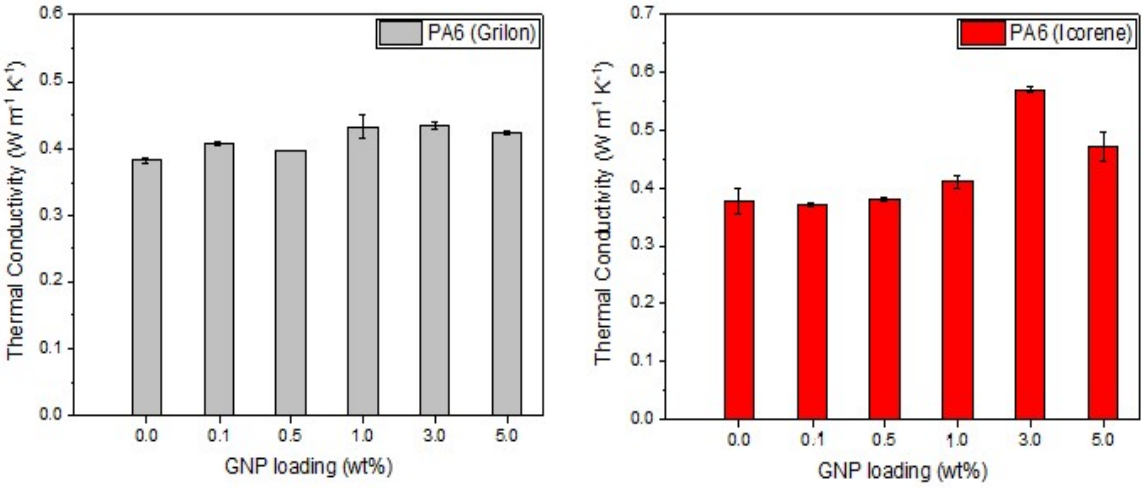

Fig. 6.25. *Thermal conductivity variation as a function of GNPs content.*

The thermal conductivity measurement was repeated 10 times by placing the sensor in different points on the sample surface.

Tab. 6.11. *Results of thermal conductivity measurements.*

GNP loading (PA6-Icorene)	**Average (W/m·K)**	**STD**
0 wt%	0.38	2.15E-2
0.1wt%	0.37	3.23E-3
0.5wt%	0.38	3.34E-3
1wt%	0.41	1.2E-2
3wt%	0.57	4.65E-3
5wt%	0.47	2.44E-2
GNP loading (PA6-Grilon)	**Average (W/m·K)**	**STD**
0 wt%	0.38	3E-3
0.1wt%	0.41	2.51E-3
0.5wt%	0.40	1.31E-3
1wt%	0.43	1.66E-2
3wt%	0.44	5.5E-3
5wt%	0.42	2.13E-3

The thermal conductivity results did not show any significant sign of improvement. This is due to the complexity of the mechanisms of heat transfer of graphene in polymer composites, which differ quite substantially from the mechanism of electric transfer.

While electric current can flow through the composites more easily, favoured by tunnelling effects across barriers, heat is transferred by the movement of vibrations (phonons) and free electrons between the conductive particles in the polymer matrix. The high number of interfaces produced between the filler and the matrix lead to phonon scattering phenomena and high interfacial thermal resistance, which drastically decrease and slow-down the phonon transfer. Therefore, a strong interface between the polymer and the additives is required in order to minimize the interfacial thermal resistance.

Recent studies have proposed the possibility to modify graphene surface in order to form an interlayer by connecting the polymer chains to the filler and decreasing the interfacial thermal resistance [122, 123]. Other researchers obtained good improvement in thermal conductivity by adding large %vol of fillers, thus achieving the formation of thermally conductive percolated structure. For instance, Gu *et al*. [124] obtained a thermal conductivity 9 times higher than the neat polymer matrix, by adding 21.4 vol% of GNPs through mechanical ball milling followed by hot pressing. The modest improvements obtained with PA6/GNPs composites can be related to the weak filler/matrix interface, also confirmed by SEM micrographs, and to the not sufficiently high level of filler loading which prevented the formation of a conductive network into the matrix. Furthermore, the presence of porosity could contribute to the reduction of the thermal conductivity, by enhancing phonon scattering. Microscopic voids can arise during the melting processes of the composites due to the presence of air bubbles which are caused by the evaporation of water contained by the hygroscopic structure of Nylon 6. This fact is in accordance with the minor improvements found during the mechanical tensile testing of the composites (see section 6.7).

6.10 Scanning Electron Microscopy (SEM)

Several micrographs of different samples have been taken by scanning electron microscopy in order to investigate the fracture surfaces of PA6/GNPs composites. The specimens used were previously subjected to cryogenic fracture, by pouring the material in liquid nitrogen, and subsequently hammered in order to obtaining surfaces as far as

possible free from plastic deformation phenomena and formation of fibrils/crazes. Figure 6.26 show micrographs relating to the GNP powder morphology.

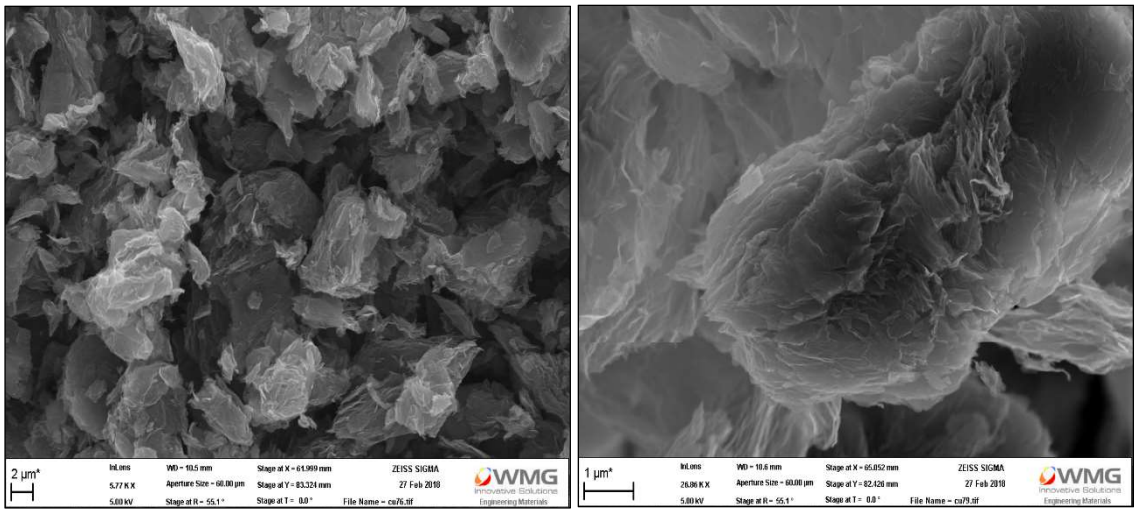

Fig. 6.26. *SEM images of GNP powder.*

It is apparent from fig. 6.26 the high irregularity in the structure of the graphene platelets which are visibly constituted by the overlapping of few layers. In the next series of figures, some of the most significant micrographs related to PA6/GNPs composites fracture surface are shown.

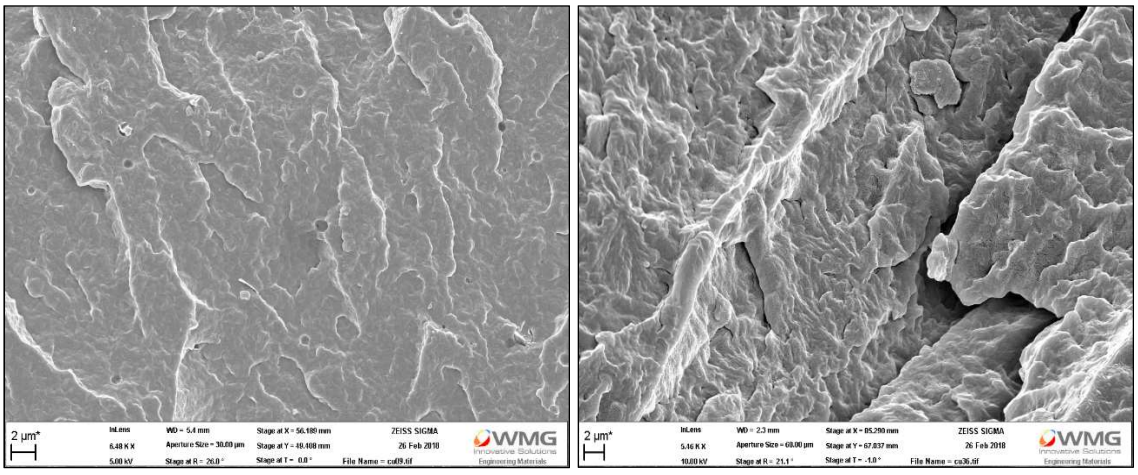

Fig. 6.27. *SEM images of neat PA6 (Grilon®) on the left, and neat PA6 (Icorene™), on the right.*

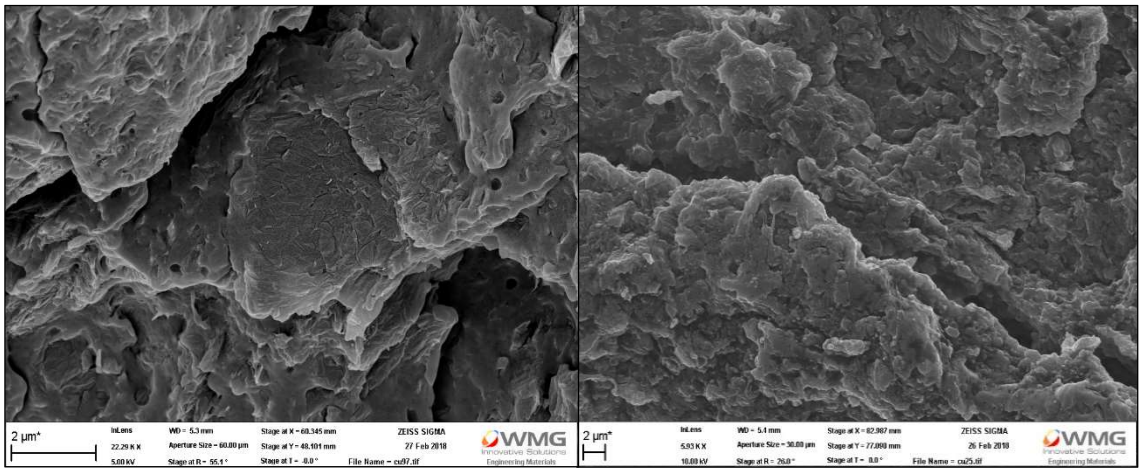

Fig. 6.28. *SEM images of PA6/5wt% GNPs (Grilon®) on the left, and PA6/5wt% GNPs (Icorene™), on the right.*

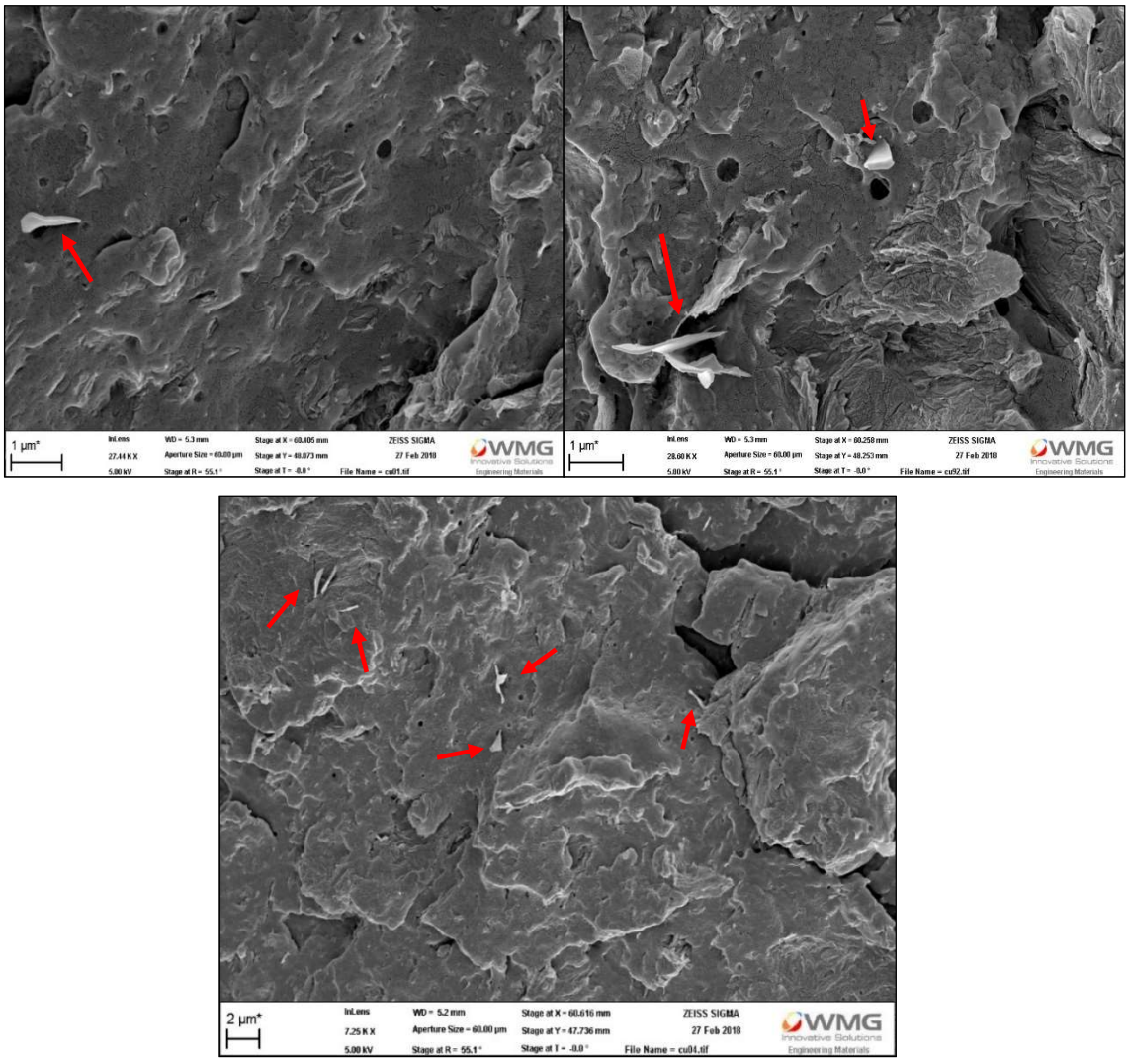

Fig. 6.29. *SEM images of PA6(Grilon®) with 5wt% of GNPs, where fillers are indicated with arrows.*

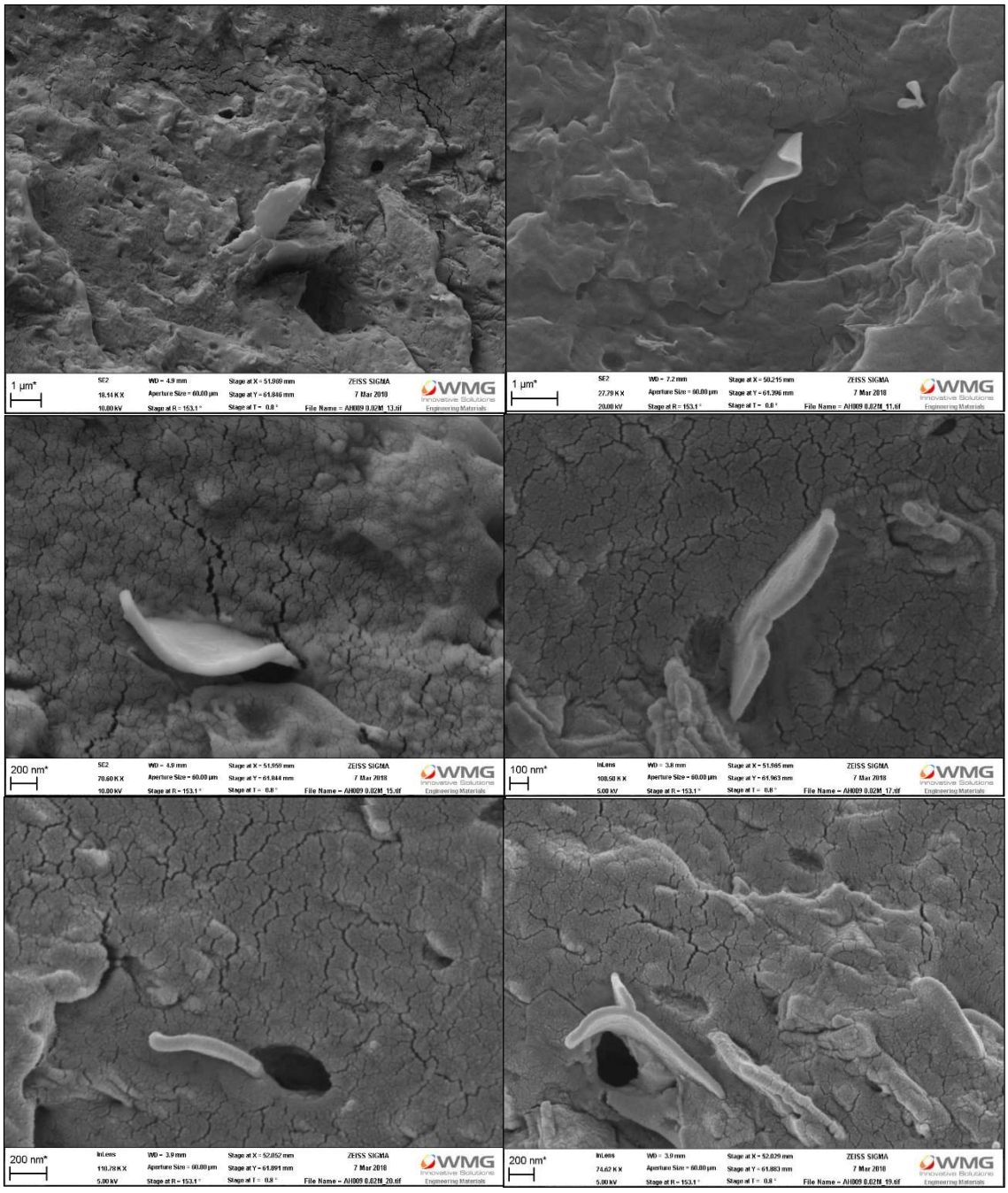

Fig. 6.30. *High magnification SEM images of PA6 (Grilon®)/5wt% GNPs.*

From SEM micrographs, it is possible to see that GNPs did not fully maintained their morphology after melt-mixing, due to the strong shear stresses which may cause bending and shortening of the fillers. Porosity is visible next to the platelets, suggesting that poor adhesion occurred between the matrix and the filler. Fig. 6.29 and other images taken at lower magnification, were not sufficiently precise to indicate the degree of dispersion of

the platelets into matrix. GNPs are partially visible, suggesting that the majority can be well incorporated by the polymer matrix. A deeper morphological analysis of the composites should be performed by using transmission electron microscopy (TEM) in order to study the distribution of the filler in the first layers of the material.

Conclusions

The present study was designed to determine the effect of the dispersion of graphene nanoplatelets (GNPs), containing oxygen functionality, on the properties of Polyamide 6 nanocomposites obtained via melt-blending process. Two Polyamides with different molecular weight have been consider to take into account the effect of different melt viscosity.

The addition of GNPs to Nylon 6 matrix did not have significant effect on the thermal stability of the unfilled polymer while some effects on the crystallinity have been revealed since it has been proved that the nanofillers acted as nucleating agent. Moreover, PA6 nanocomposites exhibited the formation of a double-peak in the crystallisation exotherms above 3wt% of GNPs, indicating that the fillers favoured the nucleation of α -form crystallites and, at the same time, they limited the complete crystallisation of the γ-phase. DMTA analysis showed a slight enhancement of the storage modulus as well as glass transition temperature with increasing filler content. Rheological results highlighted an increase in complex modulus (G') and complex viscosity (η^*) by more than one order of magnitude, passing from 1wt% to 3wt% of GNPs, at low frequencies. This marked variation is associated with the formation of a percolated rheological network, which in turn caused a change in the viscoelastic response of the composite, from that of a molten liquid to that of a "pseudo-solid" material. The rheological network formation represented a sign of a homogeneous filler dispersion through the polymer matrix. Further evidence of this rheological transition was found by observing the variation of $(\tan)^{-1}$ and of the phase angle (δ), both oriented towards a more elastic behaviour of the composite. The rheological percolation was observed above 1wt% for both Nylon 6 systems. A greater enhancement of G' and η^* was found for Icorene™ based composites, possibly due to the higher molecular weight (and therefore viscosity) of the unfilled PA6, than the Grilon® type. The mechanical characterisation showed that the addition of GNPs affected the ductility of the matrix. Indeed, the elongation at break was greatly reduced by the incorporation of more than 0.5wt% of the fillers, possibly due to the presence filler

agglomerations and porosities, which could act as failure point during the tensile test; moreover, also the tensile stress at break tended to become higher. In other words, the materials changed its behaviour, from ductile to brittle, for filler content higher than 0.5-1wt%. Young's modulus and yield stress showed only minor improvement when increasing filler content thus suggesting that there was not a very good adhesion between matrix and filler. Electrical measurements indicated a reduction of the electrical volume resistivity of about 10 orders of magnitude on the addition of up to 5wt% GNPs. The electrical percolation threshold for both composite systems was achieved between 1wt% and 3wt% GNPs, in accordance with the rheological results. Thermal conductivity measurements did not show any significant improvement of the heat transfer through the composite structure. This result suggested that, even if a percolated rheological network was achieved, the high thermal interface resistance prevented an efficient heat transport among the conductive fillers. Moreover, it seems that no perfect contact between nanofillers was achieved throughout the rheological network. This fact can explain the low improvement in heat transport, in which the phonons required a continuous conductive path to be effectively transported through the polymer matrix. On the contrary, electrical transport was possible thanks to the electron tunnelling phenomena which occur between adjacent non-contacting fillers. High degree of porosity and weak filler/matrix adhesion contributed to increase the phonon scattering phenomena, thus reducing the global thermal conductivity of the composites.

In conclusion, it can be stated that the increase in the chemical compatibility between graphene and polar polyamide matrix, by using graphene containing oxygen functionality, as shown by Raman and XPS analysis, is not enough to obtain a good matrix-filler adhesion. One of the key feature in achieving significant improvement of the polymer nanocomposites properties still remain the processing conditions. Therefore, considerably more work will need to be done in order to optimise the variable which affect the filler dispersion during the melt-mixing process. More specifically, the residence-time, screw speed and temperature profile could be adjusted gradually towards a better filler dispersion target. Although the rheological percolation has been achieved above 1wt%, a further investigation of the processing parameters and filler dimensions

should be carried out in order to reduce the percolation threshold and to improve the filler/matrix adhesion.

Bibliography

[1] Ha SM, Kwon OH, Oh YG, Kim YS, Lee SG, Won JC, Cho KS, Kim BG, Yoo Y. (2015). Thermally conductive polyamide 6/carbon filler composites based on a hybrid filler system. *Sci. Technol. Adv. Mater*. **16**, 65001.

[2] Mayoral B, Harkin-Jones E, Khanam PN, AlMaadeed M, Ouederni M, Hamilton A, et al. (2015). Melt processing and characterisation of polyamide 6/graphene nanoplatelet composites. *RSC Adv*. **5**, 52395–409.

[3] Jones WE Jr., Chiguma J, Johnson E, Pachamuthu A, Santos D. (2010). Electrically and Thermally Conducting Nanocomposites for Electronic Applications. *Materials* **3** 1478-1496.

[4] Huang X, Jiang P, Tanaka T. (2011). A review of Dielectric polymer composites with high thermal conductivity. *IEEE Electr. Insul*. **27**, 8–16.

[5] King JA, Tucker KW, Vogt BD, Weber E, Quan CL. (1999). Electrically and thermally conductive nylon 6,6. *Polym. Comp*. **20**, 643–54.

[6] Jouni M, Boudenne A, Boiteux G, Massardier V, Garnier B, Serghei A. (2013). Electrical and thermal properties of polyethylene/silver nanoparticle composites. *Polym. Compos*. **34**, 778–86.

[7] Huang X, Chunyi Z. (2016). Polymer Nanocomposites: Electrical and Thermal Properties. (Switzerland: Springer International Publishing).

[8] Allaoui A, Bai S, Cheng HM, Bai JB. (2002). Mechanical and electrical properties of a MWNT/epoxy composite. *Compos. Sci. Technol.* **62**, 1993–8.

[9] Li J, Kim JK. (2007). Percolation threshold of conducting polymer composites containing 3D randomly distributed graphite nanoplatelets. *Compos. Sci. Technol.* **67**, 2114–2120.

[10] Gojny FH, Wichmann MHG, Fiedler B, Kinloch IA, Bauhofer W, Windle AH, et al. (2006). Evaluation and identification of electrical and thermal conduction mechanisms in carbon nanotube/epoxy composites. *Polymer* **47**, 2036–45.

[11] Burger N, Laachachi A, Ferriol M, Lutz M, Toniazzo V, Ruch D. (2016). Review of thermal conductivity in composites: mechanisms, parameters and theory. *Prog. Polym. Sci.* **61**, 1-28.

[12] Riande E, Calleja RD. (2004). Electrical properties of polymers. (New York: Marcel Dekker Inc.) pp 3.

[13] Kanatzidis MG. (1990). Conductive polymers. C&EN. 36-54.

[14] Su W, Schrieffer J. R., Heeger, A. J. (1979). Solitons in polyacetylene. *Physical Review Letters*. **42** (25), 1698.

[15] Gorman CB, Ginsburg EJ, Grubbs RH. (1993). Soluble, Highly Conjugated Derivatives of Polyacetylene from the Ring-Opening Metathesis Polymerization of Monosubstituted Cyclooctratetraenes: Synthesis and the Relationship between Polymer Structure and Physical Properties. *Journal of the American Chemical Society*. **115** (4), 1397–1409.

[16] Kalaitzidou K, Fukushima H, Drzal LT. (2010). A route for polymer nanocomposites with engineered electrical conductivity and percolation threshold. *Materials*, **3** (2), 1089-1103.

[17] Taherian R. (2014). Development of an equation to model electrical conductivity of polymer-based carbon nanocomposites. *ECS Journal of Solid State Science and Technology*. **3** (6), M26-M38.

[18] Li A, Zhang C, Zhang YF. (2017). Thermal conductivity of graphene-polymer composites: Mechanisms, properties, and applications. *Polymers*, **9** (9), 437.

[19] Henry A, Chen G. (2008), High thermal conductivity of single polyethylene chains using molecular dynamics simulations. *Phys. Rev. Lett.* **101**, 235502/1-235502.

[20] Burger N, Laachachi A, Ferriol M, Lutz M, Toniazzo V, Ruch V. (2016). Review of thermal conductivity in composites: Mechanisms, parameters and theory. *Prog. Polym. Sci*. **61**, 1-28.

[21] Zongh C, Yang Q, Wang W. (2001). Correlation and prediction of the thermal conductivity of amorphous polymers. *Fluid Phase Equilb*. **181**, 195-202.

[22] Dashora P, Gupta G. (1996). On the temperature dependence of the thermal conductivity of linear amorphous polymers. *Polymer.* **37**, 231-4.

[23] Shahil KMF, Balandin AA. (2012). Graphene – multilayer graphene nanocomposites as highly efficient thermal interface materials. *Nano Lett*. **44**, 117-26.

[24] Wang F, Drzal LT, Qin Y, Huang Z. (2015). Mechanical properties and thermal conductivity of graphene nanoplatelet/epoxy composites. *J. Mater. Sci*. **12**, 861-7.

[25] Zhao YH, Wu ZH, Bai SL. (2015). Study on thermal properties of graphene foam/graphene sheets filled polymer composites. *Composites A.* **69**, 219-25.

[26] Nan CW, Liu G, Lin Y, Li M. (2004). Interface effect on thermal conductivity of carbon nanotube composites. *Appl Phys Lett*. **85**, 3549-51.

[27] Giri A, Hopkins PE, Wessel JG, Duda JC. (2015). Kapitza resistance and the thermal conductivity of amorphous superlattices. *J. Appl. Phys*. **118,** 165203, 1-6.

[28] Gulotty R, Castellino M, Jagdale P, Tagliaferro A, Balandin AA. (2013). Effects of functionalisation on thermal properties of single-wall carbon nanotube-polymer nanocomposites. *ACS Nano*. **6**, 137-58.

[29] Qian D, Dickey EC, Andrews R, Rantell T. (2002). Multiwall Carbon Nanotubes: Synthesis and Application. *Acc. Chem. Res*. **35** (12), 1008–1017.

[30] Potts JR, Dreyer DR, Bielawski CW, Ruoff RS. (2011). Graphene-based polymer nanocomposites. *Polymer.* **52**, 5-25.

[31] Dhineshkumar V, Ramasamy D, Sudha K. (2015). Nanotechnology application in food and dairy processing. *International Journal of Farm Sciences*, **5** (3), 274-288.

[32] Alexandre M, Dubois P. (200). Polymer-layered silicate nanocomposites: preparation, properties and uses of a new class of materials, *Materials Science and Engineering: R: Reports*. **28**, 1–63.

[33] Verdejo R, Bernal MM, Romasanta LJ, Lopez-Manchado MA. (2011). Graphene filled polymer nanocomposites. *J. Mater. Chem*. **21**, 3301-3310.

[34] Chen L, Hernandez Y, Feng XL, Müllen K. (2012). From Nanographenes and Graphene Nanoribbons to Graphene Sheets: Chemical Synthesis. *Angew. Chem. Int. Ed.* **51,** 7640-7654.

[35] Du X, Skachko I, Barker A, Andrei EY. (2008). Approaching ballistic transport in suspended graphene. *Nat. Nanotechnol*. **3**, 491-495.

[36] Gong L, Yin B, Li LP, Yang MB. (2015). Nylon-6/Graphene composites modified through polymeric modification of graphene, *Compos. Part B*. **73**, 49–56.

[37] Sadasivuni KK, Ponnamma D, Thomas S, Grohens Y. (2014). Evolution from graphite to graphene elastomer composites. *Prog. Polym. Sci*. **39**, 749-780.

[38] Kim HS, Bae HS, Yu J, Kim SY. (2016). Thermal Conductivity of Polymer Composites with the Geometrical Characteristics of Graphene Nanoplatelets. *Sci. Rep*. **6**, 26825.

[39] Cho JW, Paul DR. (2001). Nylon 6 nanocomposites by melt compounding. *Polymer*. **42**,1083-1094.

[40] Peltola P, Välipakka E, Vuorinen J, Syrjälä S, Hanhi K. (2006). Effect of rotational speed of twin screw extruder on the microstructure and rheological and mechanical properties of nanoclay-reinforced polypropylene nanocomposites. *Polym. Eng. Sci.* **46**, 995-1000.

[41] Lertwimolnun W, Vergnes B. (2006). Effect of processing conditions on the formation of polypropylene/organoclay nanocomposites in a twin-screw extruder. *Polym. Eng. Sci*. **46**, 314-323.

[42] Nassar N, Utracki LA, Kamal MR. (2005). Melt Intercalation in Montmorillonite/Polystyrene Nanocomposites. *Int. Polym. Proc*. **20**, 423-431.

[43] Yuan FY, Zhang HB, Li X, Ma HL, Li XZ, Yu ZZ. (2014). In situ chemical reduction and functionalization of graphene oxide for electrically conductive phenol formaldehyde composites. *Carbon.* **68**, 653-661.

[44] Sun J, Xue Q, Guo Q, Tao Y, Xing W. (2014). Excellent dielectric properties of polyvinylidene fluoride composites based on sandwich structured MnO_2/graphene nanosheets/MnO_2. *Compos Part A: Appl Sci Manuf*. **67**, 252-258.

[45] Liu K, Chen S, Luo Y, Jia D, Gao H, Hu G, Liu L. (2014). Noncovalently functionalized pristine graphene/metal nanoparticle hybrid for conductive composites. *Compos. Sci. Technol*. **94**, 1-7.

[46] Kasaliwal G, Gldel A, Potschke P. (2009). Influence of processing conditions in small-scale melt mixing and compression molding on the resistivity and morphology of polycarbonate-MWNT composites. *J. Appl, Polym. Sci.* **112**, 3494-3509.

[47] Krause B, Pötschke P, Häußler L. (2009). Influence of small scale melt mixing conditions on electrical resistivity of carbon nanotube-polyamide composites. *Compos. Sci. Technol.* **69**, 1505-1515.

[48] Chirtoc M, Horny N, Henry JF, Turgut A, Kökey I, Tavman I, Omastová M. (2012). Photothermal Characterization of Nanocomposites Based on High Density Polyethylene (HDPE) Filled with Expanded Graphite. *Int. J. Thermophys*. **33**, 2110-2117.

[49] Zhou W, Yu D, An Q. (2009). A novel polymeric coating witjh high thermal conductivity. *Polymer. Plast. Technol*. **48**, 1230-8.

[50] Mortazavi B, Baniassadi M, Bardon J, Ahzi S. (2013). Modeling of two phase random composite materials by finite element, Mori-Tanaka and strong constrast methods. *Composites Part B: Engineering*. **45**, 1117-1125.

[51] Stankovich S, Dikin DA, Dommett GH, Kohlhaas KM, Zimney EJ, Stach EA, Piner RD, Nguyen ST, Ruoff RS. (2006). Graphene-based composite materials. *Nature* **442** (7100), 282-286.

[52] Gang W, Jun L, Qiang Z, Mingqiu Z. (2006). Correlation between percolation behavior of electricity and viscoelasticity for graphite filled high density polyethylene. *Polymer*. **47**, 2442-2447.

[53] Du F, Scogna RC, Zhou W, Brand S, Fischer JE, Winey KI. (2004). Nanotube Networks in Polymer Nanocomposites: Rheology and Electrical Conductivity. *Macromolecules.* **37** (24), 9048–9055.

[54] Du J, Zhao L, Zeng Y, Zhang L, Lia F, Liu P, Liua C. (2011) Comparison of electrical properties between multi-walled carbon nanotube and graphene nanosheet/high density polyethylene composites with a segregated network structure. *Carbon*. **49**, 1094-1100.

[55] Shtein M, Nadiv R, Buzaglo M, Kahil K, Regev O. (2015). Thermally Conductive Graphene-Polymer Composites: Size, Percolation, and Synergy Effects. *Chem. Mater.* **27** (6), 2100-2106.

[56] Nan CW, Shen Y, Ma J. (2010). Physical properties pf composites near percolation. *Ann. Rev. Mat. Res*. **40**, 131-151.

[57] Min KT, Kim GH. (2011). Effect of the viscosity and processing parameters on the surface resistivity of polypropylene/multiwalled carbon nanotube and ethylene–propylene–diene/multiwalled carbon nanotube nanocomposites. *Journal of Applied Polymer Science*. **120** (1), 95-100.

[58] Ha H, Kim SC, Ha K. (2010). Effect of molecular weight of polymer matrix on the dispersion of MWNTs in HDPE/MWNT and PC/MWNT composites. *Macromolecular research*. **18** (5), 512-518.

[59] Fisher, Harry L. (1941) Collected Papers of Wallace Hume Carothers on High Polymeric Substances. *Journal of Chemical Education.* **18**, 99.

[60] Buono FJ, Feldman ML. (1979). *Kirk-Othmer Encyclopedia of Chemical Technology*. John Wiley & Sons, New York.

[61] Xenopoulos A, Clark ES. (1995). *Nylon Plastics Handbook*. M. I. Kohan (Ed), Hanser Publishers, 1995.

[62] Deopura BL, Alagirusamy R, Joshi M, Gupta B. (2008). *Polyesters and polyamides*. Elsevier.

[63] Kurauchi T, Okada A, Nomura T, Nishio T, Saegusa S, Deguchi R. (1991). Characterization and Properties of a Nylon-6-Clay Hybrid. SAE technical paper, Ser, 910584.

[64] Xu Z, Gao C. (2010). In situ polymerisation approach to graphene-reinforced Nylon-6 composites. *Macromolecules*. **43** (16), 6716-23.

[65] Pan YX, Yu ZZ, Ou YC, Hu GH. (2000). A new process of fabricating electrically conducting nylon 6/graphite nanocomposites via intercalation polymerization. *Journal of Polymer Science Part B: Polymer Physics*. **38** (12), 1626-1633.

[66] Liu T, Phang IY, Shen L, Chow SY, Zhang WD. (2004). Morphology and mechanical properties of multiwalled carbon nanotubes reinforced nylon-6 composites. *Macromolecules*, **37** (19), 7214-7222.

[67] Novoselov KS, Geim AK, Morozov SV, Jiang D, Zhang Y, Dubonos SV, Grigorieva IV, Firsov AA. (2004). Electric field effect in atomically thin carbon films. *Science*. **306**, 666–669.

[68] Spyrou K, Rudolf P. (2014). An introduction to graphene. Functionalization of graphene, 1-20.

[69] Novoselov KS, Jiang D, Schedin F, Booth TJ, Khotkevich VV, Morozov SV, Geim AK. (2005). Two-dimensional atomic crystals. *Proceedings of the National Academy of Sciences USA*. **102**, 10451.

[70] Geim AK. (2009). Graphene: Status and Prospects. *Science.* **324**, 1530-1534.

[71] Lee C, Wei X, Qunyang L, Carpick R, Kysar JW, Hone J. (2009). Elastic and frictional properties of graphene. *Physica Status Solidi*. **246**, 2562-2567.

[72] Katsnelson MI, Katsnelʹson MI. (2012). Graphene: carbon in two dimensions. *Cambridge university press*.

[73] Faccio R, Fernández-Werner L, Pardo H, Goyenola C, Denis PA, Mombrú ÁW. (2011). Mechanical and Electronic Properties of Graphene Nanostructures. *Physics and Applications of Graphene-Theory*. InTech.

[74] Vlachopoulos J, Strutt D. (2003). Polymer processing. *Materials science and technology*. **19** (9), 1161-1169.

[75] Sacher S, Wahl P, Markl D, Treffer D, Menezes JC, Koscher G, Khinast JG. (2012). PAT for Pharmaceutical Extrusion Monitoring and Supervisory Control. *AIChE Annual Meeting.*

[76] Andersen P. (2015). Fundamentals of twin-screw extrusion polymer melting: Common pitfalls and how to avoid them. *AIP Conference Proceedings* (Vol. 1664, No. 1, p. 020007). AIP Publishing.

[77] Kutz M. (2011). *Applied plastics engineering handbook: processing and materials*. William Andrew.

[78] Kamal MR, Isayev A, Liu SJ. (2009). Injection molding. In *Injection Molding* (pp. I-XXIV).

[79] Li Z. Shi Y, Liu H, Chen F, Zhang Q, Wang K, Fu Q. (2014). Effect of melting temperature on interfacial interaction and mechanical properties of polypropylene (PP) fiber reinforced olefin block copolymers (OBCs). *RSC Advances*. **4** (85), 45234-45243.

[80] Penjumras P, AbdulRahman R, Talib RA, Abdan K. (2016). Effect of silanecoupling agent on properties of biocomposites based on poly (lactic acid) and durian rind cellulose. *IOP Conference Series: Materials Science and Engineering*. 137 (1), 012006.

[81] Park CH, Lee WI. (2012). Compression molding in polymer matrix composites. *Manufacturing techniques for polymer matrix composites (PMCs)* (pp. 47-94).

[82] Roberts DR, Holder SJ. (2011). Mechanochromic systems for the detection of stress, strain and deformation in polymeric materials. *Journal of Materials Chemistry*. **21** (23), 8256-8268.

[83] Godec D. (2007). Günter Erhard: Designing with Plastics. *Polimeri: časopis za plastiku i gumu*, *27*(2), 100-100.

[84] Kohan MI. (1995). *Nylon plastics handbook*. Hanser Publishers.

[85] Ferry JD. (1980). *Viscoelastic properties of polymers*. John Wiley & Sons.

[86] Menard KP. (2008). *Dynamic mechanical analysis: a practical introduction*. CRC press.

[87] Seymour RB, Carraher CE. (2000). *Polymer chemistry* (Vol. 181). New York: Marcel Dekker.

[88] Mutlur S. (2004). Thermal analysis of composites using DSC. *Advanced topics in characterization of composites*, 11-33.

[89] Coats AW, Redfern JP. (1963). Thermogravimetric analysis. A review. *Analyst*. **88** (1053), 906-924.

[90] Mezger TG. (2006). *The rheology handbook: for users of rotational and oscillatory rheometers*. Vincentz Network GmbH & Co KG.

[91] Cox W, Merz E. (1959). Rheology of polymer melts - A correlation of dynamic and steady flow measurements. In *International Symposium on Plastics Testing and Standardization*. ASTM International.

[92] Gardiner DJ. (1989). Introduction to Raman scattering. In *Practical Raman Spectroscopy* (pp. 1-12). Springer, Berlin, Heidelberg.

[93] Stokes D. (2008). *Principles and practice of variable pressure: environmental scanning electron microscopy (VP-ESEM)*. John Wiley & Sons.

[94] Van der Heide P. (2011). *X-ray photoelectron spectroscopy: an introduction to principles and practices*. John Wiley & Sons.

[95] Griffiths PR, De Haseth JA. (2007). *Fourier transform infrared spectrometry* (Vol. 171). John Wiley & Sons.

[96] He Y. (2005). Rapid thermal conductivity measurement with a hot disk sensor: Part 1. Theoretical considerations. *Thermochimica acta*. **436** (1-2), 122-129.

[97] Do CH, Pearce EM, Bulkin BJ, Reimschuessel HK. (1987). FT–IR spectroscopic study on the thermal and thermal oxidative degradation of nylons. *Journal of Polymer Science Part A: Polymer Chemistry*. **25** (9), 2409-2424.

[98] Svoboda M, Schneider B, Štokr J. (1991). Infrared spectroscopic study of the products of thermal degradation of polyamides in inert atmosphere. *Collection of Czechoslovak chemical communications*, **56** (7), 1461-1476.

[99] Grigg MN. (2006). *Thermo-oxidative degradation of polyamide 6* (Doctoral dissertation, Queensland University of Technology).

[100] Collins PG, Bradley K, Ishigami M, Zettl DA. (2000). Extreme oxygen sensitivity of electronic properties of carbon nanotubes. S*cience.* **287** (5459), 1801-1804.

[101] Geng Y, Wang SJ, Kim JK. (2009). Preparation of graphite nanoplatelets and graphene sheets. *Journal of colloid and interface science*. **336** (2), 592-598.

[102] Song Y, Yu J, Yu L, Alam FE, Dai W, Li C, Jiang N. (2015). Enhancing the thermal, electrical, and mechanical properties of silicone rubber by addition of graphene nanoplatelets. *Materials & Design*. **88**, 950-957.

[103] Mkhoyan KA, Contryman AW, Silcox J, Stewart DA, Eda G, Mattevi C, Chhowalla M. (2009). Atomic and electronic structure of graphene-oxide. *Nano letters*. **9** (3), 1058-1063.

[104] Graf D, Molitor F, Ensslin K, Stampfer C, Jungen A, Hierold C, Wirtz L. (2007). Spatially resolved Raman spectroscopy of single-and few-layer graphene. *Nano letters*. **7** (2), 238-242.

[105] Bokobza L, Bruneel JL, Couzi M. (2014). Raman spectroscopy as a tool for the analysis of carbon-based materials (highly oriented pyrolitic graphite, multilayer graphene and multiwall carbon nanotubes) and of some of their elastomeric composites. *Vibrational Spectroscopy*. **74**, 57-63.

[106] Dixon D, Lemonine P, Hamilton J, Lubarsky G, Archer E. (2015). Graphene oxide–polyamide 6 nanocomposites produced via in situ polymerization. *Journal of Thermoplastic Composite Materials*, **28** (3), 372-389.

[107] Cheng HKF, Sahoo NG, Pan Y, Li L, Chan SH, Zhao J, Chen G. (2010). Complementary effects of multiwalled carbon nanotubes and conductive carbon black on polyamide 6. *Journal of Polymer Science Part B: Polymer Physics*, **48** (11), 1203-1212.

[108] Khanna YP, Kuhn WP. (1997). Measurement of crystalline index in nylons by DSC: complexities and recommendations. *Journal of Polymer Science Part B: Polymer Physics*, **35** (14), 2219-2231.

[109] Mayoral B, Hornsby PR, McNally T, Schiller T, Jack K, D. J. Martin DJ. (2013). Quasi-Solid State Uniaxial and Biaxial Deformation of PET/MWCNT Composites, RSC Adv. **3**, 5162-5183.

[110] AlMaadeed MA, Kahraman R, Khanam PN, Madi N. (2012). Date palm wood flour/glass fibre reinforced hybrid composites of recycled polypropylene: mechanical and thermal properties. Mater. Des. **42**, 289-94.

[111] Zhang L, Wan C, Zhang Y. (2009). Investigation on the multiwalled carbon nanotubes reinforced polyamide 6/polypropylene composites. *Polymer Engineering & Science*, **49** (10), 1909-1917.

[112] Xu Z, Gao C. (2010). In situ polymerization approach to graphene-reinforced nylon-6 composites. *Macromolecules*, **43** (16), 6716-6723.

[113] Zhou S, Yu L, Song X, Chang J, Zou H, Liang M. (2014). Preparation of highly thermally conducting polyamide 6/graphite composites via low-temperature in situ expansion. *Journal of Applied Polymer Science*, **131** (1).

[114] Du F, Scogna RC, Zhou W, Brand S, Fischer JE, Winey KI. (2004). Nanotube networks in polymer nanocomposites: rheology and electrical conductivity. Macromolecules, **37**(24), 9048-9055.

[115] Liu X, Wu Q, Berglund LA, Qi Z. (2002). Investigation on unusual crystallization behavior in polyamide 6/montmorillonite nanocomposites. *Macromolecular Materials and Engineering*, *287*(8), 515-522.

[116] Shan GF, Yang W, Yang MB, Xie BH, Li ZM, Feng JM. (2006). Effect of crystallinity level on the double yielding behavior of polyamide 6. *Polymer testing*, **25** (4), 452-459.

[117] Chávez-Medellín R, Prado LA, Schulte K. (2010). Polyamide-12/Functionalized Carbon Nanofiber Composites: Evaluation of Thermal and Mechanical Properties. *Macromolecular Materials and Engineering*, **295** (4), 397-405.

[118] Papageorgiou DG, Kinloch IA, Young RJ. (2017). Mechanical properties of graphene and graphene-based nanocomposites. *Progress in Materials Science*, **90**, 75-127.

[119] Vasileiou AA, Kontopoulou M, Gui H, Docoslis A. (2015). Correlation between the length reduction of carbon nanotubes and the electrical percolation threshold of melt compounded polyolefin composites. *ACS applied materials & interfaces*, **7** (3), 1624-1631.

[120] Fukushima H, Kalaitzidou K, Drzal LT. (2007). Electrical and barrier properties of exfoliated graphite nanoplatelet (xGnP) reinforced nanocomposites. *ICCM-16, Kyoto*.

[121] Fukushima H, Drzal LT. (2006). Nylon-exfoliated graphite nanoplatelet (xGnP) nanocomposites with enhanced mechanical, electrical and thermal properties. *NSTI Nanotech*. 282-5.

[122] Balandin AA. (2011). Thermal properties of graphene and nanostructured carbon materials. *Nature materials*, **10** (8), 569.

[123] Pu HH, Rhim SH, Hirschmugl CJ, Gajdardziska-Josifovska M, Weinert M, Chen JH. (2013). Anisotropic thermal conductivity of semiconducting graphene monoxide. *Applied Physics Letters*, **102** (22), 223101.

[124] Gu J, Li N, Tian L, Lv Z, Zhang Q. (2015). High thermal conductivity graphite nanoplatelet/UHMWPE nanocomposites. *Rsc. Advances*. **5** (46), 36334-36339.